Exploring Statistical Isotropy Violations in the CMB sky: Real-Space Analysis

विद्या वाचस्पति की
उपाधि की अपेक्षाओं की आंशिक पूर्ति में प्रस्तुत शोध प्रबंध

A thesis submitted in partial fulfillment of the requirements
of the degree of Doctor of Philosophy

द्वारा / By

दीपांशु/ Dipanshu

पंजीकरण सं. / Registration No.: 20193697

शोध प्रबंध पर्यवेक्षक / Thesis Supervisor:

Prof. तरुण सौरदीप/Tarun Souradeep

IISER PUNE

भारतीय विज्ञान शिक्षा एवं अनुसंधान संस्थान पुणे

INDIAN INSTITUTE OF SCIENCE EDUCATION AND RESEARCH
PUNE

2024

To my father, mother, and sister, Preeti— for their unwavering love, support, and belief in me throughout this journey.

CERTIFICATE

This is to certify that the work incorporated in the thesis entitled *"Characterizing Statistical Isotropy Violations in the CMB: Real-Space Analysis "* submitted by Dipanshu was carried out by the candidate under my supervision. To the best of my knowledge, the work presented here or any part of it has not been included in any other thesis submitted previously for the award of any degree or diploma from any other university or institution.

Tarun Souradeep

Date: Prof. Tarun Souradeep

September 26, 2024 Thesis Supervisor

DECLARATION

Name of Student: Dipanshu

Reg. No.: 20193697

Thesis Supervisor: Prof. Tarun Souradeep

Department: Physics

Date of joining program: August 1, 2019

Date of Pre-Synopsis Seminar: April 10, 2024

Title of Thesis: Exploring Statistical Isotropy Violations in the CMB sky: Real-Space Analysis

I declare that this written submission represents my idea in my own words and where others' ideas have been included; I have adequately cited and referenced the original sources. I declare that I have acknowledged collaborative work and discussions wherever such work has been included. I also declare that I have adhered to all principles of academic honesty and integrity and have not misrepresented or fabricated or falsified any idea/data/fact/source in my submission. I understand that violation of the above will be cause for disciplinary action by the Institute and can also evoke penal action from the sources which have thus not been properly cited or from whom proper permission has not been taken when needed.

The work reported in this thesis is the original work done by me under the guidance of Prof Tarun Souradeep.

Dipanshu

Date:

September 26, 2024

Dipanshu

(20193697)

ACKNOWLEDGEMENTS

I want to thank everyone who has been a key part of my efforts over these past five years. This Ph.D. journey has not only been a valuable academic experience but has also helped me grow personally in many ways.

The role of a Ph.D. supervisor is incredibly important, and I feel incredibly fortunate to have had the opportunity to pursue my Ph.D. under the guidance of Prof. Tarun Souradeep.. His support and guidance throughout these years have not only made me a better researcher but also an independent thinker and a better person. I am especially thankful for his generosity in sharing his expertise and knowledge, which has greatly enriched my understanding of the subject. Watching him work through complex mathematical ideas with such insight has been an invaluable learning experience. His patience, whether with difficult equations or my occasional typos, is something I'll always admire. What I am most grateful for is that he allowed me the space to explore my own ideas, yet was always there to listen and guide me when needed. He stood by me during my most challenging times, supporting my decisions—whether academic or personal—with kindness and encouragement that has meant so much to me. His belief in me and constant motivation have made a lasting impact, and I will always carry the lessons I've learned from him in both my professional and personal life. For all of this, I am deeply thankful.

I would also like to express my heartfelt thanks to my collaborators, Shriya and Akashdeep. These two brilliant young minds played a crucial role in developing my work. Their energy and enthusiasm constantly lifted my spirits, encouraging me to think differently and make significant progress. Their genius helped me tackle difficult problems with greater ease, and for that, I am deeply grateful.

I also want to extend my thanks to the entire CMB@IUCAA-IISER-RRI group.

The countless discussions we shared were invaluable to my research journey. These conversations not only deepened my understanding but also shaped my growth as a researcher. I am sincerely thankful to all the members of the group—Rajorshi, Sarvesh, Sayan, Shabbir, Debabrata, Santanu, Debajyoti, Aditya, James, Protap, Vaishali, Aritra, and Fazlu—for their insightful contributions to our cosmology discussions.

I am also deeply indebted to my RAC members—Prof. Arun Thalapillil, Prof. Sanjit Mitra and Prof. Suneeta Vardarajan—for their immense support, valuable comments, and suggestions throughout my Ph.D. tenure. Their guidance played a crucial role in helping me streamline my research and make significant advancements. I am sincerely grateful for their insights and encouragement along the way.

I am also deeply thankful to all my teachers who have shaped my thinking, taught me the foundations of physics, and guided me to become a better researcher. My journey began during my Master's at HRI, Allahabad, where two years of rigorous learning gave me a deep understanding of theoretical physics and mathematics. I would especially like to thank Prof. Ashoke Sen and Prof. Dileep Jatkar—working on projects and courses under their guidance inspired me to pursue cosmology in my Ph.D. and provided a clear direction for my career.

I am equally grateful to all the teachers at RRI Bangalore, IISER Pune, HRI Allahabad, and the Panjab University, Chandigarh, for their invaluable teaching and guidance throughout my academic journey. Their mentorship has been essential to my growth and success, and I truly appreciate the role each of them has played in shaping my path.

It has been an incredible privilege to pursue my PhD at two distinguished institutions— IISER Pune and Raman Research Institute . I am deeply grateful to both institutes for providing exceptional facilities, infrastructure, and a research-driven environment, even amidst the challenges posed by the COVID-19 pandemic.

I would like to extend my sincere appreciation to the administrative staff at both institutes for their unwavering support. In particular, I am deeply thankful to Vidya Ma'am for her invaluable assistance in coordinating meetings and managing various administrative tasks. I am also grateful to Mahima Ma'am, Dhanashree Ma'am, and Mr. Prabhakar for their dedicated efforts in handling all documentation processes, ensuring everything proceeded smoothly throughout my PhD journey.

My PhD journey has been shared with an incredible group of colleagues and friends across various institutes. I am immensely grateful to each of them for walking this path with me and teaching me invaluable life lessons along the way. While it's impossible to name everyone, I want to express my deepest gratitude to those who have left a lasting impact on me.

At RRI, I owe special thanks to Sarvesh Bhaiya, Rajorshi Da, and Samrat Bhaiya. You all guided me like elder brothers, offering unwavering support during the ups and downs of my PhD journey. Your wisdom, guidance, and life lessons have played a vital role in shaping my character. I will always carry your support in my heart. At IISER Pune, Aakash, Mayank, Ritam, Jiten, and Rajeev—thank you for the countless memories we shared, especially during the COVID-19 times. The laughter, discussions, and moments we spent together will forever be cherished. At HRI Allahabad, Ankur, Durgesh, and Arnab—you guys have been phenomenal. I am grateful to have found lifelong friends in you, the kind of friends I can call anytime to share anything. The bond we formed is truly unbreakable. Lastly, at Punjab University, Sanjay, Ankur, Gurvir, Karan, and Rohan—thank you for being the very first group of friends I made when I began hostel life. The memories we created are unforgettable, and I am grateful to you for standing by me during those formative years. To everyone at RRI, IISER, HRI, and PU, thank you for sharing this beautiful journey with me and for being a part of my academic and personal growth. The friendships and memories we've created will stay with me forever.

Lastly, I want to thank my father, mother, and my younger sister, Preeti, for their endless love, trust, and support. Whatever I am today is because of the values you taught me. I am truly grateful for everything you've done to help me become a better person. A special thanks to my sister, for being by my side during the toughest times. I will always be thankful to all of you for your constant support and belief in me.

Abstract

Observations of cosmic microwave background (CMB) anisotropies have been instrumental in advancing modern cosmology. The availability of high-resolution CMB maps has significantly enhanced our understanding of the universe's origin, dynamics, and components. The exquisitely measured maps of fluctuations in the CMB present the possibility of systematically testing the principle of statistical isotropy of the Universe. The isotropy of the CMB has been a subject of close scrutiny since the release of full-sky CMB data from missions like COBE, WMAP, and Planck. There are compelling reasons to investigate the isotropic nature of the universe.

A systematic approach based on strong mathematical formulation allows any non-statistical isotropic (nSI) feature to be traced to the nature of physical effects or observational artifacts. Bipolar spherical harmonics (BipoSH) representation has emerged as an overarching general formalism for quantifying the departures from statistical isotropy for a field on a 2D sphere. The BipoSH coefficients extend the traditional CMB angular power spectrum, offering deeper insights into the early universe. The detection of non-zero BipoSH coefficients suggests a potential violation of isotropy. Statistical isotropy, which quantifies the isotropic nature of the universe studied through isotropic angular correlation function, plays a critical role in these studies.

In this thesis, we study a natural generalization of the well-known isotropic angular correlation function that can also capture nSI features in random maps on a 2-sphere. We utilize a reduction technique for BipoSH that results in new basis functions called mBipoSH functions. In this new basis, new measures quantifying nSI features emerge as an additional set of the real space angular correlation functions that we refer to as mBipoSH angular correlation functions.

In the specific domain of our interest, which involves the detailed study of observed maps depicting the anisotropy in the CMB, these maps offer a new set of observables in real space that complement the harmonic space BipoSH representation used earlier in the literature. Introducing new approaches often helps shed new light on the nature of the phenomena underlying the observed nSI signals. As an illustrative example, we derive and plot the mBipoSH angular correlation functions for the well-known nSI effects induced in CMB maps due to the Doppler boost, Cosmic hemispherical asymmetry and Non-circular beam cases. We emphasize that the work presented in this thesis can be effectively employed in the wider context to investigate random distributions on a 2D sphere, encompassing diverse applications ranging from celestial sky maps to geographical maps.

LIST OF PUBLICATIONS

Publications included in this thesis

1. *Capturing Statistical Isotropy Violation with Generalized Isotropic Angular Correlation Functions of Cosmic Microwave Background Anisotropy.*

   Dipanshu, Tarun Souradeep and Shriya Hirve. The Astrophysical Journal 954, 181 (2023).

2. *Statistical Isotropy Violations in CMB Temperature Anisotropy: Analysis Using Minimal Bipolar Spherical Harmonics*

   Dipanshu, Akashdeep Karan and Tarun Souradeep. Prepared for Submission, arXiv:2411.11139 (2024).

TABLE OF CONTENTS

Acknowledgments iv

Abstract viii

List of Publications ix

Synopsis xviii

I Introduction 9

Chapter 1: Introduction 11

1.0.1 CMB as a perfect blackbody 12

1.0.2 Temperature anisotropy 14

1.0.3 CMB polarisation 17

1.0.4 Concordance model of cosmology 23

1.0.5 Two point angular correlation function 24

1.0.6 Weak Lensing of CMB 26

1.0.7 CMB Foregrounds 27

1.1 Summary 28

II Statistical Isotropy of CMB 33

Chapter 2: Statistical Isotropy of the CMB 35

2.1 Bipolar Spherical Harmonics 37
2.2 Properties of BipoSH coefficients 39
2.2.1 BipoSH coefficients for SI sky 39
2.2.2 Parity under BipoSH coefficients 40
2.2.3 Symmetries under BipoSH coefficients 41
2.3 Sources of SI violation 42
2.4 Discussion 43

Chapter 3: 'minimal' Bipolar Spherical Harmonics 45

3.1 Reduction of Bipolar Harmonics 46
3.1.1 Examples of the 'minimal' Harmonics expansions 54
3.2 'Minimal' Harmonics Functions 56
3.2.1 Dipole anisotropy $(L = 1)$ 59
3.2.2 $L = 2$, Quadrupole anisotropy 60
3.2.3 $L = 3$ Octopole Anisotropy 62
3.3 Symmetries of mBipoSH angular basis 63
3.3.1 Symmetries of correlation function in mBipoSH basis 64
3.3.2 Effect of rotation 65
3.3.3 Parity in mBipoSH angular functions 66
3.4 Construction of map in reduced basis 67
3.5 Discussion 68

Chapter 4: Exploring nSI effects in CMB using mBipoSH 71

4.1 Dipole anisotropy due to Doppler Boost 71

4.2 Cosmic Hemispherical Asymmetry 79
4.3 Non Circular Beam Effects 83
4.4 Real Space based Estimation Method 90
4.4.1 Minimum Variance Estimator 90
4.5 Analysis of Planck Data 97
4.6 Discussions 98

Chapter 5: Conclusion 101
5.1 Summary 101
5.1.1 BipoSH basis and its irreducible reduction 102
5.1.2 Application to the CMB sky maps 102
5.2 Future Work 103

Appendix A: Spherical coordinate system 107

Appendix B: Important Relations 111

Appendix C: mBipoSH functions 113
C.0.1 Rank 1 Reduction Formula 113
C.0.2 Rank 2 Reduction Formula 113
C.0.3 Rank 3 Reduction Formula 114

Bibliography 115

LIST OF FIGURES

1.1 Cosmic microwave background spectrum as measured by the FIRAS instrument on the COBE. Credits: COBE, M. O'Dwyer. 13

1.2 Visual representation of improvement of resolution in CMB temperature maps. The following three panels show the identical spot on the sky, as measured by COBE, WMAP and Planck sattelites. [Image Credits- NASA/JPL- Caltech/ESA] 18

1.3 The CMB temperature anisotropies map measured by Planck, foreground-cleaned using the SMICA method. The grey region depicts the noisy galactic region that has been in-painted to complete the full map. Credits: Planck Collaboration 19

1.4 CMB polarization anisotropy map as measured by Planck, with headless vectors illustrating the polarization field. Credits: Planck Collaboration 20

1.5 Pictorial representation of the E and B mode components of the CMB. Image credits: Licia Verde. 21

1.6 These are the foreground cleaned angular power spectra for temperature (top), the temperature-polarization cross-spectrum (middle), the E mode of polarization (bottom left), and the lensing potential (bottom right), measured from Planck. Credits: Planck Collaboration 22

1.7 The angular correlation function of the two-point temperature correlations. The black line shows the mean value of $C(\theta)$, and the grey region shows the cosmic variance bars corresponding to the correlation function. 25

1.8 Angular power spectra of various CMB fields probed by various CMB experiments are listed in the top panel. CMB-TT, CMB-EE, and CMB-BB represent the temperature anisotropy angular power spectra, the angular power spectrum of the E-mode of CMB polarization, and the angular power spectrum of the B-mode of CMB polarization, respectively. The B-mode power shown here is mainly contributed by the gravitational lensing of CMB photons due to large-scale structure. The middle panel displays D_ℓ^{TE}, the correlation between CMB temperature anisotropy and the E-mode of CMB polarization. The bottom panel illustrates the angular power spectrum of the lensing potential, C_ℓ^ϕ. Credits: Planck Collaboration. 29

3.1 Pictorial representation of the Euler angles. Source- Wikipedia 65

3.2 Pictorial representation of $\cos\theta$ spectrum at each point on the sphere 68

4.1 Theoretical plots for defined mBipoSH angular correlation functions for Doppler boost. 77

4.2 C_{SI} and C^1_{nSI} plotted with 1000 simulated SI CMB maps in the respective panels. 77

4.3 The mean and variance of the two mBipoSH angular correlation functions C^0_{nSI} and C^1_{nSI} plotted with 1000 SI and nSI maps generated with same random seed. 78

4.4 The left panel displays the two theoretical mBipoSH correlation functions for the nSI effect CHA, namely $C_0(\cos\theta)$ and $C_1(\cos\theta)$ along with the SI correlation function. The right panel presents the cosmic variance error bar for these mBipoSH correlation functions using 1000 simulated CHA maps generated by CoNIGS (1) compared with Doppler effect. 83

4.5 Illustration of the mBipoSH isotropic correlation functions for the non-circular beam. Top panel shows how the correlation functions vary with the change in θ_{FWHM}. The bottom panel shows how these isotropic correlation functions change with respect to e. 88

4.6 Angular mBipoSH correlation functions from SEVEM Foreground-cleaned Planck data for L=1. Green and blue lines represent the extracted mBipoSH functions from the map, while light blue and red depict theoretical Doppler boost-only plots with error bars. 97

4.7 Angular mBipoSH correlation functions from SMICA Foreground-cleaned Planck data for L=1. Green and blue lines represent the extracted mBipoSH functions from the map, while light blue and red depict theoretical Doppler boost-only plots with error bars. 98

A.1 The visual representation of the first few spherical harmonic basis components. Credit- wolfram.com/sphericalharmonics 110

Synopsis

In this thesis, we develop a mathematical framework to effectively study CMB anisotropies data distributed on a 2D sphere, with a focus on capturing features that go beyond statistical isotropy. The Bipolar Spherical Harmonics (BipoSH) basis has proven to be instrumental in quantifying such features in CMB data beyond the power spectrum.

We introduce a potential extension of the BipoSH basis to capture statistical isotropy (SI) violations using a set of isotropic, real-space angular correlation functions, termed mBipoSH angular correlation functions, which depend on the angular separation θ. These newly defined functions provide additional isotropic correlation measures for maps with SI violations.

We mathematically define these angular correlation functions for three well-known cases of SI violation: Doppler boost, cosmic hemispherical asymmetry, and non-circular beam effects. The outputs are validated using simulated maps exhibiting the relevant effects. This method introduces a new approach for studying nSI maps through real-space-based estimations, making it timely and relevant for future ground-based CMB missions.

This thesis is divided into 5 Chapters, and the outline is as follows.

Chapter 1 provides the background of CMB cosmology and outlines the main focus of the thesis. It introduces key methods and techniques used in the analysis of CMB anisotropies. The chapter also reviews the current status of CMB cosmology, with insights from major missions like COBE, WMAP, and Planck, setting the stage for the advanced analysis methods explored in this research.

In Chapter 2, we examine the statistical isotropy (SI) parameter to validate the cosmological principle. We mathematically define SI through two-point correlation functions and introduce the Bipolar Spherical Harmonics (BipoSH) framework as a tool to capture SI violations. We discuss the efficacy of Bipolar Harmonic coefficients in capturing SI violation features for randomly distributed data on a 2D sphere.

In Chapter 3, we explore the reduction of the BipoSH basis to a new, complementary and comprehensive basis. This reduction technique leads to a novel, minimal set of generalized isotropic angular correlation functions, which we referred to as mBipoSH functions in this thesis. We derive these functions mathematically and present the exact relations for the first few multipoles.

In Chapter 4, we present the effectiveness of this newly defined mBipoSH angular correlation functions by applying them to known cases of statistical isotropy (SI) violations in CMB data. We specifically investigate the Doppler boost, cosmic variance, and non-circular beam effects for this purpose, providing the exact mathematical formalism alongside an analysis of these nSI features on simulated maps. Finally, we present a mathematical framework to capture the strength of nSI effects from pixel-based measurements.

In Chapter 5, we provide a summary of the work done in this thesis and discuss the future research directions motivated by the studies conducted throughout this thesis.

Part I

Introduction

CHAPTER 1

INTRODUCTION

Our thirst for knowledge about the cosmos dates back to ancient civilizations, where diverse cosmological models attempted to explain the nature of the universe. From the belief in a flat Earth to the notion of a geocentric universe, human imagination came far but struggled to decipher the true workings of the large cosmos. In the 16th century, Nicolas Copernicus proposed a heliocentric model. The belief that Earth at the center of the solar system was replaced by the idea that the Sun takes the central position. In early 17th century, Johannes Kepler's laws of planetary motion brought further knowledge about the cosmos and revealed celestial bodies follows the elliptical path. In 1920s, a important moment arrived when Edwin Hubble peered through his telescopic lens and observed galaxies beyond our Milky Way galaxy. His observations revealed that distant galaxies were not static but actually moving away from us. From this, Hubble's Law emerged, describing the relationship between a galaxy's recessional velocity and its distance from us. From observations of redshifted light from these galaxies at various distances, it was deduced that they are receding away from our galaxy at a velocity proportional to the distances between them. Based on the observation that galaxies were moving away from us, it was hypothesized that the universe is ever expanding. This led to the implication that the universe must have been smaller and hotter in the past. If we trace back the timeline enough, we reach an epoch where temperatures were very high, preventing the existence of neutral atoms and making radiation the dominant form of energy. Moving forward from a time in such an expanding universe, when matter was composed of unbound electrons and nucleons, the "Big Bang Model" of cosmology successfully predicts the abundance of light elements (hydrogen, helium, and lithium), aligning with experimental measurements. These predictions rely on the evolution of the universe's background metric, which is described by an isotropic and homogeneous Friedmann-Robertson-Walker (FRW) metric. This provided fundamental understanding of the current universe.

During the early stages of the universe, the photons were tightly coupled to the electrons and protons and were existing in the form of baryon-photon fluid. In the epoch of recombination, which happened about 380,000 years after the Big Bang, the temperature dropped below $\sim$1 eV around the redshift of z $\sim$ 1100, which was not high enough temperature to maintain equilibrium in the baryon-photon fluid. Hence as a result of this, photons decoupled from the electrons. Due to which the fraction of free electrons dropped dramatically and photons became transparent and freely streaming from the last scattering surface as the CMB photons which we observe today. The observed CMB radiation is almost uniform across the sky and observationally indistinguishable from blackbody spectrum at a temperature of 2.725 K. However, there are small anisotropies in the temperature at the level of 10^{-5}. CMB is also linearly polarized at 10% level of temperature amplitude. These anisotropies of the CMB directly reflect the physics in the early universe and their power spectra provide us platform to determine cosmological parameters.

1.0.1 CMB as a perfect blackbody

The presence of a cosmological relic radiation, the cosmic microwave background originating from the early radiation dominated phase of the universe was one of the important predictions made by the hot big bang model of cosmology. This relic radiation was predicted to have a black body spectrum. The CMB was first serendipitously discovered by Penzias and Wilson in 1965. In 1991, the Far In-

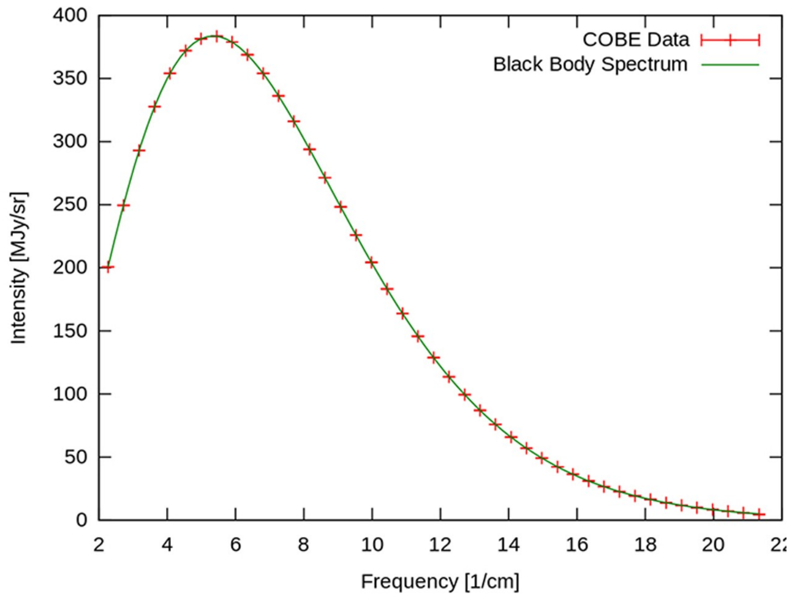

Figure 1.1: Cosmic microwave background spectrum as measured by the FIRAS instrument on the COBE. Credits: COBE, M. O'Dwyer.

fraRed Absolute Spectrophotometer (FIRAS) instrument on the NASA's Cosmic Background Explorer (COBE) satellite measured the spectrum of the CMB. The measurements obtained by FIRAS mission showed that the CMB spectrum closely matches with the blackbody radiation spectrum. The temperature of the CMB was determined to be around 2.72548 ± 0.00057 Kelvin (2) , with deviations at the level upto 10^{-5} and temperature variations of the similar magnitude. This discovery provided significant support for the Big Bang model, as this confirmed the existence of a thermal background radiation. It was a significant milestone in our understanding of the universe's origins and marking the measurement of the Cosmic Microwave Background .

A blackbody is completely defined by its temperature T and its intensity is given by the Planck law as,

$$B_v(T) = \frac{2h}{c^2}\frac{v^3}{e^{\frac{hv}{k_B T}} - 1}\,\text{ergs}^{-1}\,\text{cm}^{-2}\,\text{Hz}^{-1}\text{sr}^{-1}. \tag{1.1}$$

The blackbody nature of CMB photons is observed due to free streaming from a redshift of z $\sim$ 1100, after they decoupled from electrons. However, there are certain processes that occur in the universe's history which can cause distortions in the CMB intensity spectrum. It is still an open area of research to study these processes to understand why the CMB remains remarkably close to a thermal spectrum and how can this improve our understanding about the early universe.

1.0.2 Temperature anisotropy

The cosmic microwave background radiation has temperature variations across different directions in the sky. These anisotropies provide crucial information about our universe as they can trace their origins back to both early and late stages of the universe. The anisotropies in the CMB temperature arise from two main sources, primary anisotropies and secondary anisotropies. Primary anisotropies mainly result from effects during or before decoupling. These primary anisotropies originate from primordial quantum fluctuations that took place during the inflationary era of the universe. These tiny fluctuations later grew and became the seeds for the formation of the large-scale structure we observe today, such as galaxies and galaxy clusters. On the other hand, secondary anisotropies arise due to the interaction of decoupled CMB photons with late large scale structure of the universe. Studying these anisotropies in the CMB allows us to probe the early universe and understand the nature of primordial fluctuations which helps us to test different cosmological models. By analyzing the primary and secondary anisotropies, we can gain valuable insights into the processes and properties of our universe.

The temperature anisotropies of the cosmic microwave background are described as a continous random field. This field denoted as $\Delta T(\hat{n})$ is defined on a 2-dimensional surface of a sphere representing the sky. Here, $\hat{n} = (\theta, \phi)$ is a unit vector on the sphere, and $\Delta T(\hat{n}) = T(\hat{n}) - T_0$ represents the deviation of temperature from the mean temperature of the CMB.

The statistical properties of the CMB field can be studied by the n-point correlation functions denoted as $\langle \Delta T(\hat{n}_1)\Delta T(\hat{n}_2)\cdots\Delta T(\hat{n}_n)\rangle$. The brackets $\langle\dot{}\rangle$ denotes the ensemble average. In the context of CMB fluctuations generated during the inflationary era are assumed to be Gaussian in nature. These fluctuations arise from the quantum vacuum fluctuations of the scalar field potential. In such a case, using the Wick's theorem, it can be mathematically shown that all the information in the field is encoded in the two-point correlation function. The two-point correlation function can be represented as

$$C(\hat{n},\hat{n}') \equiv \langle \Delta T(\hat{n})\Delta T(\hat{n}')\rangle. \tag{1.2}$$

The Gaussian field on spherical surface can be naturally expanded in spherical harmonic basis as

$$\Delta T(\hat{n}) = \sum_{\ell=1}^{\infty}\sum_{m=-\ell}^{\ell} a_{\ell m} Y_{\ell m}(\hat{n}), \tag{1.3}$$

where the complex spherical harmonic coefficients $a_{\ell m}$ completely describe the temperature field. By utilizing the orthogonality of the spherical harmonics

$$\int d\hat{n}\, Y^*_{\ell m}(\hat{n}) Y_{\ell' m'}(\hat{n}) = \delta_{\ell\ell'}\delta_{mm'}, \tag{1.4}$$

we can determine the coefficients from the continuous temperature field as

$$a_{\ell m} = \int d\hat{n}\, Y^*_{\ell m}(\hat{n})\Delta T(\hat{n}) \tag{1.5}$$

These coefficients are complex random variables with zero mean and variance C_ℓ, under the assumption of orientation independence referring to the assumption of isotropic nature of the universe.

$$\langle a_{\ell m}\rangle = 0, \quad \langle a_{\ell m} a^*_{\ell' m'}\rangle = \delta_{\ell\ell'}\delta_{mm'}C_\ell. \tag{1.6}$$

An equivalent description of the CMB two-point correlation function is given by the following expression

$$C(\hat{n}_1, \hat{n}_2) = \sum_{l_1 m_1} \sum_{l_2 m_2} \langle a_{l_1 m_1} a_{l_2 m_2} \rangle Y_{l_1 m_1}(\hat{n}_1) Y_{l_2 m_2}(\hat{n}_2), \tag{1.7}$$

where the quantity inside the brackets $\langle \dot{} \rangle$ is commonly referred to as the harmonic space covariance matrix.

CMB two-point correlation function is predicted to be rotation independent due to the assumption of homogeneous and isotropic nature of the universe. Under this assumption, the CMB two-point correlation can be written as follows

$$C(\hat{n}_1, \hat{n}_2) \equiv C(\hat{n}_1 \cdot \hat{n}_2). \tag{1.8}$$

Using the expression from the equations (1.6) and (1.7), the two point correlation function becomes

$$C(\theta) = \sum_{l} \frac{2l+1}{4\pi} C_l P_l(\cos\theta), \tag{1.9}$$

where θ is the angle between the two directions given by $\hat{n}_1$ and $\hat{n}_2$, $P_l(x)$ are the Legendre polynomials, and C_l's are the coefficients of expansion in this basis, more commonly known as the CMB angular power spectrum. It provides us with a wealth of information about how the universe evolved and its fundamental properties. But since we only have one sky to probe, observations of the CMB power spectrum are limited by cosmic variance. For each multipole moment denoted as ℓ, there are 2ℓ+1 modes that contribute to the CMB signal. The cosmic variance can be quantified using a formula that represents the confidence limit for the 68% data range for the CMB power spectrum.

$$\Delta C_l = \sqrt{\frac{2}{2l+1}} \cdot C_l = \sqrt{\frac{2}{2l+1}} \cdot \frac{1}{2l+1} \sum_{m=-l}^{l} |a_{lm}|^2, \tag{1.10}$$

At higher ℓs, cosmic variance is progressively less limiting because more independent modes for the measurements of C_l are available at higher multipoles. Hence, with measurements at higher angular resolution, we can do more precise tests of theory. So using high-resolution probes becomes important for better study the CMB datasets. The COBE mission by NASA, operating from 1989 to 1993, was the first mission to detect the power spectrum from the sky. It had a resolution of 7° degrees and confirmed the presence of temperature fluctuations in the CMB sky.

Following COBE mission, the Wilkinson Microwave Anisotropy Probe (WMAP) sattelite operated from 2001 to 2010. WMAP observed the temperature and polarization of the CMB at five frequencies ranging from 23 to 94 GHz. It improved upon the COBE with a sensitivity 45 times greater and an angular resolution improved to 40 arc minutes. WMAP provided more detailed measurements of the CMB power spectrum and confirmed the different peaks with great accuracy. In 2009, the Planck satellite started observing the sky at an even higher resolution of up to 5 arc minutes as also shown in the figure 1.2 and delivered the most detailed full-sky maps to date. The figure shows the current cleaned SMICA map from the Planck satellite.

Currently, the best estimates of the CMB power spectrum are obtained by the Planck mission and they are in good agreement with the predictions made by the theory supporting the Big Bang model.

1.0.3 CMB polarisation

Photons possess not only energy/temperature but also have state of polarization, which offers an alternative means of observing the sky and testing our models. The linear polarization of the cosmic microwave background primarily arises due to Thomson scattering, which refers to the elastic scattering of a photon by a free

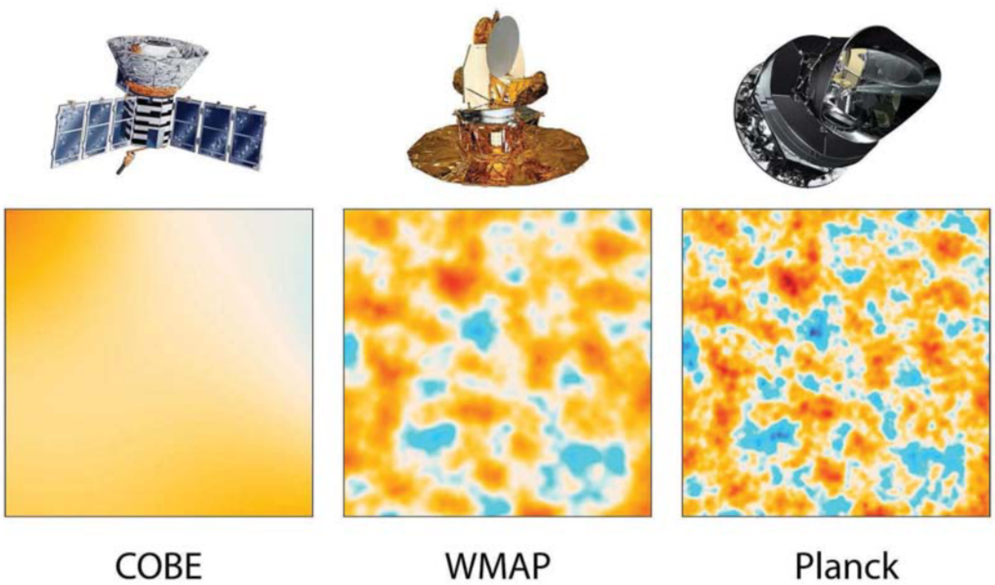

Figure 1.2: Visual representation of improvement of resolution in CMB temperature maps. The following three panels show the identical spot on the sky, as measured by COBE, WMAP and Planck sattelites. [Image Credits- NASA/JPL-Caltech/ESA]

electron. This process causes the photon to change its direction while preserving its energy and hence, wavelength. When describing both polarized and unpolarized light, we commonly use the Stokes parameters which are I, Q, U and V. These parameters are computed by taking time averages of the electric field vectors. The parameter I represents the intensity of light, which is related to its temperature and I has always a positive value. Q and U describe linear polarization in two coordinate systems, which are rotated by 45° degrees with respect to each other. The parameter V represents circular polarization, but it is not relevant for the cosmic microwave background and can be ignored for such reasons. The parameter I is a scalar quantity independent of the coordinate system. Q and U depend on angles measured relative to an arbitrary axis and as a result are dependent on the chosen coordinate system. In problems relating cosmological analysis, it is convenient to study the polarization maps in the basis elements that are independent of the

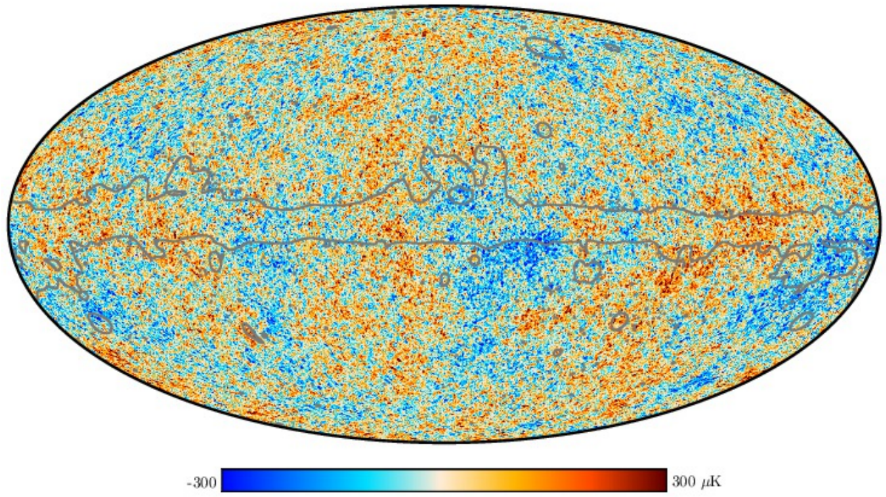

Figure 1.3: The CMB temperature anisotropies map measured by Planck, foreground-cleaned using the SMICA method. The grey region depicts the noisy galactic region that has been in-painted to complete the full map. Credits: Planck Collaboration

coordinate system. In the context of CMB polarization fields on a sphere, it is convenient to use two scalar quantities known as E-mode and B-mode to describe the CMB polarization that are coordinate independent quantities. These modes can be expanded in terms of spin ± 2 spherical harmonics, similar to the expansion of the temperature anisotropy field in spherical harmonics. The E-mode is defined as the curl-free mode in CMB polarization. On the other hand, the B-mode is defined as the gradient-free mode, which represents the component of polarization that lacks any divergence. The polarization of the CMB can be expressed using the Stokes parameters Q and U as follows:

$$(Q \pm iU)(\hat{n}) = \sum_{\ell m} a_{\pm 2,\ell m \pm 2} Y_{\ell m}(\hat{n}), \tag{1.11}$$

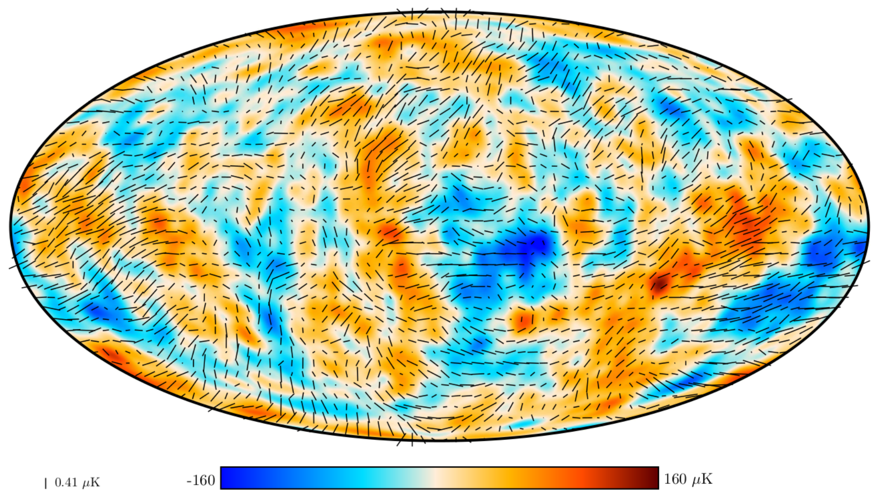

Figure 1.4: CMB polarization anisotropy map as measured by Planck, with headless vectors illustrating the polarization field. Credits: Planck Collaboration

where $a_{\pm 2,\ell m}$ are the spherical harmonic coefficients. Based on these coefficients, we define the E-mode field and B-mode field as:

$$E(\hat{n}) = \sum_{\ell m} a_{E,\ell m} Y_{\ell m}(\hat{n}) \tag{1.12}$$

$$B(\hat{n}) = \sum_{\ell m} a_{B,\ell m} Y_{\ell m}(\hat{n}), \tag{1.13}$$

where the spherical harmonic coefficients $a_{E,\ell m}$ and $a_{B,\ell m}$ are given by, $a_{E,\ell m} \equiv -\frac{1}{2}(a_{2,\ell m} + a_{-2,\ell m})$ and $a_{B,\ell m} \equiv \frac{i}{2}(a_{2,\ell m} - a_{-2,\ell m})$. For different kinds of correlations in the CMB sky, between polarization and temperature, we can express a general equation for different $C_l's$ as follows,

$$\left\langle a^{X*}_{\ell m} a^{Y}_{\ell' m'} \right\rangle = C^{XY}_{\ell} \delta_{\ell\ell'} \delta_{mm'}, \tag{1.14}$$

where X,Y could be T,E,B. Using this the temperature, E-mode and B-mode power spectra are given as C^{TT}_{ℓ}, $C^{EE}_{\ell} C^{BB}_{\ell}$. The cross-correlation, C^{TB}_{ℓ} and C^{EB}_{ℓ} are vanishing in the absence of the parity violating physics. Hence, the only other expected non-zero spectrum is the cross power spectrum C^{TE}. Figure 1.6 shows the

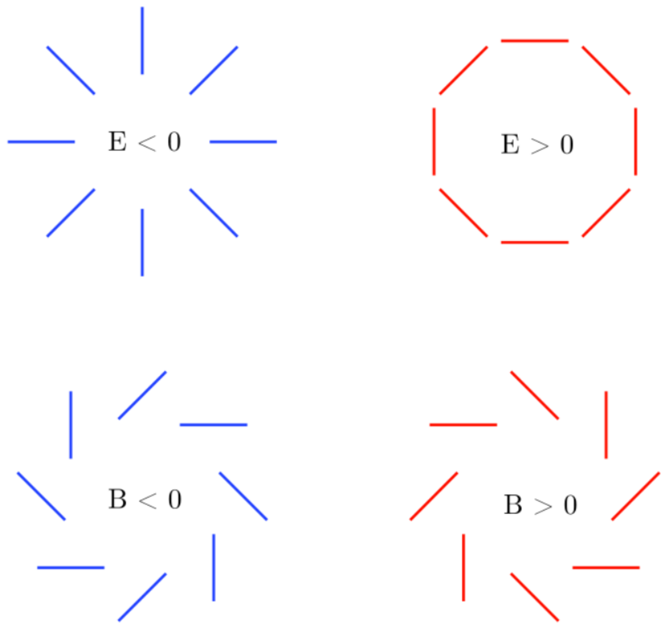

Figure 1.5: Pictorial representation of the E and B mode components of the CMB. Image credits: Licia Verde.

latest power spectrum data from the Planck collaboration. Note that, while plotting the power spectrum, using $D_\ell = \frac{\ell(\ell+1)}{2\pi} C_\ell$ is used instead of C_ℓ, this helps in visualizing the power more clearly. The factor of $\frac{\ell(\ell+1)}{2\pi}$ accounts for the way power is distributed across different angular scales in the CMB sky. This factor amplifies the power at smaller angular scales, which are higher ℓ values and compresses the power at larger angular scales or lower ℓ values such that it approximately equals the power per unit logarithmic interval in ℓ. The panel displays the different power spectrum obtained from Planck sattelite measurements of the CMB, along with the solid line representing the best-fit model. The data and theory show reasonably good agreement from the data.

The B-mode power spectrum in the CMB is not shown in plot due to its relatively weak nature compared to the dominant E-mode signal. The B-mode polarization in the CMB is supposed to be generated by primordial gravitational waves. These are generated as a consequence of inflation in the early phase of the uni-

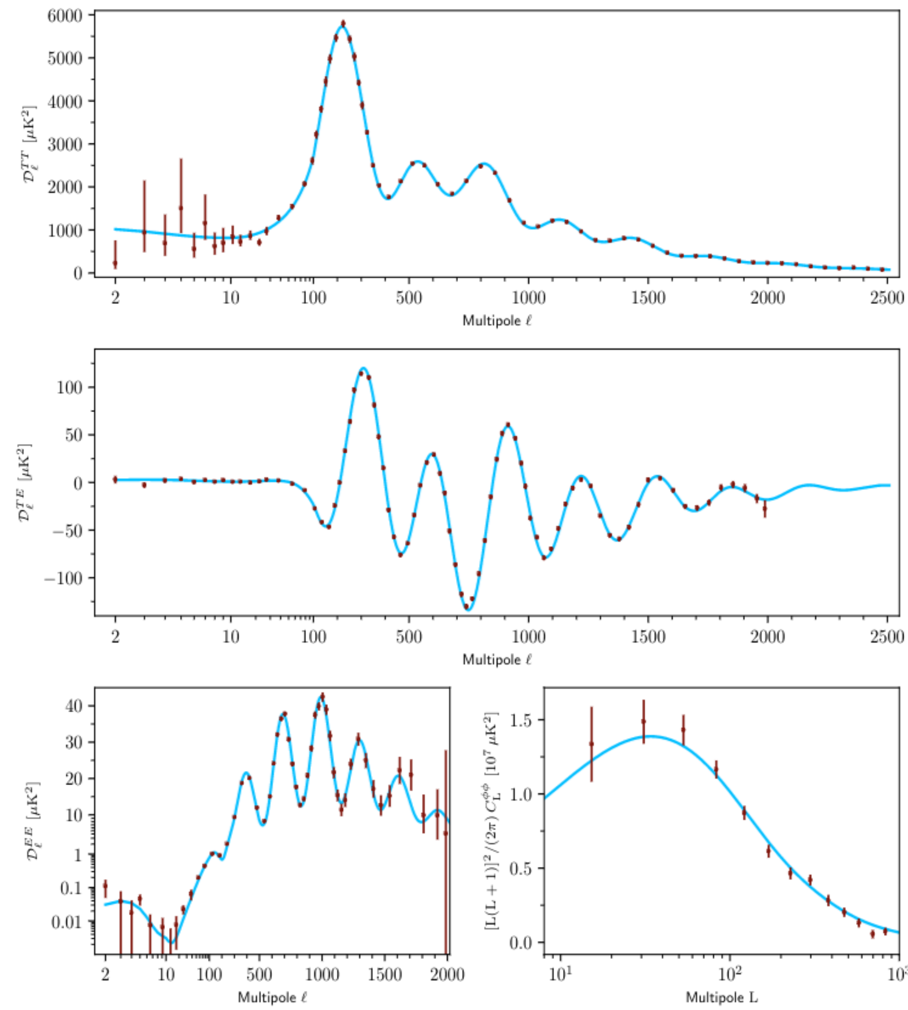

Figure 1.6: These are the foreground cleaned angular power spectra for temperature (top), the temperature-polarization cross-spectrum (middle), the E mode of polarization (bottom left), and the lensing potential (bottom right), measured from Planck. Credits: Planck Collaboration

verse. The B-mode power spectrum is related to the tensor-to-scalar ratio (r). This quantifies the amplitude of primordial gravitational waves relative to the density fluctuations (scalar perturbations) in the CMB data. Mathematically, the tensor-to-scalar ratio is commonly defined as

$$r \equiv \frac{P_{\mathrm{T}}\left(k_{0}\right)}{P_{\mathrm{S}}\left(k_{0}\right)}. \tag{1.15}$$

Compared to the measurement of CMB temperature, obtaining accurate measurements of CMB polarization poses more difficulties. The amplitude of CMB polarization anisotropy is approximately one-tenth of the amplitude observed in CMB temperature anisotropy.

1.0.4 Concordance model of cosmology

The acoustic peak structure observed in the CMB temperature angular power spectrum measured from high resolution CMB sky maps from Planck satellite gives us a wealth of information about the composition and history of the early universe. By studying accurate measurements of the first few peaks in the angular power spectrum, CMB data have provided us with significant advances to our understanding of cosmology. Using these peaks we can calculate the cosmological parameters such as the Hubble Constant (H_0) which represents the rate of expansion of the universe and the density parameters such as Ω_b which gives the density of baryonic matter Ω_c represents the density of cold dark matter and Ω_Λ refers to the density of dark energy or cosmological constant. The spectral index (n_s) defines the primordial power spectrum of density fluctuations and the optical depth (τ) measures the likelihood of scattering of CMB photons by free electrons. The amplitude of the primordial power spectrum (A_s) gives the overall level of fluctuations in the CMB. These different cosmological parameters which are derived from the CMB angular power spectrum analysis provide crucial insights into the evolution and properties of the universe.

Table 1.1: CMB Parameters and Best-Fit Values

CMB Parameter	**Best-Fit Value from Planck (2018)**
H_0 (km/s/Mpc)	67.37 ± 0.54
$\Omega_b h^2$	0.02233 ± 0.00015
$\Omega_c h^2$	0.1198 ± 0.0012100
n_s	0.965 ± 0.004
τ	0.054 ± 0.007
A_s	$2.101 \pm 0.033 \times 10^{-9}$

1.0.5 Two point angular correlation function

When studying the CMB sky, we analyze the measurements at pixels distributed on a 2D sphere from the sky. For such kind of data, the spherical harmonics basis is a natural basis for data analysis. Spherical harmonics provide a set of basis functions that can efficiently capture the CMB fluctuations information across the different angular scales. However, an alternative approach to study the CMB data is by using the two-point angular correlation function. Using this method, we directly measure the statistical correlation between the different pairs of pixels in the CMB map. It does not require the full sky measurement of the temperature fluctuation values, which is necessary, in principle, when using the spherical harmonics basis. This is because to take the spherical harmonic transformation, the complete basis is required in real space. Hence, two-point angular correlation function provides a powerful and robust tool for studying the CMB sky, most importantly in cases where partial sky is observed. It is based on the direct pixel based measurement of the CMB data and gives the spatial correlations present in the CMB fluctuations.

By calculating the angular correlation between pairs of pixels, we can study

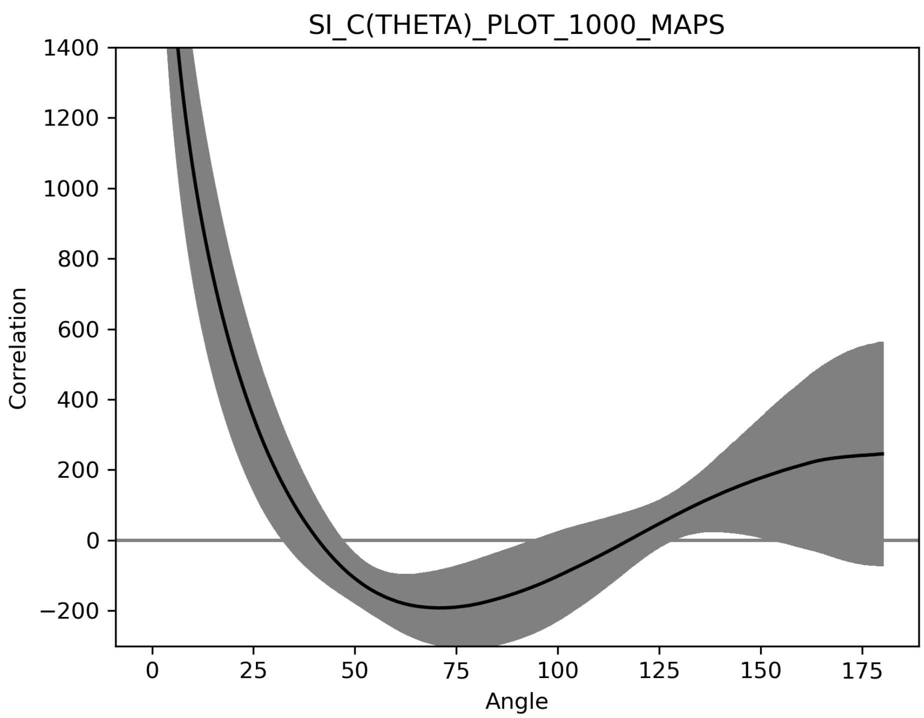

Figure 1.7: The angular correlation function of the two-point temperature correlations. The black line shows the mean value of $C(\theta)$, and the grey region shows the cosmic variance bars corresponding to the correlation function.

valuable information about the early universe using statistical properties of the CMB data. This includes the angular power spectrum and the distribution of temperature or polarization fluctuations across the sky. The two-point correlation function is calculated as the ensemble average of all pairs of pixels from the given data and provides correlation between the temperature or polarization values of different pairs of pixels in the CMB map. Upcoming ground-based surveys such as ACT and SPT, that focus on observing the specific patches of the sky at the very high resolution, the two-point correlation function may be an appropriate avenue for studying the information about the early universe. Hence, the two-point angular correlation function is a complementary approach to study the CMB data that provides the compact and robust results when working with partial sky regions.

1.0.6 Weak Lensing of CMB

The CMB photons travel through large-scale structures (LSS) before reaching us. The large scale structure have their roots in the scalar perturbations induced the Friedmann-Robertson-Walker (FRW) metric due to quantum fluctuations during the inflationary era. These matter distribution causes the CMB photons to deviate from their original geodesics. As a result of this deviation, the temperature anisotropies observed on the CMB sky are remapped by the deflection field. The new lensed temperature fluctuation field can be written as

$$\tilde{T}(\hat{\mathbf{n}}) = T(\hat{\mathbf{n}} + \vec{\Delta}). \tag{1.16}$$

Here, $\vec{\Delta}$ represents the deflection of the photon in its own direction. Under the Born approximation, using the photon geodesic equation, we can show that $\vec{\Delta}$ is related to the projected lensing potential ψ through the expression given as

$$\vec{\Delta}(\hat{\mathbf{n}}) = \vec{\nabla}\psi(\hat{\mathbf{n}}). \tag{1.17}$$

In a flat ΛCDM universe, the projected lensing potential ψ represents the gravitational lensing caused by large-scale structures. The total cumulative effect of net deflection due to weak lensing of CMB photons can be represented by the equation written as

$$\vec{d} = -2\int_0^{\chi_*} d\chi \frac{\chi_* - \chi}{\chi} \nabla_\perp \Phi(\chi\hat{n}), \tag{1.18}$$

Here, χ gives the comoving distance and χ_* is the comoving distance to the surface of the last scattering. $\nabla_\perp\Phi$ gives the transverse derivative of the gravitational potential. The lensing effect on CMB polarization signal can also induce a B-mode signal in the CMB map. Due to which it becomes important to precisely study the lensing effect and its impact on the CMB temperature and polarisation signal. The lensing power spectrum $C_L^{\phi\phi}$ can be constructed using the lensing potential. Aplot of the lensing potential is shown in the given figure 1.8 to understand the magnitude of this effect.

Studying the lensing effect on the CMB signal is also important because it provides valuable information about the distribution of matter in the LSS of the universe. By precisely studying the CMB lensing signal, we can study the matter distribution in the large scale structure and this can provide us with the new information about the dark matter distribution and matter content in the universe.

1.0.7 CMB Foregrounds

The CMB signal captured from the sky is contaminated by the presence of other astrophysical sources of photons within our galaxy. These sources include emission from interstellar thermal dust, synchrotron radiation, spinning dust emission and free free emission and some others contributions from the emission from galactic and extragalactic sources. To extract the true CMB signal from the observed map, it becomes important to account for and subtract the noise due to these contaminating sources. This process is known as foreground subtraction or foreground cleaning. Planck measured the CMB signal across nine different frequency channels, each frequency channel has different dominations from the foreground contributions. In the temperature dataset, the lower frequency ranges are primarily contaminated by the synchrotron radiation, free-free emission, and spinning dust emissions, while for high frequency measurements, the CMB map is mostly noise contaminated by the emission due to thermal dust.

In case of polarization, only synchrotron radiation and thermal dust emissions have a polarized component. Their signals dominate over the CMB signal across the entire frequency range. These foreground contributions can be separated by using knowledge of their respective spectral properties and distributions at different frequency channels. This process of removing the foregrounds is known as component separation.

By accurately studying and modeling the spectral properties of different foreground emissions and the also taking into account their frequency dependent behaviors, we can separatee the foreground components from the true CMB signal. This component separation technique allows us to get the true CMB signal from the observed sky map, which is important for precisely studying cosmological parameters and the study of the early universe phenomena.

1.1 Summary

With the discovery and confirmation of the cosmic microwave background signal, it became possible to study the universe in great detail. The figure 1.8 shown in

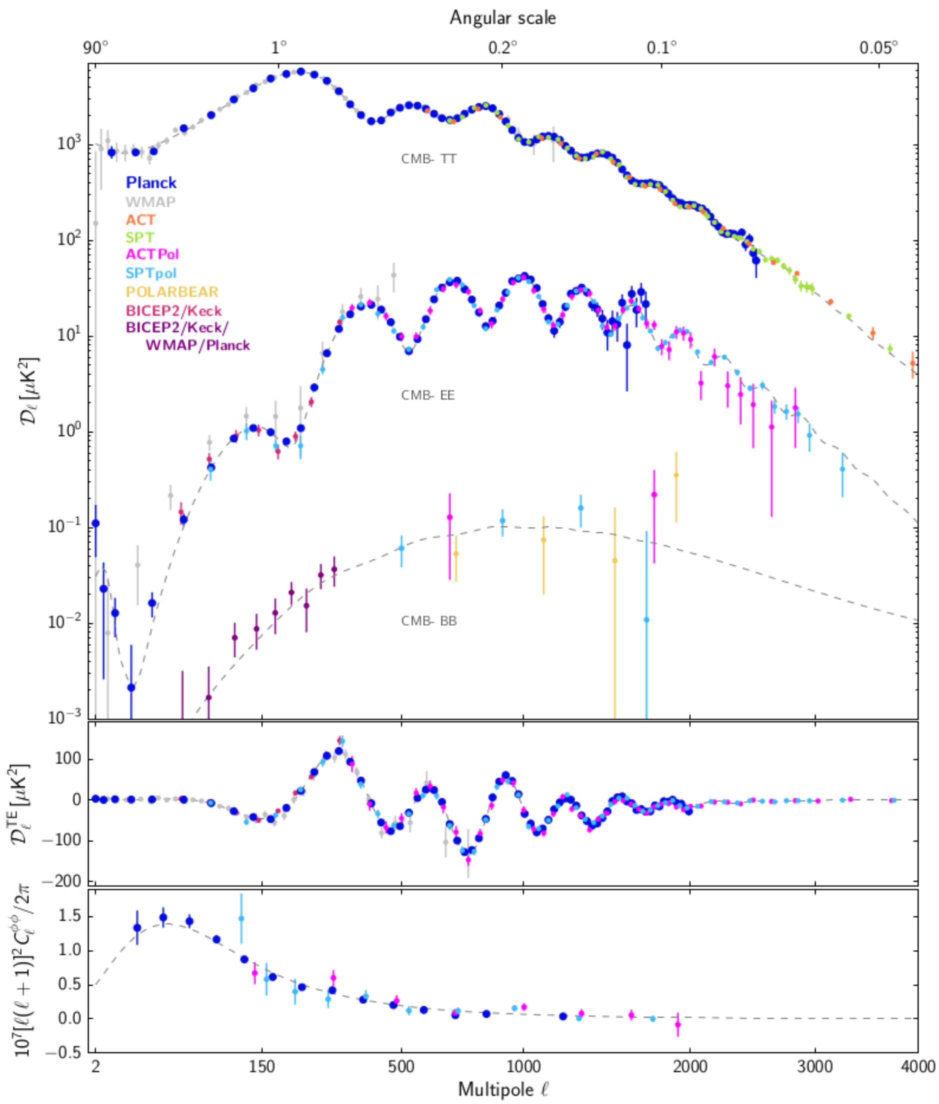

Figure 1.8: Angular power spectra of various CMB fields probed by various CMB experiments are listed in the top panel. CMB-TT, CMB-EE, and CMB-BB represent the temperature anisotropy angular power spectra, the angular power spectrum of the E-mode of CMB polarization, and the angular power spectrum of the B-mode of CMB polarization, respectively. The B-mode power shown here is mainly contributed by the gravitational lensing of CMB photons due to large-scale structure. The middle panel displays D_ℓ^{TE}, the correlation between CMB temperature anisotropy and the E-mode of CMB polarization. The bottom panel illustrates the angular power spectrum of the lensing potential, C_ℓ^{ϕ}. Credits: Planck Collaboration.

this context represents different quantities, such as the temperature power spectrum C_L^{TT}, the E-mode and B-mode polarization power spectrum C_L^{EE}, C_L^{BB}, and the lensing potential power spectrum $C_L^{\phi\phi}$, which have been measured by various CMB missions. These measurements demonstrate a strong agreement between theoretical predictions and the high-resolution CMB data.

The availability of high-resolution CMB maps has transformed our ability to investigate the origin and dynamics of the universe and its components. By analyzing these sky maps, we can explore deviations in the large-scale structure of the universe, challenging the foundational principles of cosmology that are based on the assumptions of homogeneity and isotropy. This provides a unique opportunity to validate fundamental cosmological theories by comparing observed data with theoretical predictions.

The exquisitely measured maps of temperature fluctuations in the CMB signal offer the potential source to test the principle of statistical isotropy (SI) of the universe. This thesis focuses on studying deviations in CMB data from statistical isotropy and exploring various other large-scale effects. In this thesis , we define a new mathematical approach to study these deviations corresponding to a known physical phenomena. Through systematic observations, we can identify non-statistical isotropy (nSI) features in the data and trace them back to known physical effects or observational artifacts using a strong mathematical framework. By understanding and quantifying these deviations, we can obtain important insights into the underlying processes and phenomena that have influenced the universe on largest scales.

The goal of this research is to contribute to the field of cosmology by providing a rigorous mathematical analysis of CMB data distributed on the spherical surface beyond the limitations of the assumptions of Statistical isotropy. The study aims to investigate the implications of deviations from statistical isotropy and their connections to other known large-scale effects. Through these efforts, we hope to deepen our understanding of the universe and make valuable contributions to refining and validating cosmological theories.

Part II

Statistical Isotropy of CMB

CHAPTER 2

STATISTICAL ISOTROPY OF THE CMB

> *"Just the variety of theories we've discovered so far, and their incompleteness, leads me to wonder if there is such a thing as a complete theory. Or is there just a succession of approximations all the way down?"*
> -— "James Peebles"

The ΛCDM model of cosmology is built on the assumptions of isotropy and homogeneity of the universe. These basic fundamental assumptions imply that the universe is expected to have the same statistical properties in all directions in the sky, i.e., isotropy and is expected to have the same statistical properties independent of the position from which it is observed, called as homogeneity. These assumptions employed to construct a simplified cosmological model and have to be observationally validated as they form the foundation of the current model of cosmology.

Investigating the homogeneity of the Universe directly presents significant challenges, but we can better understand its isotropy by studying the Cosmic Microwave Background (CMB), which appears to be highly isotropic. To assess statistical homogeneity of a random field $\Phi(\mathbf{x})$, we observe that all its moments are unaffected by arbitrary translations with respect to vector $\mathbf{a}$. The average value $\langle\Phi(\mathbf{x})\rangle$ remains constant and can be set to zero. The two-point correlation function, denoted as $C(\mathbf{x_1}, \mathbf{x_2})$, captures the relationship between $\Phi(\mathbf{x_1})$ and $\Phi(\mathbf{x_2})$. Notably, this function in case of homogeneous field depends solely on the difference vector $\mathbf{x_1} - \mathbf{x_2}$, indicating translational invariance when we replace $\mathbf{a}$ with $-\mathbf{x_2}$. Generalizing to n-point correlation functions, statistical homogeneity leads us to the conclusion that their expectation values remain invariant under translations $\mathbf{a}$.

Moreover, statistical isotropy (SI) asserts that the n-point correlation functions are rotationally invariant under any arbitrary rotation $\mathbf{R}$. Consequently under the condition of statistical isotropy, the n-point correlation function $\langle\Phi(\mathbf{x_1})\Phi(\mathbf{x_2})...\Phi(\mathbf{x_n})\rangle$ equals $\langle\Phi(\mathbf{Rx_1})\Phi(\mathbf{Rx_2})...\Phi(\mathbf{Rx_n})\rangle$. This isotropy leads to the simplified expression $C(\mathbf{x_1},\mathbf{x_2}) = \langle\Phi(\mathbf{x_1})\Phi(\mathbf{x_2})\rangle = C(|\mathbf{x_1}-\mathbf{x_2}|)$ for the two-point correlation function.

In mathematical terms, the two-point correlation function is dependent upon the dot product of the directions $\hat{n}_1$ and $\hat{n}_2$ rather than individual direction dependency

$$C(\hat{n}_1,\hat{n}_2) \equiv C(\hat{n}_1\cdot\hat{n}_2).$$

Thus, this correlation function, which depends on the angle θ between the directions, is known as a statistical isotropic correlation function. It is essential to distinguish between statistical isotropy and Gaussianity, which are distinct concepts. While statistical isotropy guarantees that the expectation values of n-point correlation functions are rotationally invariant, Gaussianity relates to the statistical distribution underlying the measurable quantity. In a Gaussian distribution, odd higher-point correlation functions are zero, and the even-point correlation functions can be expressed in terms of the two-point function using the Wick's theorem. As a result of underlying Gaussianity, all statistical information of the field is encapsulated in the two-point correlation function.

For isotropic Gaussian models, the two-point correlation function and power spectrum capture all essential information about the field, making it relatively straightforward to describe. However, in non-statistical isotropic cases, even if the field is Gaussian, the isotropic two-point correlation function(diagonal elements) alone is insufficient; additional information from the full covariance matrix, including off-diagonal elements, is needed to fully describe the field. For non-

Gaussian fields, higher-order moments must be considered to capture the complete statistical properties of the field.

However, for our current study to capture the non-statistical isotropy of the universe, we will focus on Gaussian fields well supported by the current observations, where the two-point correlation is sufficient to study the field's characteristics.

Hence, to conclude, an examination of the complete covariance matrix is essential for investigating isotropy under the Gaussian field. In instances of statistical isotropy, the non-diagonal entries of the matrix are zero, and any departure from statistical isotropy is reflected in the non-diagonal elements of the matrix. To comprehensively understand these deviations and study the structural intricacies of the early universe, the utilization of appropriate mathematical constructs becomes important.

2.1 Bipolar Spherical Harmonics

The correlation function for the cosmic microwave background (CMB), as discussed in the preceding chapter, is defined as $C(\hat{n}, \hat{n}') \equiv \langle \Delta T(\hat{n}) \Delta T(\hat{n}') \rangle$. Utilizing the spherical harmonic transformation, it can be expressed in the following form

$$C(\hat{n}_1, \hat{n}_2) = \sum_{l_1 m_1} \sum_{l_2 m_2} \langle a_{l_1 m_1} a_{l_2 m_2} \rangle Y_{l_1 m_1}(\hat{n}_1) Y_{l_2 m_2}(\hat{n}_2).$$

To capture the non-diagonal elements of the covariance matrix and systematically explore statistical isotropy (SI) violations in cosmic microwave background (CMB) sky maps, Hajian and Souradeep (3; 4) introduced a novel generalized basis called Bipolar Spherical Harmonic basis. This new mathematical approach enhances the efficacy of studying SI violation signatures in CMB datasets. The Bipolar Spherical Harmonic (BipoSH) functions form a comprehensive and orthonormal basis in the $S^2 \times S^2$ space, exhibiting crucial bi-directional dependencies. They are wellsuited for exploring the most general form of the Cosmic Microwave Background (CMB) two-point correlation function, which depends on two directions $\hat{n}_1$ and $\hat{n}_2$. This exploration is particularly relevant in cases where statistical isotropy is not observed under the assumption of Gaussianity. The most general two-point correlation function for a gaussian random field defined on a 2D sphere can be expressed in the BipoSH basis as

$$C(\hat{n}_1, \hat{n}_2) = \sum_{LM} \sum_{l_1 l_2} A^{LM}_{l_1 l_2} \{Y_{l_1}(\hat{n}_1) \otimes Y_{l_2}(\hat{n}_2)\}_{LM}.$$

The coefficients $A^{LM}_{l_1 l_2}$ are known as BipoSH coefficients, and the tensor product of the two spherical harmonics defined as $\{Y_{l_1}(\hat{n}_1) \otimes Y_{l_2}(\hat{n}_2)\}_{LM}$ is referred to as BipoSH functions. These BipoSH functions are connected to the spherical harmonic functions through the expression

$$Y^{l_1, l_2}_{LM}(\hat{n}_1, \hat{n}_2) \equiv \{Y_{l_1}(\hat{n}_1) \otimes Y_{l_2}(\hat{n}_2)\}_{LM} = \sum_{m_1, m_2} C^{LM}_{l_1 m_1 l_2 m_2} Y_{l_1 m_1}(\hat{n}_1) Y_{l_2 m_2}(\hat{n}_2), \tag{2.1}$$

where $C^{LM}_{l_1 m_1 l_2 m_2}$ denotes the Clebsch-Gordon coefficients. These coefficients adhere to the constraints $|l_1 - l_2| \leq L \leq l_1 + l_2$ and $m_1 + m_2 = M$. Consequently, the indices on the BipoSH coefficients also satisfy these constraints.

The BipoSH coefficients can be determined using the inverse transform of the two-point correlation function, $C(\hat{n}_1, \hat{n}_2)$ by performing the inverse transformation and multiplying both sides of equation by $\{Y_{l'_1}(\hat{n}_1) \otimes Y_{l'_2}(\hat{n}_2)\}^*_{L'M'}$, the resulting expression, denoted as $A^{LM}_{l_1 l_2}$, is obtained. This involves integrating over all angles and using the orthogonality property of BipoSH functions. The BipoSH coefficients can be written as

$$
\begin{aligned}
A_{l_1 l_2}^{LM} &= \int d\Omega_{\hat{n}_1} \int d\Omega_{\hat{n}_2} C(\hat{n}_1, \hat{n}_2) Y_{l_1}(\hat{n}_1) \otimes Y_{l_2}(\hat{n}_2)^{*}_{LM} \\
&= \int d\Omega_{\hat{n}_1} \int d\Omega_{\hat{n}_2} C(\hat{n}_1, \hat{n}_2) Y_{LM}^{l_1, l_2}(\hat{n}_1, \hat{n}_2). \qquad (2.2)
\end{aligned}
$$

It is important to note here that the upper indices "L" provide us with the order of SI violation, hence depicting the harmonic decomposition of the non-SI correlations expansions in the CMB sky. Lower indices provide us with the scale of the map, showing the harmonic decomposition of the map.

Using the definition of BipoSH from eq. (2.1), the BipoSH coefficients can be written in terms of spherical harmonics covariance matrix can be expressed as

$$
A_{l_1 l_2}^{LM} = \sum_{m_1 m_2} \langle a_{l_1 m_1} a^{*}_{l_2 m_2} \rangle (-1)^{m_2} C_{l_1 l_2 m_1 - m_2}^{LM}.
$$

It is evident from the above expression that BipoSH coefficients captures the general structure of the covariance matrix, providing a natural framework for studying non-statistical isotropy violations encoded in the non-diagonal entries of the covariance matrix.

2.2 Properties of BipoSH coefficients

2.2.1 BipoSH coefficients for SI sky

Given the condition of statistical isotropy (SI) for the Cosmic Microwave Background (CMB) sky, the covariance matrix becomes diagonal. This results in non-vanishing Bipolar Spherical Harmonic (BipoSH) coefficients only for $L = 0$.

When substituting the diagonal covariance matrix of a SI CMB sky, denoted as C_l in equation , into the expression for $A_{ll'}^{LM}$ as in equation , we obtain

$$A_{ll'}^{LM} = \sum_{mm'} C_l \delta_{ll'} \delta_{m-m'} (-1)^{m'} C_{lml'm'}^{LM}$$
$$= C_l \delta_{l'} \delta_{M0} \sum_m (-1)^m C_{lml-m}^{LM}.$$

Utilizing the summation rules of Clebsch-Gordan equations, as expressed in equation , the above expression simplifies to

$$A_{ll'}^{LM} = (-1)^l C_l (2l+1)^{1/2} \delta_{ll'} \delta_{L0} \delta_{M0}.$$

This equation characterizes the statistical isotropy condition in bipolar harmonic space. Notably, this condition arises as a result of the sum over m. Consequently, A_{00}^{00} contains all the information about the correlation function and is related to the power spectrum C_l. The well recognised power spectrum C_l of CMB sky is thus recognized as a subspace of the BipoSH space.

2.2.2 Parity under BipoSH coefficients

The Bipolar Spherical Harmonic (BipoSH) coefficients can be expressed in terms of even and odd parity components, in accordance with the spherical harmonics. The decomposition is given by the equation

$$A_{ll'}^{LM} = A_{ll'}^{\oplus} \frac{\left[1 + (-1)^{l+l'+L}\right]}{2} + A_{ll'}^{\ominus} \frac{\left[1 - (-1)^{l+l'+L}\right]}{2}. \tag{2.3}$$

Here, $A_{ll'}^{\oplus}$ represents the even parity component, and $A_{ll'}^{\ominus}$ represents the odd parity component. For even parity BipoSH coefficients (where $l_1 + l_2 - L$ is even), they transform similarly to standard Spherical Harmonics

$$A_{l_1 l_2}^{LM} = (-1)^M A_{l_1 l_2}^{LM}.$$

On the other hand, odd parity BipoSH coefficients (where $l_1 + l_2 - L$ is odd) transform as

$$A^{LM}_{l_1 l_2} = (-1)^{M+1} A^{LM}_{l_1 l_2}.$$

Typically, most physical effects result in even-parity BipoSH coefficients. However, certain cosmological effects and systematics can lead to parity-violating effects, which are interesting to study using BipoSH coefficients. Examples of such effects include weak lensing due to tensor (odd parity) perturbations, chiral GW background etc. When there's parity-violating physics, like a chiral GW background, we anticipate a non zero correlation between odd and even parity Bipolar Spherical Harmonics. Hence, BipoSH coefficients provide a powerful tool to explore various cosmological phenomena, including those that involve parity-violating effects.

2.2.3 Symmetries under BipoSH coefficients

The correlation function's reality, denoted as $C(\hat{n}_1, \hat{n}_2) = C^*(\hat{n}_1, \hat{n}_2)$, implies a specific relationship in the Bipolar Spherical Harmonic (BipoSH) coefficients. This reality condition leads to the following symmetry between M and $-M$ modes, as

$$A^{LM}_{l_1 l_2} = (-1)^{l_1+l_2-L+M} A^{*L-M}_{l_1 l_2}.$$

Additionally, BipoSH coefficients with $M = 0$ and $l_1 + l_2 - L$ even are purely real, while those with $M = 0$ and $l_1 + l_2 - L$ odd are purely imaginary. Furthermore, the symmetric nature of the correlation function, $C(\hat{n}_1, \hat{n}_2) = C(\hat{n}_2, \hat{n}_1)$, results in the following relation for BipoSH coefficients

$$A^{LM}_{l_1 l_2} = (-1)^{l_1+l_2-L} A^{LM}_{l_2 l_1}.$$

If the given correlation function remains invariant under reflection about the xy-plane, where $\{\theta, \phi\}$ transforms as $\{\theta \to \pi - \theta, \phi \to \phi\}$, the associated Spherical

Harmonic (SH) functions undergo the transformation $\hat{P}_{\rm r} Y_{lm}(\theta,\phi) = (-1)^{l+m} Y_{lm}(\theta,\phi)$. Consequently, BipoSH functions under this reflection symmetry transform as $\hat{P}_{\rm r}\{Y_{l_1}(\hat{n}_1) \otimes Y_{l_2}(\hat{n}_2)\}_{LM} = (-1)^{l_1+l_2+M}\{Y_{l_1}(\hat{n}_1) \otimes Y_{l_2}(\hat{n}_2)\}_{LM}$, leading to the relationship among BipoSH coefficients

$$A^{LM}_{l_1 l_2} = (-1)^{l_1+l_2+M} A^{LM}_{l_1 l_2}.$$

This symmetry implies that $l_1 + l_2 + M$ is always even. Similarly, if the correlation function remains invariant under inversion of the coordinate system, denoted as $\hat{P}_i C(\hat{n}_1, \hat{n}_2) = C(\hat{n}_1, \hat{n}_2)$, where $\{\theta, \phi\}$ transforms as $\{\theta \to \pi - \theta, \phi \to \pi + \phi\}$, the transformation of SH functions becomes $\hat{P}_i Y_{lm}(\theta,\phi) = (-1)^l Y_{lm}(\theta,\phi)$. Under such a point parity transformation, BipoSH coefficients are related as

$$A^{LM}_{l_1 l_2} = (-1)^{l_1+l_2} A^{LM}_{l_1 l_2}.$$

Hence, BipoSH coefficients efficiently capture the symmetries inherent in the correlation function, offering a powerful tool for probing and exploring the symmetries embedded in the universe through the analysis of the two-point correlation function of the Cosmic Microwave Background.

2.3 Sources of SI violation

A foreground-cleaned map derived from the Planck satellite observations gives temperature fluctuations of the CMB relative to the mean temperature. The observed fluctuations across different pixels in the HEALPix-resolved map can have various sources of non trivial effects, including beam convolution, noise, residual foregrounds, and other theoretical factors. These diverse contributors may introduce features that potentially violate statistical isotropy in the CMB map.

The observed CMB map from Planck/WMAP satellite is a realization of a Gaussian field with covariance structure $C = C_T + C_N + C_{\rm res}$, where C_T denotes the theoretical covariance of Cosmic Microwave Background (CMB) temperature fluctuations, C_N represents the noise covariance matrix, and $C_{\rm res}$ accounts for the covariance of residuals from foregrounds. The potential breakdown of statistical isotropy can manifest in any of these components. Broadly, these effects fall into two categories. Theoretical effects, motivated by early universe CMB theory and intrinsic to the actual Cosmic Microwave Background (CMB) sky, are denoted as ΔT. Three examples of such effects are discussed, including weak lensing of the CMB photons, Doppler boost due to relative motion of the observer with respect to the rest frame of CMB and cosmic hemispherical asymmetry (CHA). On the other hand, certain observational artifacts or systematics in an optimally cleaned CMB map manifest themselves as violations of statistical isotropy. Examples of these effects include non-circular beam, incomplete sky coverage (masking), and anisotropic noise. These effects have been thoroughly studied and quantified through the utilization of the BipoSH basis.

2.4 Discussion

The isotropic characteristics of the CMB sky have been under scrutiny since the release of the CMB full sky missions such as COBE/WMAP/Planck. There are strong motivations to study the isotropic nature of the universe. BipoSH coefficients represent a natural extension of the CMB angular power spectrum, offering a wealth of information about the early universe. The measurement of non-vanishing BipoSH coefficients serves as a crucial indicator, revealing a potential violation of one of the fundamental assumptions underlying the construction of cosmological principle—namely, isotropy. Statistical isotropy, a parameter defined for probing the isotropic nature of the universe using correlations in the CMB data, becomes a key aspect in this context. Notably, all the estimators discussed in this chapter possess the advantage of being inherently model-independent. Violations of statistical isotropy can occur either due to theoretical anomalies or instrumental artifacts. The BipoSH basis has proven to be a successful tool in the literature for investigating such effects. Its successful application extends to the study of cross-correlations in the temperature (T), E-mode polarization (E), and B-mode polarization (B) data of the CMB.

CHAPTER 3

'MINIMAL' BIPOLAR SPHERICAL HARMONICS

The BipoSH formalism is derived from the tensor product of two spherical harmonics bases, which are in turn decomposed from a pixel-based Gaussian field. This formalism is a most general framework for analyzing data distributed on a two-dimensional sphere. By utilizing the natural generalization of the two-point correlation function, BipoSH effectively captures essential information regarding such data. The BipoSH formalism reveals signatures of statistical isotropy violations in terms of the harmonic scale of the sky, denoted by l. In this chapter, we introduce a potential extension of the BipoSH basis to capture the SI violation features using a set of isotropic, real space, angular correlation function of angular separation θ. To establish the mathematical formalism for performing the real space transformation of the Bipolar functions, capturing the nSI features, we utilize the special reduction formulae studied by Manakov et al (5).

The motivation behind exploring real-space-based methods comes from various considerations. First, in the Cosmic Microwave Background (CMB) anisotropy bipolar harmonics expansion with relatively small rank L often contribute significantly to most of the known sources of non-statistical isotropy features such as Doppler boost, CHA etc. By going to the real-space domain, we can effectively reduce the number of functions required to study these nSI effects.

Another crucial reason is based on the fact that, as we measure temperature information in pixels on sphere from the CMB sky, understanding real-space correlations in a non-statistically isotropic sky becomes crucial. This becomes especially important with upcoming missions dedicated to studying the CMB, which are often heavily masked and/or limited in sky coverage. Developing a real space based estimator is therefore timely for complete and comprehensive study of CMB non-statistical isotropic effects.

Moreover, the new method may reveal certain unknown signatures that could prove crucial in understanding early universe phenomena. These insights may potentially provide valuable information about the intricacies and physics of the early universe.

3.1 Reduction of Bipolar Harmonics

Bipolar spherical harmonics as defined in the previous chapter, represent tensors of rank L. Following general mathematical principles, a tensor with a rank of L should be constructed using L vectors, each formed from its arguments.

Utilizing this approach, we perform the reduction of the Bipolar Spherical Harmonic (BipoSH) basis. This reduction process of BipoSH functions yields L functions, which, when expressed in theta space, manifest as measurable quantities known as two point correlation functions in the $2D$ spherical sky.

To derive this method, we begin with the expansion of bipolar harmonics basis functions using arbitrary l_1 and l_2, creating a superposition of a small number of harmonics defined by the equation

$$\mathcal{Y}^{k}_{LM}(\hat{n}_1, \hat{n}_2) = Y^{L-k,k}_{LM}(\hat{n}_1, \hat{n}_2), \text{ where } k = 0, 1, ..., L. \tag{3.1}$$

This equation represents the reduced bipolar harmonic functions based on the idea that L vectors are sufficient to explain the Bipolar basis (5). The right-hand side of the equation represents the BipoSH basis. Here, we define the reduced bipolar basis functions, where the internal ranks l_1 and l_2 depend on the superscript k and the harmonic rank L. Different k values represent different basis vectors in this reduced basis.

These new set of harmonics share the same rank L but have the smallest possible ranks for their internal tensors, and the sum of these internal tensors equal L. The basis composed of set of harmonics given by $\mathcal{Y}^{k}_{LM}$ represent the simplest possible bipolar harmonics of rank L and can be readily analyzed to study the nSI effects in the CMB data. From this, we can infer that, in general, the entire set of BipoSH can be reduced to these $L+1$ functions in this new basis such that internal ranks of this are limited to L. All other combinations of internal ranks beyond the value of L can be formed using combining these defined L vectors, constructed in the appropriate manner.

In order to establish the relationship between any general bipolar harmonic basis element in terms of our reduced 'minimal' harmonics basis, we use the concept of vector differentiation (6). Given that we are dealing with spherical harmonics we use the familiar orbital angular momentum operators to enact the differential operation.

In the study of the simplest case for multipole with angular momentum quantum number $L = 1$, considering both internal ranks l and l' being equal, the 'minimal' harmonic possible should be given by the tensor of rank 1. According to parity rules, $L + l + l'$ is odd, indicating an axial vector (odd parity) formed from the two respective directions on which the bipolar harmonics are constructed. It can be demonstrated that, as a result, the expression $Y^{ll'}_{1M}(n_1, n_2)$ is proportional to $i(\hat{n}_1 \times \hat{n}_2)$. This is due to the fact that the vector resulting from the cross product $(\hat{n}_1 \times \hat{n}_2)$ is the only axial vector that can be formed exclusively from the vectors n_1 and n_2. Hence this represents the 'minimal' basis to study the bipolar harmonic basis.

Generalizing this idea involves employing the rules of vector differentiation for the Legendre polynomial. For example, we can express the Legendre polynomial in the form of bipolar spherical harmonics as follows

$$P_l\left(\hat{n}_1 \cdot \hat{n}_2\right) = \frac{4\pi}{2l+1} \sum_m Y_{lm}(\hat{n}_1) Y^*_{lm}(\hat{n}_2) = (-1)^l 4\pi Y^{ll}_{00}(\hat{n}_1, \hat{n}_2). \tag{3.2}$$

This follows from the definition of bipolar harmonics and its formula for tensor product expansion, as discussed in the preceding chapter. For the discussed case of bipolar harmonic $Y^{ll'}_{1M}(n_1, n_2)$, calculating its explicit form can be accomplished by operating the del operator as

$$\nabla P_l\left(\hat{n} \cdot \hat{n}'\right) = \frac{\mathrm{d}P_l(\cos\theta)}{\mathrm{d}\cos\theta} \nabla \frac{\boldsymbol{r} \cdot \boldsymbol{r}'}{rr'} = \frac{1}{r} P^{(1)}_l(\cos\theta)\left(\hat{n}' - \left(\hat{n} \cdot \hat{n}'\right)\hat{n}\right). \tag{3.3}$$

where, $P^{(k)}_l(x) = (\mathrm{d}/\mathrm{d}x)^k P_l(x)$, the k th derivative of P_l and $\hat{n} = \boldsymbol{r}/r, \hat{n}' = \boldsymbol{r}'/r'$. When we apply the orbital angular momentum operator given by $\hat{l} = -\mathrm{i}[\vec{\mathbf{r}} \times \vec{\nabla}]$ to the Legendre polynomials, it gives the following relation

$$\hat{\boldsymbol{l}} P_l\left(\hat{n}_1 . \hat{n}_2\right) = -\mathrm{i}\left[\hat{n}_1 \times \hat{n}_2\right] P^{(1)}_l\left(\hat{n}_1 . \hat{n}_2\right). \tag{3.4}$$

This relation is achieved using the previous result of the operation of the del operator acting on the Legendre polynomials. On the other hand, the action of the angular momentum operator acts as either a raising or lowering operator on the spherical harmonics, given by the Spherical components of the operator $\hat{\mathbf{L}}$, which act on $Y_{lm}(\vartheta, \varphi)$ according to relations given as

$$\widehat{L}_{\pm 1} Y_{lm}(\vartheta, \varphi) = \mp \sqrt{\frac{l(l+1) - m(m \pm 1)}{2}} Y_{lm \pm 1}(\vartheta, \varphi), \tag{3.5}$$

$$\widehat{L}_0 Y_{lm}(\vartheta, \varphi) = m Y_{lm}(\vartheta, \varphi). \tag{3.6}$$

The following relation can be written in a more compact form as

$$\widehat{L}_\mu Y_{lm}(\vartheta, \varphi) = \sqrt{l(l+1)} C^{lm+\mu}_{lm1\mu} Y_{lm+\mu}(\vartheta, \varphi). \tag{3.7}$$

Using this relation on the right side of equation (3.2), we get the result as

$$\hat{\boldsymbol{l}} P_l\left(\hat{n}_1 \cdot \hat{n}_2\right) = 4\pi(-1)^l \sqrt{\frac{l(l+1)}{3(2l+1)}} Y_{10}^{ll}\left(\hat{n}_1, \hat{n}_2\right). \tag{3.8}$$

Comparing both results from equations (3.4) and (3.8), we obtain the final result for the bipolar spherical harmonics as

$$Y_{10}^{ll}\left(\hat{n}_1, \hat{n}_2\right) = -\mathrm{i}\left[\hat{n}_1 \times \hat{n}_2\right] P_l^{(1)}\left(\hat{n}_1 \cdot \hat{n}_2\right)(-1)^l \frac{\sqrt{3(2l+1)}}{4\pi\sqrt{l(l+1)}}. \tag{3.9}$$

From here, we can naively see that the ∇ operator works as a raising and a lowering operator for bipolar harmonics. Using this method, we can construct the explicit 'minimal' form of the bipolar harmonics. This is a very basic example, and we can generalize this method using the angular momentum operator as raising and lowering operators for higher multipole bipolar harmonics. Generally, the method for calculating the higher-order multipole is more complicated. We need to construct the lowering and raising operators valid for the tensor product of the spherical harmonics. We can then use this to create a complete basis for our new reduced 'minimal' basis functions.

To construct the appropriate formalism, using the spherical harmonics representation in the form

$$Y_{lm}(\boldsymbol{r}/r) = \sqrt{\frac{(2l+1)!!}{4\pi l!}} \frac{1}{r^l} \{\boldsymbol{r}\}_{lm},$$

where $\{\boldsymbol{r}\}_{lm}$ is a symmetric tensor of rank l, with its corresponding projection labeled by m. This tensor represents the components of the position vector $\boldsymbol{r}$ in a spherical basis, providing a convenient representation for the expansion of functions in terms of spherical harmonics.

Using the relation $\{\nabla \otimes \boldsymbol{r}\}_{a\alpha} = -\sqrt{3}\delta_{a0}\delta_{\alpha 0}$, we can derive the tensor product of the gradient operator ∇ with the spherical harmonic function $Y_{lm}(\boldsymbol{r}/r)$. This product simplifies the expression and allows for a more efficient computation of differential operators in spherical coordinates.

$$\left\{\nabla \otimes r^l Y_l(\boldsymbol{r}/r)\right\}_{kq} = -\delta_{k,l-1}(2l+1)\sqrt{\frac{l}{2l-1}} r^{l-1} Y_{l-1,q}(\boldsymbol{r}/r).$$

The angular momentum operator for rank L is denoted as $\{\hat{\boldsymbol{l}}\}_{LM}$. Using the notation of angular momentum operators and introducing the subsequent index ∇ operator from the angular momentum operator, the raising operator for spherical harmonics follows as

$$\left\{\{\nabla\}_k \otimes r^l Y_{lm}(\boldsymbol{r}/r)\right\}_L = \delta_{L,l-k}(-1)^k \frac{2l+1}{2l-2k+1}\left[\frac{(2l)!}{2^k(2l-2k)!}\right]^{\frac{1}{2}} r^{l-k} Y_{l-k,m}(\boldsymbol{r}/r). \tag{3.10}$$

The utilization of $\hat{\boldsymbol{n}} = \frac{\boldsymbol{r}}{r}$ and $\hat{\boldsymbol{n}'} = \frac{\boldsymbol{r}'}{r'}$ is to optimize the ∇ operator, which operates on derivatives with respect to radial variables. So, the corresponding rank decreasing operator is

$$\hat{\mathcal{O}}^{l-}_{kq}(r,\nabla) = (-1)^k \frac{2l-2k+1}{2l+1}\sqrt{\frac{2^k(2l-2k)!}{(2l)!}} \frac{1}{r^{l-k}} \{\nabla\}_{kq} r^l.$$

Similarly, the rank increasing operator for the spherical harmonics is

$$\hat{\mathcal{O}}^{l+}_{kq}(r,\nabla) = (-1)^k \sqrt{\frac{2^k(2l+2k+1)(2l)!}{(2l+1)(2l+2k)!}} r^{l+k+1} \{\nabla\}_{kq} \frac{1}{r^{l+1}}.$$

This was derived using the identity given as

$$\left\{\nabla \otimes \frac{1}{r^{l+1}} Y_l(\boldsymbol{r}/r)\right\}_{kq} = -\delta_{k,l+1}(2l+1)\sqrt{\frac{l+1}{2l+3}} \frac{1}{r^{l+2}} Y_{l+1,q}(\boldsymbol{r}/r),$$

Together, these raising and lowering operators can be simply written as

$$\left\{\hat{\mathcal{O}}_k^{l\pm} \otimes Y_l(\boldsymbol{r}/r)\right\}_{jm} = \delta_{j,l\pm k} Y_{l\pm k,m}(\boldsymbol{r}/r).$$

This expression helps to construct the relationship involving bipolar harmonics

$$\begin{aligned}&\left\{\left\{\hat{\mathcal{O}}_p^{l-}(r_1,\nabla_1)\ \otimes\hat{\mathcal{O}}_q^{l+}(r_2,\nabla_2)\right\} \otimes \{Y_l(\boldsymbol{r_1}/r_1) \otimes Y_l(\boldsymbol{r_2}/r_2)\}\right\}_{LM} \\ &\qquad = \Pi_{L,l-p,l-q} \left\{\begin{matrix} q & p & L \\ l & l & 0 \\ l-q & l-p & L \end{matrix}\right\} Y_{LM}^{l-k,l+q}(\boldsymbol{r_1}/r_1, \boldsymbol{r_2}/r_2).\end{aligned} \tag{3.11}$$

In this equation, the operator $\hat{\mathcal{O}}_p^{l-}(r_1,\nabla_1)$ acts as a *rank-lowering* operator on the spherical harmonic $Y_l(\boldsymbol{r_1}/r_1)$, while $\hat{\mathcal{O}}_q^{l+}(r_2,\nabla_2)$ is a *rank-increasing* operator for the corresponding harmonic $Y_l(\boldsymbol{r_2}/r_2)$. These operators modify the rank of the harmonics, combining to form bipolar spherical harmonics $Y_{LM}^{l-k,l+q}(\boldsymbol{r_1}/r_1, \boldsymbol{r_2}/r_2)$. The term $\Pi_{L,l-p,l-q} = \sqrt{(2L+1)(2l-2p+1)(2l-2q+1)}$ is a normalization factor that ensures proper scaling, while the expression within the curly brackets represents a $9j$ symbol, which is crucial for evaluating the coupling of angular momenta in this configuration. The resulting function $Y_{LM}^{l-k,l+q}(\boldsymbol{r_1}/r_1, \boldsymbol{r_2}/r_2)$ is the final combined bipolar harmonic expressed in terms of the modified ranks.

Utilizing this raising and lowering operators defined for the framework of bipolar spherical harmonics basis, we can formally represent a general bipolar harmonic in terms of action of the gradient operator tensor on the Legendre polynomials as

$$\begin{aligned}&Y_{jm}^{ll'}(\hat{n}_1,\hat{n}_2) \\ &= (-1)^{j+q} \frac{\sqrt{(2l+1)(2l'+1)}}{4\pi(2n+1)!} c_j(l,l') \left\{\{\nabla\}_{k+\lambda_p} \otimes \{\nabla'\}_{j-k}\right\}_{jm} r^q r'^q P_q(\boldsymbol{r}\cdot\boldsymbol{r}'/rr').\end{aligned}$$

Here, $c_j(l,l')$ can be expressed as

$$c_j(l,l') = \left[\frac{2^{j+\lambda_p}(l+l'+j+1)!(2j+\lambda_p+1)!(l+l'-j)!}{(j+\lambda_p+l-l')!(j+\lambda_p+l'-l)!}\right]^{1/2},$$

$q = \frac{1}{2}\left(l+l'+j+\lambda_p\right), k = \frac{1}{2}\left(l-l'+j-\lambda_p\right)$, and the parameter λ_p characterizes the parity properties inherent in the spherical harmonics.

Utilizing the above defined relationships, we derive the subsequent reduction formulas for the expansions of any bipolar harmonic in the form of the 'minimal' harmonic basis.

The relation between the bipolar spherical harmonics and 'minimal' bipolar spherical harmonic functions with the product of the θ-dependent functions a_λ can be obtained as

$$Y^{l_1,l_2}_{LM}(\hat{n}_1,\hat{n}_2) = \sum_{\lambda=\lambda_p}^{L} a^{\lambda_p}_{\lambda}(l_1,l_2,L,\cos\theta)Y^{\lambda,L+\lambda_p-\lambda}_{LM}(\hat{n}_1,\hat{n}_2), \tag{3.12}$$

where the parameter λ_p characterizes the space inversion property that conveys information about the parity of BipoSH functions expressed as

$$\lambda_p = \begin{cases} 0 & \text{for even } (l_1+l_2-L) \\ 1 & \text{for odd } (l_1+l_2-L)\,, \end{cases} \tag{3.13}$$

indicates that the BipoSH function $Y^{l_1 l_2}_{LM}$ behaves as a tensor for even parity and a pseudo-tensor for odd parity and $\cos(\theta)$ is defined as dot product of the directions $\hat{n}_1 \cdot \hat{n}_2$.

The above relation provides us with the 'minimal' bipolar spherical harmonic basis, which is limited to the index L corresponding to the rank of the given bipolar harmonic tensor. The combination of these basis functions multiplied by new important functions a_λ creates the full, complete, and orthogonal basis for the bipolar harmonics. These angular separation θ-dependent functions are the key functions for constructing correlations on the SI violated 2D sphere.The explicit form of the 'minimal' bipolar harmonic functions constructed in this new basis can be expanded as follows

For the case when $\lambda_p = 0$ (where $l_1 + l_2 - L$ is even), the reduced bipolar harmonic basis can be written as

$$Y^{ll'}_{jm}(\hat{n}_1, \hat{n}_2) = \sum_{s=0}^{j} a^0_s(l, l', j, \cos\theta)\mathcal{Y}^s_{jm}(\hat{n}_1, \hat{n}_2),$$

and for the case when $\lambda_p = 1$ (where $l_1 + l_2 - L$ is odd)

$$Y^{ll'}_{jm}(\hat{n}, \hat{n}') = \sum_{s=0}^{j-1} a^1_s(l, l', j, \cos\theta)\left\{\left[\hat{n}, \hat{n}'\right] \otimes \mathcal{Y}^s_{j-1}(\hat{n}, \hat{n}')\right\}_{jm}.$$

The given reduction process constraints our analysis to only a few internal ranks up to L. The tensor with rank $l + l' \geq L$ can be written using L 'minimal' BipoSH basis functions with its coefficients being functions of l, l', and $\theta = \cos^{-1}(\hat{n}_1 \cdot \hat{n}_2)$.

In equation (3.12), the coefficients $a^{\lambda_p}_s$ can be explicitly expressed in functional form as

$$\begin{aligned}
&a^{\lambda_p}_s(l, l', j, \cos\theta)\\
=&\mathrm{i}^{\lambda_p}(-1)^{l'}\left[\frac{2^j(2l+1)\,(2l'+1)\,(2j+1)!\,(l+l'-j)!s!\,\left(j-s-\lambda_p\right)!}{q\,(j-l+l')!\,(j-l'+l)!(2s+1)!!\,\left(2j-2s-2\lambda_p+1\right)!!}\right]^{\frac{1}{2}}\\
&\times\sum_{t=0}^{t_{\max}}(-1)^{s+t}\begin{pmatrix}\frac{1}{2}\,(j'-l)\\ t\end{pmatrix}\begin{pmatrix}j-\lambda_p-t\\ s\end{pmatrix}\frac{(q-\lambda_p)!!}{(q-\lambda_p-2t)!!}P^{(j-t)}_{j'-t-s}(\cos\theta)
\end{aligned} \tag{3.14}$$

where $q = l + l' + j + 1$, $j' = j + l' - \lambda_p$, $t_{\max} = \min\left\{j - \lambda_p - s; \frac{1}{2}\,(j' - l)\right\}$, and

$\begin{pmatrix} m \\ n \end{pmatrix}$ represents the binomial coefficient. The polynomials $P_n^{(m)}$ follow the symmetry relation given as $P_n^{(m)}(x) + (2n-3)P_{n+1}^{(m-1)}(x) - P_{n+2}^{(m)}(x) = 0$. Upon examining the functional form of the a_λ functions, it becomes apparent that the necessary symmetry for transposing l and l' is absent, thereby deviating from the definition of bipolar harmonics. This observation suggests that the equation does not represent the comprehensive form for a_λ. Consequently, we apply these equations exclusively only when l is less than l', corresponding to coefficients $s \geq \frac{L}{2}$. For the remaining coefficients, we employ a symmetry relation given as

$$a_\lambda(l_1, l_2, L, \cos\theta) = a_{L-\lambda_p-\lambda}(l_2, l_1, L, \cos\theta). \tag{3.15}$$

to determine the exhaustive reduced set of 'minimal' bipolar harmonics. This yields the complete set of 'minimal' bipolar harmonics in an equivalently reduced form, satisfying the requirements of the completeness property of bipolar harmonics.

3.1.1 Examples of the 'minimal' Harmonics expansions

Spherical harmonics expansions are constrained by Clebsch-Gordan coefficients satisfying the triangularity conditions $|l_1 - l_2| \leq L \leq l_1 + l_2$ and $m_1 + m_2 = M$.

For the multipole $L = 1$, we can have $l_1 = l_2$, $l_1 = l_2 + 1$, or $l_1 = l_2 - 1$. The different terms can be obtained as

$$Y_{1M}^{ll}(\hat{n}_1, \hat{n}_2) = a_1(l_1, l_2, 1, \cos\theta) Y_{1M}^{11}(\hat{n}_1, \hat{n}_2), \tag{3.16}$$

$$
\begin{aligned}
Y_{LM}^{l+1,l}(\hat{n}_1,\hat{n}_2) &= \sum_{\lambda=\lambda_p}^{L} a_\lambda(l+1,l,1,\cos\theta) Y_{LM}^{\lambda,L-\lambda}(\hat{n}_1,\hat{n}_2) \\
&= a_0(l+1,l,1,\cos\theta) Y_{1M}^{0,1}(\hat{n}_1,\hat{n}_2) + a_1(l+1,l,1,\cos\theta) Y_{1M}^{1,0}(\hat{n}_1,\hat{n}_2),
\end{aligned}
\tag{3.17}
$$

$$
\begin{aligned}
Y_{LM}^{l,l+1}(\hat{n}_1,\hat{n}_2) &= \sum_{\lambda=\lambda_p}^{L} a_\lambda(l,l+1,1,\cos\theta) Y_{LM}^{\lambda,L-\lambda}(\hat{n}_1,\hat{n}_2) \\
&= a_0(l+1,l,1,\cos\theta) Y_{1M}^{0,1}(\hat{n}_1,\hat{n}_2) + a_1(l+1,l,1,\cos\theta) Y_{1M}^{1,0}(\hat{n}_1,\hat{n}_2).
\end{aligned}
\tag{3.18}
$$

Similarly for the multipole L = 2, we can have 5 different possible combinations of $l_1 = l_2, l_1 = l_2 + 1, l_1 = l_2 + 2, l_1 = l_2 - 1, l_1 = l_2 - 2$. One such term could be expanded as

$$
\begin{aligned}
Y_{2M}^{l,l+1}(\hat{n}_1,\hat{n}_2) &= \sum_{\lambda=\lambda_p}^{L} a_\lambda(l,l+1,2,\cos\theta) Y_{2M}^{\lambda,L-\lambda}(\hat{n}_1,\hat{n}_2) \\
&= a_1(l,l+1,2,\cos\theta) Y_{2M}^{1,2}(\hat{n}_1,\hat{n}_2) + a_2(l,l+1,2,\cos\theta) Y_{2M}^{2,1}(\hat{n}_1,\hat{n}_2)
\end{aligned}
\tag{3.19}
$$

So we can see from here that the 'minimal' Harmonics reduces the expansion to certain values of l_1 and l_2 for a given L. And a_λ captures the information about l_1 and l_2 in the already known function form.

Further analysis of the aforementioned set of 'minimal' BipoSH basis functions reveals that the tensor $Y_{LM}^{l_1 l_2}$ has $L + 1 - \lambda_p$ different basis components. Using this reduction mechanism for bipolar harmonics, we can construct equivalent compact and complementary θ-dependent 'minimal' BipoSH basis functions for any given value of multipole L.

3.2 ’Minimal’ Harmonics Functions

The application of the Bipolar Spherical Harmonics basis has emerged as an effective method for investigating non-statistical isotropic signatures present in the Cosmic Microwave Background (CMB) sky. Within the CMB temperature and polarisation field map, numerous sources contribute to violations of statistical isotropy, such as Doppler boost, Cosmic Hemispherical Asymmetry (CHA), weak lensing, and non-circular beam effects etc. The BipoSH formalism has demonstrated success in analyzing these effects.

Studies of these CMB effects have revealed that these non-statistical effects are most relevant at very low multipole values (L values). Therefore, there has always been a need for a new, simpler basis that can effectively represent these features in the mimimal form. Additionally, using this new representation might uncover new insights into CMB anisotropy, which could be crucial for understanding the early universe. It can be seen that in the bipolar harmonic basis, the nSI violation feature could be spread over the entire range of l from zero to infinity, whereas reduced bipolar harmonics limit our study in real space functions of angular separation, θ having a finite domain of 0 to 180 degrees and the internal rank is restricted to L. Further, real space approach may present a promising avenue for partial sky observations/data.

In this section, we will incorporate our previously defined reduced bipolar basis into the CMB framework. We’ll explore how isotropy violations in the CMB can be expressed using statistical isotropic correlation functions with a ’minimal’ number of angular multipole functions.

The correlation function in terms of BipoSH functions is given as

$$C(\hat{n}_1, \hat{n}_2) = \sum_{L,M,l_1,l_2} A^{LM}_{l_1 l_2} Y^{l_1 l_2}_{LM}(\hat{n}_1, \hat{n}_2) \tag{3.20}$$

Utilizing the reduction mechanism of the bipolar harmonics basis, the most general two-point correlation function from equations (3.12) and (3.20) can be expressed in the form of the reduced bipolar harmonic basis as

$$C\left(\hat{n}_1, \hat{n}_2\right) = \sum_{L,M,l_1,l_2} A^{LM}_{l_1 l_2} \sum_{\lambda=\lambda_p}^{L} a^{\lambda_p}_{\lambda}(l_1, l_2, L, \cos\theta) Y^{\lambda, L+\lambda_p-\lambda}_{LM}(\hat{n}_1, \hat{n}_2). \tag{3.21}$$

The above equation can be easily recasted to another form in case of even parity by exchanging the summations as follows

$$C(\hat{n}_1, \hat{n}_2) = \sum_{L,M} \sum_{\lambda=0}^{L} \left[\sum_{l_1,l_2} A^{LM}_{l_1 l_2} a_\lambda(l_1, l_2, L, \cos\theta) \right] Y^{\lambda, L-\lambda}_{LM}(\hat{n}_1, \hat{n}_2), \tag{3.22}$$

$$C(\hat{n}_1, \hat{n}_2) = \sum_{L,M} \sum_{\lambda=0}^{L} \left[\alpha^{L,M}_{\lambda}(\cos\theta) \right] Y^{\lambda, L-\lambda}_{LM}(\hat{n}_1, \hat{n}_2). \tag{3.23}$$

Now, it is interesting to note that the expression inside the square brackets takes different $L+1$ different values for a given multipole L in our newly defined reduced bipolar basis. These values correspond to the θ-dependent correlation functions expanded in the general nSI sky, which we define as the the 'minimal' Bipolar (mBipoSH) correlation functions. These functions encapsulate the nSI feature in our study.

From the above analysis, the mBipoSH angular correlation functions for any given multipole L in a nSI CMB sky can be expressed as a product of BipoSH coefficients and newly defined a_λ coefficients as

$$C_\lambda(\theta) = \alpha^{L,M}_{\lambda}(\cos\theta) = \sum_{l_1 l_2} A^{LM}_{l_1 l_2} a_\lambda(l_1, l_2, L, \cos\theta). \tag{3.24}$$

This equation shows that the 'minimal' harmonic functions of θ encapsulate the information stored in the 2D SI violated map that can be represented in real space θ coordinates.

Utilizing the definition of bipolar spherical harmonics in terms of spherical harmonics, this expression can be further rephrased as

$$\alpha_{\lambda}^{L,M}(\cos\theta) = \sum_{l_1 l_2}\sum_{m_1 m_2} a_{l_1 m_1} a^{*}_{l_2 m_2} (-1)^{m_2} C^{LM}_{l_1 m_1 l_2 -m_2} a_{\lambda}(l_1, l_2, L, \cos\theta). \tag{3.25}$$

It is clear from this equation that our real-space-based estimator can then be expressed in terms of the temperature or polarization data collected by the CMB mission represented using spherical harmonics coefficients a_{lm}. This reduced basis allows us to study nSI violation features in real space. Additionally, we demonstrate that these new estimators based on angular separation θ are essentially combinations of isotropic correlation functions, forming a general structure on the 2D sphere. Analogous to the BipoSH coefficients, which are studied as the natural generalization of the power spectrum of the CMB, such that under the condition of $L = 0$, the BipoSH coefficients reduce to the well-known C_l. Analogously the mBipoSH angular correlation functions are a natural generalization of the standard isotropic correlation function of the CMB such at under SI condition, the mBipoSH representation reduces to a single angular correlation function

$$\alpha_0^{0,0}(\cos\theta) = C(\theta) = \sum_{l} \frac{2l+1}{4\pi} C_l P_l(\cos\theta).$$

The higher-order 'minimal' bipolar harmonic function can be shown to to have the derivatives of the Legendre polynomial up to the L^{th} order in its analytical form, where L corresponds to the multipole associated with the SI violation feature. In the next section, we will construct several lower-rank mBipoSH angular functions in their analytical forms.

3.2.1 Dipole anisotropy $(L = 1)$

To construct the analytical expression for mBipoSH basis functions corresponding to the bipolar harmonics basis, we begin with the $L = 1$ order of statistical isotropy (SI) violation, which introduces direction dependence in the cosmic microwave background (CMB) sky map. For even parity in the CMB sky, this relationship can be expressed as follows

$$Y^{ll'}_{1m}\left(\boldsymbol{n},\boldsymbol{n}'\right) = -\frac{1}{4\pi}\sqrt{\frac{3}{l_{\max}}}\left[(-1)^{l}P^{(1)}_{l}(x)[\boldsymbol{n}]_{1M} + (-1)^{l'}P^{(1)}_{l'}(x)[\boldsymbol{n}]'_{1m}\right]. \tag{3.26}$$

In this equation, the functions $P^{(1)}_{l}(x)$ and $P^{(1)}_{l'}(x)$ are associated Legendre polynomials of degree l and l' with order 1, these polynomials capture the angular dependence of the tensor components. The terms $[\boldsymbol{n}]_{1M}$ and $[\boldsymbol{n}]'_{1m}$ denote the specific projections of the spin-1 tensor components in the directions $\boldsymbol{n}$ and $\boldsymbol{n}'$, respectively.

For odd parity cases with $l' = l$, the correlation can be expressed using Bipolar Spherical Harmonic (BipoSH) and modified BipoSH (mBipoSH) functions, which account for deviations from statistical isotropy in the field.

$$Y^{ll}_{1m}\left(\boldsymbol{n},\boldsymbol{n}'\right) = \frac{\mathrm{i}(-1)^{l+1}}{4\pi}\left[\frac{3(2l+1)}{l(l+1)}\right]^{\frac{1}{2}} P^{(1)}_{l}(x)\left[\boldsymbol{n}\times\boldsymbol{n}'\right]_{1m}. \tag{3.27}$$

and in this case the mBiposh angular correlation functions can be represented as

$$\alpha^{1,M}_{\lambda}(\cos\theta) = \sum_{l} A^{1M}_{ll+1}a_{\lambda}(l, l+1, 1, \cos\theta) \tag{3.28}$$

$$\alpha^{1,0}_{0}(\cos\theta) = \sum_{l} A^{10}_{ll+1}\left[\frac{-\sqrt{3}}{4\pi\sqrt{l+1}}(-1)^{l}P^{(1)}_{l}(\cos\theta)\right] \tag{3.29}$$

$$\alpha^{1,0}_{1}(\cos\theta) = \sum_{l} A^{10}_{ll+1}\left[\frac{-\sqrt{3}}{4\pi\sqrt{l+1}}(-1)^{l+1}P^{(1)}_{l+1}(\cos\theta)\right]. \tag{3.30}$$

To compute 'minimal' BipoSH angular functions for odd parity, this corresponds to having only l, l' type correlations in maps having dipolar $(L = 1)$ anisotropic characteristics. The mBipoSH functions can be defined in case with a new parameter λ_p as

$$\alpha^{1,M}_{\lambda,\lambda_p}(\cos\theta) = \sum_l A^{1M}_{ll} a^1_\lambda(l,l,1,\cos\theta), \tag{3.31}$$

using the same approach of these functions, these odd parity angular function is

$$\alpha^{1,0}_{1,1}(\cos\theta) = \sum_l A^{10}_{ll} \frac{i(-1)^{l+1}}{4\pi} \left[\frac{3(2l+1)}{l(l+1)}\right]^{\frac{1}{2}} P^{(1)}_l(\cos\theta). \tag{3.32}$$

From here, it is important to highlight that there is only one correlation function associated with dipolar anisotropy in the case of odd parity. Furthermore from the above equations, it can be concluded that for odd parity, there are L number of mBipoSH angular correlation functions corresponding to the L multipole of SI violation.

3.2.2 $L = 2$, Quadrupole anisotropy

The mBipoSH functions can also be constructed for $L = 2$ quadrupole anisotropy. In this case, for even parity, we have l, l' and $l, l \pm 2$ correlations, while for odd parity, we have $l, l \pm 1$ correlations.

The corresponding relationship between bipolar harmonics and mBipoSH angular functions for this case can be expressed as

$$\begin{aligned} Y^{ll}_{2m}(\boldsymbol{n},\boldsymbol{n}') = \frac{(-1)^{l+1}}{4\pi} \left[\frac{30(2l+1)}{(2l-1)l(l+1)(2l+3)}\right]^{\frac{1}{2}} &\Big(P^{(1)}_l(x)\left\{\boldsymbol{n}\otimes\boldsymbol{n}'\right\}_{2m} \\ &+P^{(2)}_l(x)\left\{[\boldsymbol{n}\times\boldsymbol{n}']\otimes[\boldsymbol{n}\times\boldsymbol{n}']\right\}_{2m}\Big). \end{aligned} \tag{3.33}$$

This equation corresponds to the correlation between l and l within the context of L=2 anisotropy. To express the l, $l \pm 2$ correlations in the 'minimal' bipolar basis, the analytical form can be written as

$$Y^{ll'}_{2m}\left(\boldsymbol{n},\boldsymbol{n}'\right) = \frac{(-1)^l}{4\pi}\sqrt{\frac{5}{l_{\max}\left(2l_{\max}-1\right)\left(l_{\max}-1\right)}} \left(P^{(2)}_l(x)\{\boldsymbol{n}\otimes\boldsymbol{n}\}_{2m} - 2P^{(2)}_{(l+l')/2}(x)\left\{\boldsymbol{n}\otimes\boldsymbol{n}'\right\}_{2m} + P^{(2)}_{l'}(x)\left\{\boldsymbol{n}'\otimes\boldsymbol{n}'\right\}_{2m}\right). \tag{3.34}$$

Here, as previous case, $l_{\max}$ represents the maximum value between l and l'. The mBipoSH angular correlation functions can be constructed in the form

$$\alpha^{2,M}_{\lambda}(\cos\theta) = \sum_l A^{20}_{ll} a_\lambda(l,l,2,\cos\theta) + A^{20}_{ll+2} a_\lambda(l,l+2,2,\cos\theta) \quad \text{where } \lambda = 0,1,2. \tag{3.35}$$

The various values of λ represent different mBipoSH functions corresponding to L=2. The coefficients a_λ can be readily computed using (3.14). The exact form of these distinct a_λ coefficients can be expressed as

$$\begin{aligned}
a_1(l,l,2,\cos\theta) &= (-1)^l\sqrt{\frac{10(2l+1)}{3l(2l+3)(2l-1)(l+1)}}\left((2l+3)P^1_l(\cos\theta) - 2P^2_{l+1}(\cos\theta)\right)\\
a_1(l,l+2,2,\cos\theta) &= (-1)^l\sqrt{\frac{5}{9}\frac{1}{(2l+3)(l+2)(1+1)}}\times 2\left((2l+5)P^1_{l+2}(\cos\theta) - P^2_{l+3}(\cos\theta)\right)\\
a_0(l,l,2,\cos\theta) = a_2(l,l,2,\cos\theta) &= (-1)^l\sqrt{\frac{4(2l+1)}{(2l+3)(2l-1)(l+1)l}}P^2_l(\cos\theta)\\
a_2(l,l+2,2,\cos\theta) &= (-1)^l\sqrt{\frac{2}{3}\frac{1}{(2l+3)(l+2)(l+1)}}P^2_{l+2}(\cos\theta)\\
a_0(l,l+2,2,\cos\theta) = a_2(l+2,l,2,\cos\theta) &= (-1)^l\sqrt{\frac{2}{3}\frac{1}{(2l+3)(l+2)(l+1)}}P^2_l(\cos\theta)
\end{aligned} \tag{3.36}$$

The mBipoSH functions can be constructed using this set of a_λ coefficients. The correlations for l and $l+1$ corresponding to odd parity have the following form

$$\begin{aligned} Y^{ll'}_{2m}\left(\boldsymbol{n},\boldsymbol{n}'\right) =& \mathrm{i}\frac{(-1)^l}{4\pi}\sqrt{\frac{10}{ll'\left(l_{\max}+1\right)}}\left(P^{(2)}_l(x)\left\{\boldsymbol{n}\otimes\left[\boldsymbol{n}\times\boldsymbol{n}'\right]\right\}_{2m}\right. \\ & \left.+P^{(2)}_{l'}(x)\left\{\boldsymbol{n}'\otimes\left[\boldsymbol{n}'\times\boldsymbol{n}\right]\right\}_{2m}\right). \end{aligned} \tag{3.37}$$

Similarly, by using the same approach, we can calculate the two mBipoSH angular correlation functions for odd parity corresponding to $L=2$.

3.2.3 $L=3$ Octopole Anisotropy

The mBipoSH correlation functions can also be evaluated for a SI violated map having octopole anisotropy. The reduced bipolar basis can be written as

$$\begin{aligned} Y^{ll'}_{3m}\left(\boldsymbol{n},\boldsymbol{n}'\right) =& \mathcal{C}\left(l,l'\right)\Big[P^{(3)}_l(x)\{\boldsymbol{n}\}_{3m}+P^{(3)}_{l'}(x)\left\{\boldsymbol{n}'\right\}_{3m} \\ & -\left(3P^{(3)}_{l'+1}(x)-\frac{\left(l'-l+3\right)\left(l+l'+4\right)}{2}P^{(2)}_{l'}(x)\right)\left\{\boldsymbol{n}\otimes\left\{\boldsymbol{n}'\right\}_2\right\}_{3m} \\ & -\left(3P^{(3)}_{l+1}(x)-\frac{\left(l-l'+3\right)\left(l+l'+4\right)}{2}P^{(2)}_{l}(x)\right)\left\{\boldsymbol{n}'\otimes\left\{\boldsymbol{n}\right\}_2\right\}_{3m}\Big] \end{aligned}$$

This expression is valid for the combinations corresponding to even parity $l=l'\pm1;l'\pm3$ and for the odd parity combinations $l=l';l'\pm2$, the reduced bipolar basis can also be constructed as

$$\begin{aligned} Y^{ll'}_{3m}\left(\boldsymbol{n},\boldsymbol{n}'\right) =& -\mathrm{i}\mathcal{C}\left(l,l'\right)\Big[P^{(3)}_l(x)\left\{\left[\boldsymbol{n}\otimes\boldsymbol{n}'\right\}\times\{\boldsymbol{n}\}_2\right]_{3m}+P^{(3)}_{l'}(x)\left\{\left[\boldsymbol{n}\otimes\boldsymbol{n}'\right\}\otimes\left\{\boldsymbol{n}'\right\}_2\right]_{3m} \\ & +\left(\frac{\left(l'-l+2\right)\left(l+l'+3\right)}{2}P^{(2)}_{l'}(x)-2P^{(3)}_{l'+1}(x)\right)\left\{\left[\boldsymbol{n}\otimes\boldsymbol{n}'\right\}\times\left\{\boldsymbol{n}\otimes\boldsymbol{n}'\right\}_2\right]_{3m}\Big]. \end{aligned}$$

where the function $\mathcal{C}\left(l,l'\right)$ can be written as

$$\mathcal{C}\left(l,l'\right)=\frac{6(-1)^{l'+1}}{\pi}\left[\frac{210(2l+1)\left(2l'+1\right)\left(l+l'-3\right)!}{\left(l-l'+3\right)!\left(l'-l+3\right)!\left(l+l'+4\right)!}\right]^{\frac{1}{2}}.$$

For the specific case with correlations between l and $l+1$ within the octupole anisotropy, mBipoSH functions given by even parity can be systematically formulated as

$$\alpha_{\lambda}^{L,M}(\cos\theta) = \sum_{l} A_{ll+1}^{LM} a_{\lambda}(l, l+1, L, \cos\theta) \tag{3.38}$$

$$\alpha_{0}^{3,0}(\cos\theta) = \sum_{l} A_{ll+1}^{30} \mathcal{F}\left(l, l+1\right) P_{l}^{(3)}(\cos\theta) \tag{3.39}$$

$$\alpha_{1}^{3,0}(\cos\theta) = \sum_{l} A_{ll+1}^{30} \mathcal{F}\left(l, l+1\right) \left(-3P_{l+2}^{(3)}(\cos\theta) - 2\left(l+l'+4\right) P_{l+1}^{(2)}(\cos\theta)\right) \tag{3.40}$$

$$\alpha_{2}^{3,0}(\cos\theta) = \sum_{l} A_{ll+1}^{30} \mathcal{F}\left(l, l+1\right) \left(-3P_{l+1}^{(3)}(\cos\theta) - 2\left(l+l'+4\right) P_{l}^{(2)}(\cos\theta)\right) \tag{3.41}$$

$$\alpha_{3}^{3,0}(\cos\theta) = \sum_{l} A_{ll+1}^{30} \mathcal{F}\left(l, l+1\right) P_{l+1}^{(3)}(\cos\theta), \tag{3.42}$$

where the function $\mathcal{F}\left(l, l+1\right)$ can be expressed as

$$\mathcal{F}\left(l, l'\right) = \frac{6(-1)^{l'+1}}{\pi} \left[\frac{210(2l+1)\,(2l'+1)\,(l+l'-3)!}{(l-l'+3)!\,(l'-l+3)!\,(l+l'+4)!}\right]^{\frac{1}{2}} \tag{3.43}$$

. These distinct sets of four isotropic correlation functions capture any octupole anisotropy correlations between harmonic scale l and $l+1$ within the Cosmic Microwave Background map. The above set of useful expressions form BipoSH are reproduced in appendix.

3.3 Symmetries of mBipoSH angular basis

The mBiposh angular basis provides a natural basis to study CMB two-point correlation function with under statistical isotropy condition it gives the standard rotational invariant CMB two-point correlation function.

3.3.1 Symmetries of correlation function in mBipoSH basis

The symmetric property of two point correlation function implies $C\left(\hat{n}_1, \hat{n}_2\right) = C\left(\hat{n}_2, \hat{n}_1\right)$. Correlation function in terms of BipoSH functions is

$$C\left(\hat{n}_1, \hat{n}_2\right) = \sum_{l_1, l_2, L, M} A^{LM}_{l_1 l_2} \left\{ Y_{l_1}\left(\hat{n}_1\right) \otimes Y_{l_2}\left(\hat{n}_2\right) \right\}_{LM}. \tag{3.44}$$

Here we observe that index ℓ_1 corresponds to $\hat{n}_1$, such that upon exchanging directions $\hat{n}_1 \leftrightarrow \hat{n}_2$, the correlation function transforms into

$$C\left(\hat{n}_2, \hat{n}_1\right) = \sum_{l_2, l_1, L, M} A^{LM}_{l_2 l_1} \left\{ Y_{l_2}\left(\hat{n}_2\right) \otimes Y_{l_1}\left(\hat{n}_1\right) \right\}_{LM}. \tag{3.45}$$

For the case of mBipoSH angular correlation functions represented as sets of isotropic correlation functions for a complete correlation function, it can be shown through a simple calculation that under the exchange of the direction they interchangeably transform into each other, such that the set of these functions remains the same. This ensures the invariance of the correlation function under the exchange of directions. Explicitly for the case of $L = 1$ dipole anisotropy, under the interchange of $\hat{n}_1 \leftrightarrow \hat{n}_2$, the angular correlation mBipoSH function $\tilde{\alpha}^{1,0}_0(\cos\theta)$ is given by

$$\tilde{\alpha}^{1,0}_0(\cos\theta) = \sum_{\ell} A^{10}_{\ell\ell+1} \left[\frac{-\sqrt{3}}{4\pi\sqrt{\ell+1}} (-1)^{\ell+1} P^{(1)}_{\ell+1}(\cos\theta) \right]. \tag{3.46}$$

Utilizing the property of Clebsch-Gordan coefficients:

$$\begin{aligned} \tilde{\alpha}^{1,0}_0(\cos\theta) &= \sum_{\ell} A^{10}_{\ell\ell+1} \left[\frac{-\sqrt{3}}{4\pi\sqrt{\ell+1}} (-1)^{\ell+1} P^{(1)}_{\ell+1}(\cos\theta) \right] \\ &= \alpha^{1,0}_1(\cos\theta). \end{aligned} \tag{3.47}$$

Similarly, this property holds for the other isotropic correlation function also. Therefore, it is evident from this calculation that the total angular correlation function remains invariant under the exchange of directions.

3.3.2 Effect of rotation

To study the effect of rotation on the 'minimal' bipolar angular basis, we need to generalize the effect of rotation to the spherical harmonics. The effect of rotation on the bipolar spherical harmonics can be studied through the operation of Wigner D matrices, as shown in the equation

$$\hat{D}(\alpha,\beta,\gamma)\left\{Y_{l_1}\left(\hat{n}_1\right)\otimes Y_{l_2}\left(\hat{n}_2\right)\right\}_{LM} = \sum_{M} D^{L}_{MM}(\alpha,\beta,\gamma)\left\{Y_{l_1}\left(\hat{n}_1\right)\otimes Y_{l_2}\left(\hat{n}_2\right)\right\}_{LM}. \tag{3.48}$$

The rotation operator given by $\hat{D}(\alpha,\beta,\gamma)$ is expressed in terms of the Wigner D-functions $D^{M'}_{M}$, where α,β,γ represent the Euler angles characterizing any general rotation on the 2D sphere. These three Euler angles describe a sequence of three successive rotations $\{\alpha,\beta,\gamma\}$ on the sphere, as illustrated in the figure 3.1. These

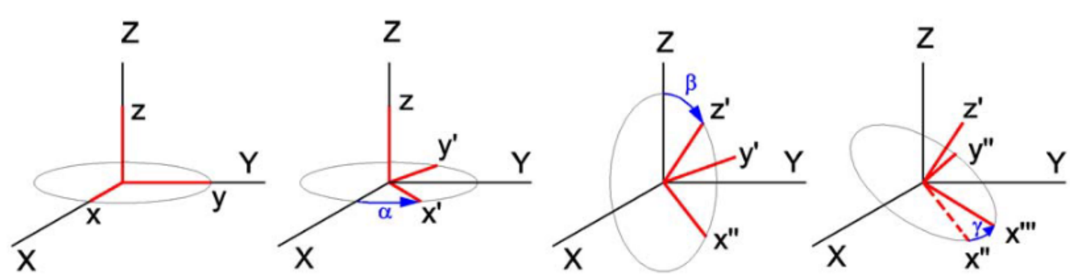

Figure 3.1: Pictorial representation of the Euler angles. Source- Wikipedia

angles defined as, coordinate system $S\{x,y,z\}$ is rotated about the z-axis by an angle α (where $0 \leq \alpha < 2\pi$). Subsequently, it is rotated about the new y-axis by an angle β (where $0 \leq \beta < \pi$), and finally, it is rotated about the new z-axis by an angle γ (where $0 \leq \gamma < 2\pi$).

To extend these calculations to the 'minimal' bipolar spherical harmonic basis, the effect of rotation can be calculated as follows

$$Y^{l_1 l_2}_{LM}(\hat{n}_1, \hat{n}_2) = \sum_{\lambda=0}^{L} a_\lambda(l_1, l_2, L, \cos\theta) Y^{\lambda, L-\lambda}_{LM}(\hat{n}_1, \hat{n}_2) \tag{3.49}$$

$$\begin{aligned}\hat{D}(\alpha,\beta,\gamma) Y^{l_1 l_2}_{LM}(\hat{n}_1, \hat{n}_2) &= \sum_{M} D_{MM}{}^{L}(\alpha,\beta,\gamma) \sum_{\lambda=0}^{L} a_\lambda(l_1, l_2, L, \cos\theta) Y^{\lambda, L-\lambda}_{LM}(\hat{n}_1, \hat{n}_2) \\ &= \sum_{\lambda=0}^{L} a_\lambda(l_1, l_2, L, \cos\theta) \sum_{M} D_{MM}{}^{L}(\alpha,\beta,\gamma) Y^{\lambda, L-\lambda}_{LM}(\hat{n}_1, \hat{n}_2).\end{aligned} \tag{3.50}$$

Since $\cos\theta$ remains invariant under axis rotation, we observe from the calculation that the Wigner-D function rotates the mBipoSH basis similarly to the BipoSH basis. Given that mBipoSH angular functions are independent of specific directions $\hat{n}_1$ and $\hat{n}_2$, but solely dependent on the angle difference between directions, they are therefore invariant under axis rotation.

3.3.3 Parity in mBipoSH angular functions

Parity violation features are naturally encoded in the mBipoSH basis.

$$\begin{aligned} Y^{l_1, l_2}_{LM}(\hat{n}_1, \hat{n}_2) &= \sum_{\lambda=\lambda_p}^{L} a_\lambda(l_1, l_2, L, \cos\theta)\, Y^{\lambda, L+\lambda_p-\lambda}_{LM}(\hat{n}_1, \hat{n}_2), \\ \lambda_p &= \begin{cases} 0 & \text{for even } (l_1 + l_2 - L) \\ 1 & \text{for odd } (l_1 + l_2 - L). \end{cases} \end{aligned} \tag{3.51}$$

It is evident from the above equation that the parameter λ_p captures the parity information of the BipoSH representation in the case of mBipoSH angular basis. Since the correlation function in the case of reduced mBipoSH basis can be expanded in terms of angular correlation functions, the expression is given by

$$C\left(\hat{n}_1, \hat{n}_2\right) = \sum_{L,M,l_1,l_2} A^{LM}_{l_1,l_2} \sum_{\lambda=\lambda_p}^{L} a^{\lambda_p}_{\lambda}(l_1, l_2, L, \cos\theta) Y^{\lambda, L+\lambda_p-\lambda}_{LM}(\hat{n}_1, \hat{n}_2). \tag{3.52}$$

The different expansion factors of λ_p carry information about different angular correlation functions corresponding to odd parity functions. Even parity functions are represented by $\lambda_p = 0$, while odd parity functions are represented by $\lambda_p = 1$. In absence of parity violating processes, only even parity correlation functions are present. This means that correlation functions associated with $\lambda_p = 1$ should disappear in such cases. In cases of large-scale phenomena involving parity violation, these correlation functions with $\lambda_p = 1$ directly correspond to their counterparts in the Bipolar Spherical Harmonics (BipoSH) within the mBipoSH basis.

Similarly, within the mBipoSH angular basis, any non-zero cross-correlation in angular correlation functions of different parity signifies the existence of parity-violating phenomena in real space (θ-space). Thus, the mBipoSH basis plays a critical role in investigating parity violation in real space.

3.4 Construction of map in reduced basis

It is interesting to note this mathematical structure defining a reduced basis having real space functions opens a new avenue towards a visual representation of SI violations in a set of sky maps. The mBipoSH angular correlations functions product with spherical harmonics basis can be summed over to construct the θ- dependent angular function at each point on the 2D sphere.

$$\zeta_\lambda(\hat{n}_1, \cos\theta) = \sum_{LM} \alpha^{LM}_{\lambda}(\cos\theta) Y_{LM}(\hat{n}_1). \tag{3.53}$$

These $\zeta_\lambda(\hat{n}_1, \cos\theta)$ functions represent the $\cos\theta$ spectrum ranging from -1 to 1 for any defined pixel on the sphere as shown in the picture.

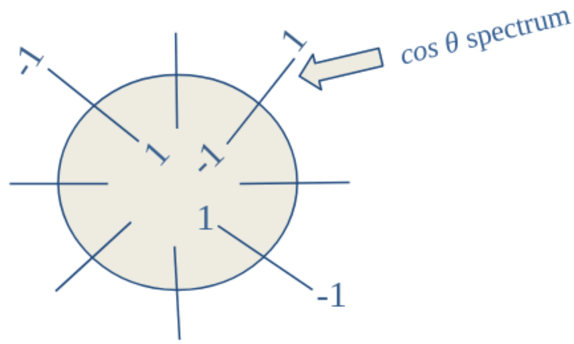

Figure 3.2: Pictorial representation of $\cos\theta$ spectrum at each point on the sphere

This formalism introduces a novel quantitative measure for examining random data distributed on a 2D sphere. The ζ functions serve as a 'minimal' construct in $\mathbf{S}^2 \times \mathbf{S}^1$ and can effectively represent the underlying pattern in the nSI CMB map. Such visualisation of the nSI part of the correlation function could be crucial for analyzing the unknown nSI features with upcoming high-resolution CMB data.

3.5 Discussion

The bipolar spherical harmonics representation has emerged as a comprehensive framework for quantifying deviations from statistical isotropy for a random field on a 2D sphere. In this chapter, we adopt a lesser-known reduction technique of the BipoSH basis, termed 'minimal' harmonics in the original paper by Manakov et al (5). This reduction technique of BipoSH leads to a novel 'minimal' generalized set of isotropic angular correlation functions, defined as mBipoSH functions. These new set of real space based functions serve as observable measures of non-statistical isotropy (nSI) features in a CMB sky map. In our specific domain of interest, these functions provide a new set of observables in real space, complementing the harmonic space BipoSH representation prevalent in the literature. To derive this 'minimal' set, we employ the mathematical theorem stating that BipoSH, being a tensor of rank L, can be constructed out of to L vectors. We construct this 'minimal' basis by defining raising and lowering operators for the bipolar basis. It is important to note that in this basis, the nSI effects at multipole L can be studied by $L+1$ different isotropic angular correlation functions in the case of even parity, and L correlation functions in the case of odd parity. This new basis can be effectively employed in a broader context to investigate random distributions on a 2D sphere, spanning diverse applications from celestial sky maps to geophysical, planetary and other maps on 2D sphere.

CHAPTER 4

EXPLORING NSI EFFECTS IN CMB USING mBipoSH

Planck and WMAP collaboration data releases have suggested intriguing hints of deviations from statistical isotropy in CMB maps beyond known effects. Departures from statistical isotropy can stem from various sources, including known physical effects and observational artifacts. Some well-studied effects include Doppler boost, weak lensing of CMB photons by large-scale structure, and systematics such as non-circular beam have been investigated using the BipoSH representation (7–10).

In this chapter, we will apply our new minimal bipolar basis to these well-known sources of nSI effects and demonstrate the efficacy of our method in capturing these effects in real space-based estimators. Additionally, we will construct a minimum variance estimator corresponding to these effects to quantify their strength. As this method provides an estimation of the nSI strength in terms of real-space estimators, it could prove useful for upcoming ground-based missions. These missions will provide partial-sky CMB maps with high resolution, such as those from ACT (Atacama Cosmology Telescope) and SPT (South Pole Telescope), as well as experiments like CMB-S4.

4.1 Dipole anisotropy due to Doppler Boost

Our motion today with respect to the cosmic rest frame causes a dipole anisotropy in the CMB temperature and polarization fields, with an inferred velocity ($\beta \equiv |v|/c = 1.23 \times 10^{-3}$). The Doppler boost of the CMB sky in this moving observer frame leads to observable nSI features in CMB due to well-known relativistic effects of modulation and aberration of the CMB temperature field. Modulation, a frequency-dependent effect, changes the brightness of the CMB sky, either enhancing or diminishing it, depending on the direction of motion. On the other hand, aberration, which is frequency-independent phenomenon, deflects the original directions of incoming CMB photons. Doppler boost nSI effect has been reliably measured by Planck collaboration (11).

The temperature of the Cosmic Microwave Background (CMB) in the direction $\hat{n}'$ in the CMB rest frame is represented as $T'(\hat{n}')$. Observed CMB temperature in the direction $\hat{n}$ due to this effect, denoted as $T(\hat{n})$, is given as

$$T(\hat{n}) = \frac{T'(\hat{n}')}{\gamma(1 - \hat{n} \cdot \boldsymbol{\beta})},$$

where $\gamma = (1 - \beta^2)^{-\frac{1}{2}}$ is the Lorentz factor and $\beta \equiv |\boldsymbol{\beta}|$. $\hat{n}$ is related to $\hat{n}'$ as

$$\hat{n} = \frac{\hat{n}' \cdot \hat{\boldsymbol{\beta}} + \beta}{1 + \hat{n}' \cdot \boldsymbol{\beta}}\hat{\boldsymbol{\beta}} + \frac{\hat{n}' - (\hat{n}' \cdot \hat{\boldsymbol{\beta}})\hat{\boldsymbol{\beta}}}{\gamma(1 + \hat{n}' \cdot \boldsymbol{\beta})}.$$

The intensity corresponding to the CMB temperature field can be given as

$$I_\nu(\hat{n}) = \frac{2h\nu^3}{c^2} \frac{1}{\exp\left[\frac{h\nu}{k_B T(\hat{n})}\right] - 1}.$$

The transformed CMB temperature field, after having only first order terms in β

$$\delta T(\hat{n}) = \delta T'(\hat{n} - \nabla(\hat{n} \cdot \boldsymbol{\beta}))(1 + \hat{n} \cdot \boldsymbol{\beta}).$$

Therefore, the effective relationship between temperature fluctuations excluding the dipole term and intensity fluctuations can be expressed as

$$\delta T(\hat{n})_I = \frac{\delta I_\nu(\hat{n})}{dI_\nu/\,dT|_{T_0}} = \delta T'(\hat{n} - \nabla(\hat{n}\cdot\boldsymbol{\beta}))\,(1 + b_\nu \hat{n}\cdot\boldsymbol{\beta})\,,$$

where $\boldsymbol{\beta}$ refers to the boost velocity vector and b_ν captures the frequency dependence of the Doppler boost given by

$$b_\nu = \frac{\nu}{\nu_0}\coth\left(\frac{\nu}{2\nu_0}\right) - 1, \tag{4.1}$$

and the local velocity β_{1M} defined in the harmonic basis as

$$\beta_{1M} = \int \boldsymbol{\beta}.\hat{n} Y^*_{1M}(\hat{n}) d\hat{n} \tag{4.2}$$

with the notation $\Pi_{l_1 l_2 \dots l_n} = \sqrt{(2l_1+1)(2l_2+1)\dots(2l_n+1)}$. This effect can be captured in the covariance matrix upto the first order in β as

$$\begin{aligned}\langle a_{lm} a^*_{l'm'}\rangle =& C_l \delta_{ll'}\delta_{mm'} \\ &+ (-1)^{m'} \frac{\Pi_{ll'}}{\sqrt{12\pi}} \sum_{N=-1}^{1} \beta_{1N} \left[\left(b_\nu(l) - \frac{1}{2}\left\{ l(l+1) - l'\left(l'+1\right) + 2 \right\} \right) C_l \right. \\ &\left. + \left(b_\nu\left(l'\right) - \frac{1}{2}\left\{ l'\left(l'+1\right) - l(l+1) + 2 \right\} \right) C_{l'} \right] C^{10}_{l0l'0} C^{1N}_{lml'-m'}.\end{aligned} \tag{4.3}$$

In the BipoSH representation, this effect induces a non-zero even parity dipolar $(L = 1)$ BipoSH coefficient in the CMB map via the l , l +1 correlations of Spherical harmonic space covariance matrix (9). The term $b_\nu(l)$ represents the Doppler boost's frequency dependence through ν, while its dependence on l captures the corresponding scale-dependent effects. The Planck collaboration has employed the BipoSH formalism to measure this effect (12) using a quadratic estimator. More recently, a fully Bayesian approach utilizing publicly available Planck data has provided a 5σ confirmation of this non-statistically isotropic (nSI) effect (13).

We illustrate our new minimal BipoSH representation for this well-understood and quantified case of SI violation in the CMB map. We explicitly derive the expressions to compute the two non-zero mBipoSH angular correlations functions expected in a Doppler boosted CMB map for this even parity effect at $L = 1$. We also outline the derivation of an appropriate estimator for these mBipoSH angular correlation functions from a CMB map.

The nSI signature of Doppler boost is captured by the BipoSH coefficients as

$$\tilde{A}^{1M}_{l,l+1|TT} = \beta^{1M} D^{TT}_{l} \frac{\Pi_{l,l+1}}{\Pi_1} C^{10}_{l,0,l+1,0}, \tag{4.4}$$

where BipoSH spectra is defined as

$$D^{TT}_{l} = \frac{1}{\sqrt{4\pi}} \left[(l + b_\nu) C^{TT}_{l} - (l + 2 - b_\nu) C^{TT}_{l+1} \right]. \tag{4.5}$$

The mBipoSH angular correlation functions for Doppler boost effect can be constructed using the method used in the previous chapter as

$$\alpha^{1M}_{\lambda}(\cos\theta) = \sum_{l} A^{1M}_{l,l+1} a_\lambda(l, l+1, 1, \cos\theta). \tag{4.6}$$

The above reduction process for the Doppler boost effect corresponding to multipole $(L = 1)$ can be simplified in terms of the correlation function as

$$C\left(\hat{n}_1, \hat{n}_2\right) = C_{SI}(\cos\theta) + C_{nSI}(\hat{n}_1, \hat{n}_2), \tag{4.7}$$

where $C_{SI}(\cos\theta)$ represents the standard isotropic correlation function for the true CMB field and the $C_{nSI}(\hat{n}_1, \hat{n}_2)$ is the nSI correlation function corresponding to Doppler boost effect $(L = 1)$ along the $\boldsymbol{\beta}$ direction can be written in terms of minimal isotropic angular correlation functions as

$$C_{nSI}\left(\hat{n}_1,\hat{n}_2\right)=\sum_{\lambda=0}^{1}C_\lambda(\cos\theta)f_\lambda\left(\hat{n}_1,\hat{n}_2\right). \tag{4.8}$$

The above eq. (4.8) provides an explicit expression to compute the angular correlation function $C_{nSI}\left(\hat{n}_1,\hat{n}_2\right)$ for the Doppler-boosted CMB temperature map.

The function $C_\lambda(\cos\theta)$ represents two distinct angular correlation functions, while $f_\lambda\left(\hat{n}_1,\hat{n}_2\right)$ are distinct functions of directions for $\lambda=0,1$. For the $L=1$ case, the functions $f_\lambda\left(\hat{n}_1,\hat{n}_2\right)$ take the form of $f_0\left(\hat{n}_1,\hat{n}_2\right)\equiv[\hat{n}_1]_{10}=\hat{n}_1.\hat{d}$ and $f_1\left(\hat{n}_1,\hat{n}_2\right)\equiv[\hat{n}_2]_{10}=\hat{n}_2.\hat{d}$ (where the indices represent the zeroth component of the rank-1 tensor). These indices specify the projection of the respective vector along the boost direction ($\hat{d}$). We obtain the complete expression for $C_{nSI}\left(\hat{n}_1,\hat{n}_2\right)$ from eq.(4.8) as

$$C_{nSI}\left(\hat{n}_1,\hat{n}_2\right)=C_0(\cos\theta)\hat{n}_1.\hat{d}+C_1(\cos\theta)\hat{n}_2.\hat{d}. \tag{4.9}$$

The explicit form of these two isotropic angular functions can be written as

$$C_0(\cos\theta)=\sum_l\beta^{10}D_l^{TT}\frac{\Pi_{l,l+1}}{\Pi_1}C^{10}_{l,0,l+1,0}\left[\frac{-\sqrt{3}}{4\pi\sqrt{l+1}}(-1)^lP_l^{(1)}(\cos\theta)\right] \tag{4.10}$$

$$C_1(\cos\theta)=\sum_l\beta^{10}D_l^{TT}\frac{\Pi_{l,l+1}}{\Pi_1}C^{10}_{l,0,l+1,0}\left[\frac{-\sqrt{3}}{4\pi\sqrt{l+1}}(-1)^{l+1}P_{l+1}^{(1)}(\cos\theta)\right]. \tag{4.11}$$

These functions represent the angle-dependent correlation functions for the Doppler-boosted CMB temperature map. It is interesting to note that both the angular correlation functions depend on the first derivative of Legendre polynomials $P_\ell^{(1)}(\cos\theta)$, indicating that the nSI signal is related to gradients induced in the temperature map. This represents the generalization of the well-studied standard statistical isotropic correlation function $C_{SI}(\cos\theta)$.

Furthermore, it should also be noted that the magnitudes of the two correlation functions are close but not identical, as evidenced by their explicit mathematical expressions. Since the correlation function is symmetric under the exchange of its arguments, eq. (4.9) is consistent with the symmetric property of the correlation function as the index specified to the mBipoSH correlation functions is in accordance with its direction's index. This can be shown as

$$C\left(\hat{n}_1, \hat{n}_2\right) = C_0(\cos\theta)\hat{n}_1.d + C_1(\cos\theta)\hat{n}_2.d \tag{4.12}$$

Under the switching of $\hat{n}_1 \leftrightarrow \hat{n}_2$, the angular correlation mBipoSH function becomes

$$C_0(\cos\theta) = \sum_{\ell} 2\pi \frac{D_l^{TT}}{l(l+1)} \frac{\Pi_{ll+1}}{\sqrt{4\pi}\Pi_1} C^{10}_{l+10l0} \left[\frac{-\sqrt{3}}{4\pi\sqrt{\ell+1}} (-1)^{l+1} P^{(1)}_{l+1}(\cos\theta) \right]. \tag{4.13}$$

Using the property of CG coefficients,

$$C_0(\cos\theta) = \sum_{\ell} 2\pi \frac{D_l^{TT}}{l(l+1)} \frac{\Pi_{ll+1}}{\sqrt{4\pi}\Pi_1} C^{10}_{l0l+10} \left[\frac{-\sqrt{3}}{4\pi\sqrt{\ell+1}} (-1)^{l+1} P^{(1)}_{l+1}(\cos\theta) \right] = C_1(\cos\theta). \tag{4.14}$$

Hence,

$$C\left(\hat{n}_2, \hat{n}_1\right) = C_1(\cos\theta)\hat{n}_2 + C_0(\cos\theta)\hat{n}_1 = C\left(\hat{n}_1, \hat{n}_2\right). \tag{4.15}$$

This shows that the correlation function is symmetric under $\hat{n}_1 \leftrightarrow \hat{n}_2$.

The figure 4.1 displays the two mBipoSH angular isotropic correlation functions for the nSI Doppler boost effect, which are $C_0(\cos\theta)$ and $C_1(\cos\theta)$ with parameters $b_\nu = 3$ for $\nu = 217$ GHz with $\beta = 1.23 \times 10^{-3}$ along with SI isotropic correlation function. These plots are generated assumings angular power spectrum C_l^{TT} computed for the best-fit ΛCDM model parameters using CAMB (14). This representation makes it evident that the departures from SI temperature fluc-

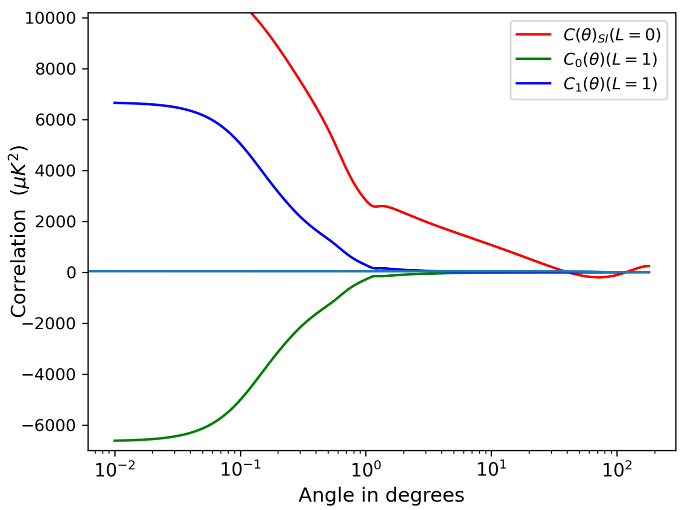

Figure 4.1: Theoretical plots for defined mBipoSH angular correlation functions for Doppler boost.

tuations in a Doppler-boosted map are primarily correlated at small angular separations ($\theta > 1^\circ$) only.

To demonstrate this effect on the simulated maps, we generated 1000 Doppler-boosted CMB maps at 217 GHz using CoNIGS. These maps were generated with a known velocity amplitude of $\beta = 1.23 \times 10^{-3}$ in the known dipole direction. Additionally, we generated 1000 statistically isotropic (SI) maps using the same initial random seed.

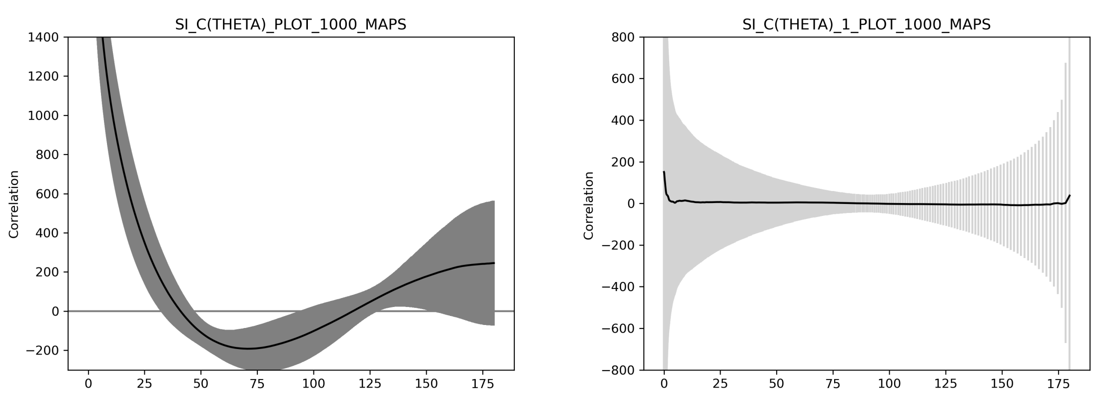

Figure 4.2: C_{SI} and C^1_{nSI} plotted with 1000 simulated SI CMB maps in the respective panels.

In the left panel of figure 4.2, the solid black line depicts the mean of C_{SI} over the 1000 maps, while the light black region represents the 1 sigma variance of the values. This plot agrees with the well-known standard isotropic correlation function, and the error bars approximate well to the cosmic variance limit. In the right panel, a similar plot is shown for the C^1_{nSI} angular correlation function for the SI maps. The Doppler boost effect is null in the SI maps, as expected.

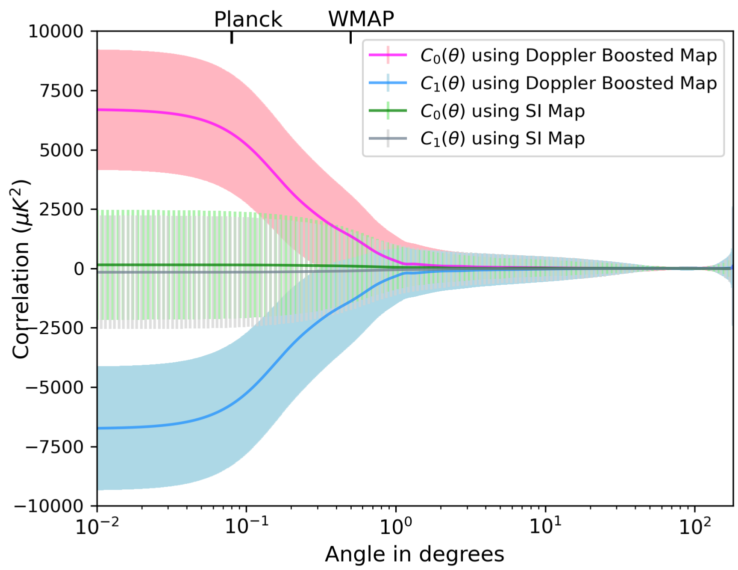

Figure 4.3: The mean and variance of the two mBipoSH angular correlation functions C^0_{nSI} and C^1_{nSI} plotted with 1000 SI and nSI maps generated with same random seed.

The figure 4.2 illustrates the two isotropic correlation functions plotted with nSI maps agrees well with theoretical plots corresponding to the effect, exhibiting non-zero effects at small angles or large l values.

From this plot 4.3, we can readily infer that the Doppler boost signal has higher SNR at smaller angular scales. Hence COBE and WMAP (15), with low resolution, were unable to resolve the Doppler boost effect on small scale CMB fluctuations as the errors bar overlap with that of the SI maps without the effect. However, the Planck mission (11), with its higher resolution, was able to resolve the Doppler boost signal emphatically at 5σ (12), which is clearly visible with the plotted mBipoSH correlation functions. Therefore, real-space angular correlation functions serve the purpose of studying the nSI effect at the suitable resolution. This becomes crucial for verifying certain non-trivial large-scale effects with upcoming high-resolution maps. It is worth noting that this is the first time isotropic correlation functions for the nSI-violated map have been studied in the literature.

4.2 Cosmic Hemispherical Asymmetry

Much like the Doppler boost nSI effect, the Cosmic Hemispherical Asymmetry (CHA) stands out as a well-discussed nSI effect in cosmic microwave background sky maps, manifesting as an $L = 1$ dipole anisotropy. CHA is phenomenologically modeled as a dipolar modulation of a statistically isotropic (SI) CMB sky. Similar to the analysis of the Doppler boost, the study of CHA involves exploring the $l, (l+1)$ correlations in the Bipolar Spherical Harmonics (BipoSH) basis. The CMB temperature anisotropy field, modulated by the dipole in the direction $\hat{n}$, is mathematically expressed as

$$\Delta T(\hat{n}) = (1 + A\hat{p} \cdot \hat{n})\Delta T^{SI}(\hat{n}).$$

Here, $\Delta T^{SI}(\hat{n})$ is the SI CMB temperature field and $\Delta T(\hat{n})$ is the observed nSI temperature field. The direction of the dipolar modulation is specified by $\hat{p} \equiv \left(\theta_p, \phi_p\right)$ with A representing the amplitude of the dipolar modulation.

In the context of cosmic hemispherical asymmetry, the amplitude of dipole modulation is studied to exhibit scale-dependent characteristics. In this scenario, the scale-dependent modulation field is described using the amplitude function $A(l)$ and the dipole direction vector $\hat{p}$, expressed in terms of the spherical harmonic basis as

$$A(l)\hat{p}\cdot\hat{n} = \sum_{N=-1}^{1} m_{1N}(l) Y_{L=1,N}(\hat{n}).$$

The equations that describe the amplitude A and direction (θ_p, ϕ_p) in terms of the spherical harmonic coefficients m_{10}, m^r_{11}, and m^i_{11} are given as

$$A(l) = \sqrt{\frac{3}{4\pi}}\sqrt{m_{10}(l)^2 + 2m^r_{11}(l)^2 + 2m^i_{11}(l)^2}, \quad \theta_p = \cos^{-1}\left[\frac{m_{10}(l)}{A(l)}\sqrt{\frac{3}{4\pi}}\right]$$
$$\text{and } \phi_p = -\tan^{-1}\left[\frac{m^i_{11}(l)}{m^r_{11}(l)}\right].$$

In this study, the dipole modulation amplitude $A(l)$ is modeled using the power-law model as investigated in Shaikh et al (16). The power-law model expresses the dipole modulation amplitude A as

$$A(l) = A\left(l_p\right)\left(\frac{l}{l_p}\right)^{\alpha},$$

where $A\left(l_p\right)$ represents the amplitude at a selected multipole l_p, the power-law dependence of the amplitude can be expressed in the form of spherical harmonic coefficients of the dipole modulation field as

$$m_{1N}(l) = m_{1N}\left(l_p\right)\left(\frac{l}{l_p}\right)^{\alpha}.$$

The CHA effect can be effectively modeled by capturing the correlations between

l and $l+1$ in the BipoSH basis. The covariance matrix can be represented as

$$\begin{aligned} S_{l_1m_1l_2m_2} &\equiv \left\langle a_{l_1m_1}a^*_{l_2m_2}\right\rangle = C_{l_1}\delta_{l_1l_2}\delta_{m_1m_2} \\ &+ \frac{\Pi_{l_1l_2}}{\sqrt{12\pi}}\left[\sum_{N=-1}^{1}\left(m_{1N}\left(l_1\right)C_{l_1}(-1)^{l_1+l_2+1} + m_{1N}\left(l_2\right)C_{l_2}\right)C^{10}_{l_10l_20}C^{1N}_{l_1m_1l_2m_2}\right. \\ &+ \left.\sum_{l'_1m'_1}C_{l'_1}\Pi^2_{l'_1}C^{10}_{l_10l'_10}C^{10}_{l_20l'_10}\sum_{N_1,N_2}m_{1N_1}\left(l'_1\right)m^*_{1N_2}\left(l'_1\right)C^{1N_1}_{l_1m_1l'_1m'_1}C^{1N_2}_{l_2m_2l'_1m'_1}\right]. \end{aligned} \tag{4.16}$$

Using the mathematical framework defined above for CHA, the BipoSH coefficients can be written as

$$A^{1N}_{ll+1}\left(l_p,\alpha\right) = m_{1N}\left(l_p\right)G^1_{ll+1},$$

where G^1_{ll+1} is the shape factor for the cosmic hemispherical asymmetry nSI signal. Specifically, here

$$G^1_{ll+1} \equiv \frac{\Pi_{ll+1}}{\sqrt{12\pi}}\left[\left(\frac{l}{l_p}\right)^{\alpha}C_l + \left(\frac{l+1}{l_p}\right)^{\alpha}C_{l+1}\right]C^{10}_{l0l+10}.$$

The most general correlation function for a nSI map can be expressed in terms of mBipoSH angular functions as

$$C(\hat{n}_1,\hat{n}_2) = \sum_{L,M}\sum_{\lambda=0}^{L}\alpha^{L,M}_{\lambda}(\cos\theta)Y^{\lambda,L-\lambda}_{LM}(\hat{n}_1,\hat{n}_2). \tag{4.17}$$

The nSI CMB sky map corresponding to cosmic hemispherical asymmetry effect will include the dipole signal $(L=1)$ in addition to the standard isotropic (SI) contribution at $L=0$. This can be expanded as follows

$$C(\hat{n}_1,\hat{n}_2) = C_{SI}(\cos\theta) + \sum_{M=(-1,0,1)}\sum_{\lambda=0}^{1}\alpha^{1,M}_{\lambda}(\cos\theta)Y^{\lambda,1-\lambda}_{1M}(\hat{n}_1,\hat{n}_2). \tag{4.18}$$

As the direction of dipole modulation is modeled as $'p,'$ designating this as our primary direction in the BipoSH basis, it follows that only the $M = 0$ component will persist, having other M components null. Employing these, we obtain correlation function having SI and nSI part as

$$C(\hat{n}_1, \hat{n}_2) = C_{SI}(\cos\theta) + \alpha_0^{1,0}(\cos\theta)[n_1]_{1,0} + \alpha_1^{1,0}(\cos\theta)[n_2]_{1,0}. \tag{4.19}$$

Calculating the mBipoSH angular functions using the equation (3.14) and the relation $[n]_{1,0} = \hat{n} \cdot \hat{p}$, the correlation function can be expanded as

$$C_{nSI}\left(\hat{n}_1, \hat{n}_2\right) = C_0(\cos\theta)\hat{n}_1.\hat{p} + C_1(\cos\theta)\hat{n}_2.\hat{p} \tag{4.20}$$

Here, $C_0(\cos\theta)$ and $C_1(\cos\theta)$ represent the set of two isotropic angular correlation functions corresponding to dipole anisotropy associated with CHA. These functions can be expressed as

$$C_0(\cos\theta) = \sum_l m_{1N}\left(l_p\right) G^1_{ll+1}\left[\frac{-\sqrt{3}}{4\pi\sqrt{l+1}}(-1)^l P_l^{(1)}(\cos\theta)\right] \tag{4.21}$$

$$C_1(\cos\theta) = \sum_l m_{1N}\left(l_p\right) G^1_{ll+1}\left[\frac{-\sqrt{3}}{4\pi\sqrt{l+1}}(-1)^{l+1} P_{l+1}^{(1)}(\cos\theta)\right]. \tag{4.22}$$

In the left panel of figure 4.4, we present the theoretical mBipoSH angular correlation functions generated using the best-fit ΛCDM model parameters obtained from CAMB. The right panel displays the mean of two mBipoSH angular correlation functions generated from 1000 different maps corresponding to the CHA effect and the Doppler effect. The shaded region represents the variance of the mBipoSH functions calculated from the SI maps.

From Figure 4.4, it becomes evident that the cosmic hemispherical effect exhibits minimal impact at extremely small angles, especially in comparison to the

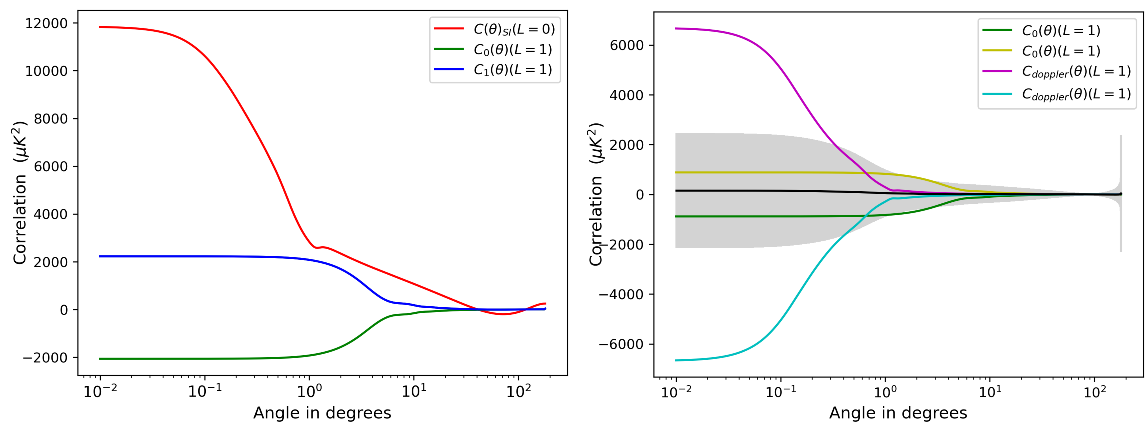

Figure 4.4: The left panel displays the two theoretical mBipoSH correlation functions for the nSI effect CHA, namely $C_0(\cos\theta)$ and $C_1(\cos\theta)$ along with the SI correlation function. The right panel presents the cosmic variance error bar for these mBipoSH correlation functions using 1000 simulated CHA maps generated by CoNIGS (1) compared with Doppler effect.

pronounced influence of the Doppler boost effect. However, as the angles increase, the cosmic hemispherical effect progressively becomes more dominant compare to the Doppler effect. Analysis of the error bar plot leads us to the conclusion that the signal strength of the cosmic hemispherical anomaly resides within the confines of the cosmic variance bars delineated in the Statistical Isotropic plots. Consequently, drawing a decisive inference regarding the presence of the cosmic hemispherical effect versus random realizations of the cosmic microwave background (CMB) sky is inconclusive at this juncture. This agrees with previously used methods, which have detected the signal of CHA at a significance level of around 3σ, consistently referring in the same direction. It is noteworthy that different statistical methods lead to approximately similar conclusionss.

4.3 Non Circular Beam Effects

The observed cosmic microwave background anisotropy on the sky results from convolving the intrinsic cosmological CMB signal with the instrumental beam response function. Inevitable deviations from circular symmetry in instrumental beams coupled with specific scan strategies from the instrument can lead to detectable violations of Statistical Isotropy (SI) in CMB datasets. Typically the most prominent deviation from circularity focusses on the $L = 2$ quadrupole effect as measured in WMAP-7 data. This is evident when modeling the anisotropic beam as an elliptical case. This approach enables a new direction to the investigation of deviations from circular symmetry in instrumental beams through SI violations in the CMB data.

To quantify SI violation for the non-circular beam case, studying its effect in the BipoSH basis leads to expansion coefficients known as beam-BipoSH coefficients ($B^{LM}_{l_1 l_2}$). For an ideal circularly symmetric beam, only the $L = 0$ beam-BipoSH coefficients are non-vanishing. However, the breakdown of circular symmetry further induces $L \neq 0$ modes in these coefficients.

The observed CMB temperature results from the convolution of the actual underlying CMB temperature with the instrument beam can be expressed as

$$\widetilde{\Delta T}\left(\hat{n}_1\right) = \int d\Omega_{\hat{n}_2} B\left(\hat{n}_1, \hat{n}_2\right) \Delta T\left(\hat{n}_2\right).$$

Here, $\Delta T\left(\hat{n}_2\right)$ is the underlying true sky temperature along $\hat{n}_2$ and $\widetilde{\Delta T}\left(\hat{n}_1\right)$ is the temperature measured along the direction $\hat{n}_1$. The factor $B\left(\hat{n}_1, \hat{n}_2\right)$ is known as the beam response function and gives the sensitivity of the detector around the pointing direction, $\hat{n}_1$.

The beam response function can be expanded in terms of BipoSH basis as

$$B\left(\hat{n}_1, \hat{n}_2\right) = \sum_{l_1 l_2 LM} B^{LM}_{l_1 l_2} Y^{l_1 l_2}_{LM}, \tag{4.23}$$

$B^{LM}_{l_1 l_2}$ represents the beam-BipoSH coefficients. The observed beam convolved temperature can be related to the spherical harmonic coefficients, $a_{\ell m}$ of the underlying

CMB signal in the terms of these beam-BipoSH coefficients as

$$\widetilde{\Delta T}\left(\hat{n}_1\right) = \sum_{l_1 m_1} \sum_{lmLM} (-1)^m a_{lm} B^{LM}_{l_1 l} C^{LM}_{l_1 m_1 l -m} Y_{l_1 m_1}\left(\hat{n}_1\right).$$

The spherical harmonic coefficients corresponding to beam convolved temperature can be given as

$$\tilde{a}_{l_1 m_1} = \sum_{lmLM} (-1)^m a_{lm} B^{LM}_{l_1 l} C^{LM}_{l_1 m_1 l -m},$$

We compute the covariance matrix for these spherical harmonic coefficients as

$$\left\langle \tilde{a}_{l_1 m_1} \tilde{a}_{l_2 m_2} \right\rangle = \sum_{lmLM} \sum_{l'm'L'M'} (-1)^{m+m'} \left\langle a_{lm} a_{l'm'} \right\rangle \times B^{LM}_{l_1 l} B^{LM}_{l_2 l'} C^{LM}_{l_1 m_1 l -m} C^{L'M'}_{l_2 m_2 l' -m'}.$$

Under the condition of underlying CMB signal to be statistically isotropic, which implies $\langle a_{lm} a_{l'm'} \rangle = (-1)^m C_l \delta_{ll'} \delta_{m-m'}$, the covariance matrix becomes

$$\left\langle \tilde{a}_{l_1 m_1} \tilde{a}_{l_2 m_2} \right\rangle = \sum_{lmLM} \sum_{L'M'} (-1)^m C_l B^{LM}_{l_1 l} B^{L'M'}_{l_2 l} C^{LM}_{l_1 m_1 l -m} C^{L'M'}_{l_2 m_2 l m}.$$

Using the covariance matrix, the BipoSH coefficients can be evaluated to be

$$\tilde{A}^{L_1 M_1}_{l_1 l_2} = \sum_{lLL'MM'} C_l B^{LM}_{l_1 l} B^{L'M'}_{l_2 l} \times \sum_{m m_1 m_2} (-1)^m C^{LM}_{l_1 m_1 l -m} C^{L'M'}_{l_2 m_2 l m} C^{L_1 M_1}_{l_1 m_1 l_2 m_2}$$

We can simplify the product of three Clebsch-Gordan coefficients using the identity involving a 6-j symbol given as (6)

$$\sum_{\alpha\beta\delta} (-1)^{a-\alpha} C^{c\gamma}_{a\alpha b\beta} C^{e\epsilon}_{d\delta b\beta} C^{f\varphi}_{d\delta a-\alpha} = K_1 \prod_{cf} C^{e\epsilon}_{c\gamma f\varphi} \left\{ \begin{array}{ccc} a & b & c \\ e & f & d \end{array} \right\},$$

where $K_1 = (-1)^{b+c+d+f}$ and $\prod_{cf} = \sqrt{(2c+1)(2f+1)}$.

Hence, the BipoSH coefficients that capture the non-circular (NC) nSI effect from the observed two-point temperature correlation function can be expressed in terms of the Beam-BipoSH coefficients as

$$\tilde{A}^{L_1 M_1}_{l_1 l_2}$$
$$= \sum_{lLML'M'} C_l B^{LM}_{l_1 l} B^{L'M'}_{l_2 l} (-1)^{l_1+L'-L_1} \sqrt{(2L+1)\,(2L'+1)} C^{L_1 M_1}_{LML'M'} \left\{ \begin{array}{ccc} l & l_1 & L \\ L_1 & L' & l_2 \end{array} \right\}$$

The beam-BipoSH spectrum does not just depend on NC-beam harmonics. It also depends on how the scan pattern on the sky of the experiment, which is described by the orientation of the beam relative to the local longitude quantified by the angle $\rho(\hat{n})$ for different pointing directions ($\hat{n} \equiv (\theta, \phi)$). The formula for beam-BipoSH can be dealt with more easily when the scanning pattern makes $\rho(\hat{n})$ stay the same. We call this kind of scanning pattern a 'parallel-transport' (PT) scan, as mentioned in (17; 18). This means the beam's orientation stays constant compared to the local longitude wherever you look in the sky. This idealised scanning method leads to $M = 0, M' = 0, M_1 = 0$. In that case, the BipoSH coefficients can be written as

$$\tilde{A}^{L_1 0}_{l_1 l_2} = \sum_{lLL'} C_l B^{L0}_{l_1 l} B^{L'0}_{l_2 l} (-1)^{l_1+L'-L_1} \times \sqrt{(2L+1)\,(2L'+1)} C^{L_1 0}_{L0L'0} \left\{ \begin{array}{ccc} l & l_1 & L \\ L_1 & L' & l_2 \end{array} \right\}.$$

The non-circular beam effect can be computed within the $L = 2$ multipole using the PT scan strategy. This involves correlations of the types $l\ l$ and $l\ (l-2)$ in harmonic space. By applying this condition, the BipoSH coefficients can be expressed as

$$\begin{aligned}\tilde{A}^{20}_{ll} &= \frac{(-1)^l 2\sqrt{5} C_l B^{00}_{ll} B^{20}_{ll}}{\left(\prod_l\right)^3 C^{20}_{l0l0}} \\ \tilde{A}^{20}_{ll+2} &= \frac{\sqrt{5}(-1)^l}{\prod_{ll+2} C^{20}_{l0l+20}} \times \left[\frac{C_l B^{00}_{ll} B^{20}_{l+2l}}{\prod_l} + \frac{C_{l+2} B^{00}_{l+2l+2} B^{20}_{ll+2}}{\prod_{l+2}}\right]\end{aligned} \tag{4.24}$$

Utilizing the formalism established in the preceding section, the correlation function can be expanded in terms of mBipoSH angular correlation functions in a similar manner for this particular case, as

$$C(\hat{n}_1, \hat{n}_2) = C_{SI}(\cos\theta) + \sum_{\lambda=0}^{2} \alpha^{2,0}_{\lambda}(\cos\theta) Y^{\lambda, 2-\lambda}_{20}(\hat{n}_1, \hat{n}_2). \tag{4.25}$$

The equation can be simplied to set of isotropic correlation functions as

$$\begin{aligned}C(\hat{n}_1, \hat{n}_2) = C_{SI}(\cos\theta) + C_0(\cos\theta) f_0(\hat{n}_1, \hat{n}_2) + C_1(\cos\theta) f_1(\hat{n}_1, \hat{n}_2) \\ + C_2(\cos\theta) f_2(\hat{n}_1, \hat{n}_2).\end{aligned} \tag{4.26}$$

where $C_0(\cos\theta)$, $C_1(\cos\theta)$, and $C_2(\cos\theta)$ are the three mBipoSH angular correlation functions that define the theta space correlations corresponding to the NC beam nSI effect. Additionally, $f_\lambda(\hat{n}_1, \hat{n}_2)$ represents rank-2 tensor functions dependent on the directions of the measurement. The analytic form of these three angular correlation functions can be expressed using the expressions (4.25) and (4.26) as

$$C_\lambda(\cos\theta) = \sum_l \left(A^{20}_{ll} a_\lambda(l, l, 2, \cos\theta) + A^{20}_{ll+2} a_\lambda(l, l+2, 2, \cos\theta) \right) \quad \text{where } \lambda = 0, 1, 2. \tag{4.27}$$

We can readily compute the coefficients a_λ from the equation (3.14) defined in previous chapter and subsequently determine the mBipoSH isotropic angular functions as follows

$$C_0(\cos\theta) = \sum_l \frac{(-1)^l 2\sqrt{5} C_l B^{00}_{ll} B^{20}_{ll}}{\left(\prod_l\right)^3 C^{20}_{l0l0}} \frac{(-1)^{l+1}}{4\pi} \left[\frac{30(2l+1)}{(2l-1)l(l+1)(2l+3)}\right]^{\frac{1}{2}} P^{(2)}_l(\cos\theta) +$$
$$\frac{\sqrt{5}(-1)^l}{\prod_{l-2l} C^{20}_{l-20l0}} \left[\frac{C_{l-2} B^{00}_{l-2l-2} B^{20}_{ll-2}}{\prod_{l-2}} + \frac{C_l B^{00}_{ll} B^{20}_{l-2l}}{\prod_l}\right]$$
$$\frac{(-1)^l}{4\pi} \sqrt{\frac{5}{(l+2)\,(2l+3)\,(l+1)}} P^{(2)}_l(\cos\theta) \tag{4.28}$$

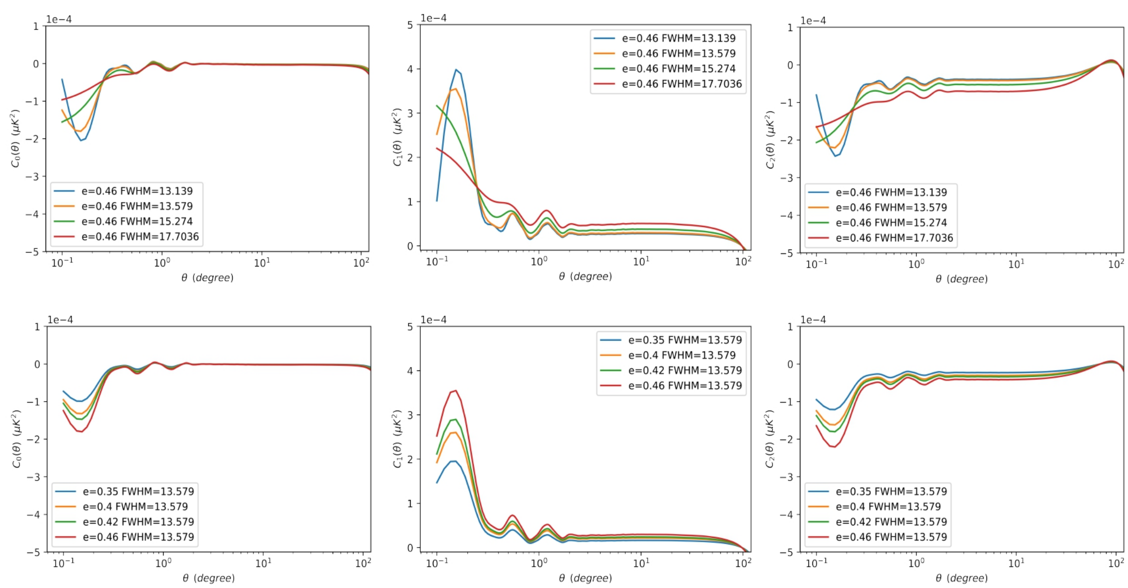

Figure 4.5: Illustration of the mBipoSH isotropic correlation functions for the non-circular beam. Top panel shows how the correlation functions vary with the change in θ_{FWHM}. The bottom panel shows how these isotropic correlation functions change with respect to e.

$$C_1(\cos\theta) = \sum_l \frac{(-1)^l 2\sqrt{5} C_l B^{00}_{ll} B^{20}_{ll}}{(\prod_l)^3 C^{20}_{l0l0}} \frac{(-1)^{l+1}}{4\pi} \left[\frac{30(2l+1)}{(2l-1)l(l+1)(2l+3)}\right]^{\frac{1}{2}} P^{(1)}_l(\cos\theta) +$$
$$\frac{\sqrt{5}(-1)^l}{\prod_{l-2l} C^{20}_{l-20l0}} \left[\frac{C_{l-2} B^{00}_{l-2l-2} B^{20}_{ll-2}}{\prod_{l-2}} + \frac{C_l B^{00}_{ll} B^{20}_{l-2l}}{\prod_l}\right]$$
$$\frac{(-1)^l}{4\pi} \sqrt{\frac{5}{(l+2)\,(2l+3)\,(l+1)}} (-2) P^{(2)}_{l+1}(\cos\theta) \tag{4.29}$$

$$C_2(\cos\theta) = \sum_l \frac{(-1)^l 2\sqrt{5} C_l B^{00}_{ll} B^{20}_{ll}}{(\prod_l)^3 C^{20}_{l0l0}} \frac{(-1)^{l+1}}{4\pi} \left[\frac{30(2l+1)}{(2l-1)l(l+1)(2l+3)}\right]^{\frac{1}{2}} P^{(2)}_l(\cos\theta)$$
$$+ \frac{\sqrt{5}(-1)^l}{\prod_{l-2l} C^{20}_{l-20l0}} \left[\frac{C_{l-2} B^{00}_{l-2l-2} B^{20}_{ll-2}}{\prod_{l-2}} + \frac{C_l B^{00}_{ll} B^{20}_{l-2l}}{\prod_l}\right]$$
$$\frac{(-1)^l}{4\pi} \sqrt{\frac{5}{(l+2)\,(2l+3)\,(l+1)}} P^{(2)}_{l+2}(\cos\theta). \tag{4.30}$$

These equations represent the mBipoSH isotropic angular correlation functions for quadrupole anisotropy with l,l and l,$l+2$ like correlations.

The analytic forms for the three distinct mBipoSH angular correlation functions can be plotted for the $L = 2$ non-circular (NC) beam case, as shown in the figure 4.3. It is deduced from the plots that the nSI effect associated with the NC beam can be effectively captured by a set of three isotropic angular correlation functions in the theta-space. This results in noticeable signatures in the correlation functions, assuming a PT scan. Therefore, mBipoSH correlation functions can prove to be crucial in mitigating systematic effects for various experiments. We intend to extend the calculation to more generalized scanning strategies in future studies.

4.4 Real Space based Estimation Method

In this section, our objective is to develop a minimum variance-based pixel space estimator for the mBipoSH isotropic angular correlation functions. This estimator will help us to effectively study the signal strength of non-statistically isotropic effects present in the CMB data. By using this approach, we aim to study and analyze large scale nSI effects.

Additionally, our proposed mBipoSH method is applicable to partial sky data missions like ACT (Atacama Cosmology Telescope) and SPT (South Pole Telescope) as it captures the features in theta-space based estimators. This adaptability is important as partial sky data missions face challenges due to incomplete sky coverage. By using our estimator, we aim to study accurate and reliable analysis of nSI effects with partial sky data.

4.4.1 Minimum Variance Estimator

To derive a Minimum Variance Estimator for mBipoSH functions similar to (19–21), we start with the expression

$$\hat{\alpha}^{LM}_{\lambda}(\cos\theta) = \alpha^{LM}_{\lambda}(\cos\theta) + \Gamma_{LM} G^{L}_{\lambda}(\cos\theta)\,,$$

Here, $\hat{\alpha}^{LM}_{\lambda}(\cos\theta)$ represents the observed mBipoSH coefficient, while $\alpha^{LM}_{\lambda}(\cos\theta)$ denotes the mBipoSH coefficient for a statistically isotropic (SI) field, whose ensemble average tends to zero. The term $\Gamma_{LM} G^{L}_{ll'}$ serves as the source of SI violation, with $G^{L}_{\lambda}(\cos\theta)$ representing the shape factor.

To illustrate this, we begin with a scenario of $L = 1$ anisotropy. In the case of Doppler boost, $\alpha^{LM}_{\lambda}(\cos\theta)$ is non-zero for a single sky. To measure the β_{1M}

parameter, we define the estimator $\hat{\beta}_{LM}$ for $L = 1$.

$$\hat{\beta}_{1M} = \sum_{\theta} \frac{\alpha_{\lambda}^{1M}(\cos\theta)}{G_{\lambda}^{1}(\cos\theta)} + \beta_{1M} \,. \tag{4.31}$$

To estimate the significance of signal, β from the estimator, $\hat{\beta}$, we need to evaluate the variance of the estimator for SI sky.

$$\begin{aligned}(\hat{\sigma}_{\beta})^2 \equiv \left\langle \hat{\beta}^{*}_{1M}\hat{\beta}_{1M'} \right\rangle = \sum_{\theta_1\theta_2} \frac{\left\langle \alpha_{\lambda}^{*1M}(\cos\theta_1)\alpha_{\lambda'}^{1M'}(\cos\theta_2) \right\rangle}{G_{\lambda}^{1}(\cos\theta_1)G_{\lambda'}^{1}(\cos\theta_2)} + |\beta_1|^2 \,, \\ (\hat{\sigma}_{\beta})^2 = N_1 + |\beta_1|^2,\end{aligned} \tag{4.32}$$

where N_1 can be written as,

$$N_1 = \sum_{\theta_1\theta_2} \frac{\left\langle \alpha_{\lambda}^{*1M}(\cos\theta_1)\alpha_{\lambda'}^{1M'}(\cos\theta_2) \right\rangle}{G_{\lambda}^{1}(\cos\theta_1)G_{\lambda'}^{1}(\cos\theta_2)}. \tag{4.33}$$

To calculate the two point correlation function of mBipoSH functions, We have

$$\alpha_{\lambda}^{L,M}(\cos\theta) = \sum_{m_1 m_2} \sum_{\ell_1 \ell_2} a_{l_1 m_1} a^{*}_{l_2 m_2} (-1)^{m_2} C^{LM}_{l_1 m_1 l_2 - m_2} a_{\lambda}(l_1, l_2, L, \cos\theta). \tag{4.34}$$

Expanding the two point correlation function as

$$\begin{aligned}
&\left\langle \alpha_{\lambda}^{*LM}(\cos\theta_1)\alpha_{\lambda'}^{*L'M'}(\cos\theta_2)\right\rangle \\
&= \sum_{m_1m_2}\sum_{\ell_1\ell_2} a_{l_1m_1}a^*_{l_2m_2}(-1)^{m_2}C^{LM}_{l_1m_1l_2-m_2}a_\lambda(l_1,l_2,L,\cos\theta_1) \\
&\times \sum_{m_3m_4}\sum_{\ell_3\ell_4}\left(a_{l_3m_3}a^*_{l_4m_4}\right)^*(-1)^{m_4}C^{L'M'}_{l_3m_4l_3-m_4}a_{\lambda'}(l_3,l_3,L',\cos\theta_2) \\
&= \sum_{m_1m_2m_3m_4}\sum_{\ell_1\ell_2\ell_3\ell_4}(-1)^{m_2}C^{LM}_{l_1m_1l_2-m_2}a_\lambda(l_1,l_2,L,\cos\theta_1) \\
&(-1)^{m_4}C^{L'M'}_{l_3m_4l_3-m_4}a_{\lambda'}(l_3,l_3,L',\cos\theta_2)(-1)^{m_3+m_4} \\
&\left\langle a_{l_1m_1}a^*_{l_2m_2}a_{l_3-m_3}a^*_{l_4-m_4}\right\rangle .
\end{aligned} \tag{4.35}$$

In order to evaluate the expectation value $\left\langle a_{l_1m_1}a^*_{l_2m_2}a_{l_3m_3}a^*_{l_4m_4}\right\rangle$ for Gaussian random variables, we use the expression:

$$\left\langle x_ix_jx_kx_l\right\rangle = \left\langle x_ix_j\right\rangle\left\langle x_kx_l\right\rangle + \left\langle x_ix_k\right\rangle\left\langle x_jx_l\right\rangle + \left\langle x_ix_l\right\rangle\left\langle x_jx_k\right\rangle .$$

Applying this to our case, we have the expression as

$$\begin{aligned}
\left\langle a_{l_1m_1}a^*_{l_2m_2}a_{l_3m_3}a^*_{l_4m_4}\right\rangle &= \left\langle a_{l_1m_1}a^*_{l_2m_2}\right\rangle\left\langle a_{l_3m_3}a^*_{l_4m_4}\right\rangle + \left\langle a_{l_1m_1}a_{l_3m_3}\right\rangle\left\langle a^*_{l_2m_2}a^*_{l_4m_4}\right\rangle \\
&+ \left\langle a_{l_1m_1}a^*_{l_4m_4}\right\rangle\left\langle a_{l_2m_2}a^*_{l_3m_3}\right\rangle \\
&= C_{l_1}C_{l_3}\delta_{l_1l_2}\delta_{m_1m_2}\delta_{l_3l_4}\delta_{m_3m_4} \\
&+ C_{l_1}C_{l_2}\delta_{l_1l_3}\delta_{m_1m_3}\delta_{l_2l_4}\delta_{m_2m_4} \\
&+ C_{l_1}C_{l_2}\delta_{l_1l_4}\delta_{m_1m_4}\delta_{l_3l_2}\delta_{m_3m_2}
\end{aligned}$$

These terms contribute to the four-point function. We show that the first term is the SI part as

$$
\begin{aligned}
&\left\langle \alpha_{\lambda}^{*LM}(\cos\theta_1)\alpha_{\lambda'}^{*L'M'}(\cos\theta_2)\right\rangle_{SI} \\
&= \sum_{m_1m_2m_3m_4}\sum_{\ell_1\ell_2\ell_3\ell_4}(-1)^{m_2}C^{LM}_{l_1m_1l_2-m_2}a_\lambda(l_1,l_2,L,\cos\theta_1)(-1)^{m_3+m_4} \\
&(-1)^{m_4}C^{L'M'}_{l_3m_4l_3-m_4}a_{\lambda'}(l_3,l_4,L',\cos\theta_2)C_{l_1}C_{l_3}\delta_{l_1l_2}\delta_{m_1m_2}\delta_{l_3l_4}\delta_{m_3m_4} \\
&= \sum_{m_1m_3}\sum_{\ell_1\ell_3}(-1)^{m_1+m_3}C^{LM}_{l_1m_1l_1-m_1}C^{L'M'}_{l_3m_3l_3-m_3} \\
&a_\lambda(l_1,l_1,L,\cos\theta_1)a_{\lambda'}(l_3,l_3,L',\cos\theta_2)C_{l_1}C_{l_3} \\
&= \sum_{\ell_1\ell_3}\left(\sum_{m_1}(-1)^{m_1}C^{LM}_{l_1m_1l_1-m_1}\right)\left(\sum_{m_3}(-1)^{m_3}C^{L'M'}_{l_3m_3l_3-m_3}\right) \\
&a_\lambda(l_1,l_1,L,\cos\theta_1)a_{\lambda'}(l_3,l_3,L',\cos\theta_2)C_{l_1}C_{l_3}
\end{aligned}
\tag{4.36}
$$

Using relations for CG coefficients:

$$
\begin{aligned}
\sum_{\alpha}(-1)^{a-\alpha}C^{c0}_{a\alpha a-\alpha} &= \prod_{a}\delta_{c0} \\
\sum_{\alpha\beta}C^{c\gamma}_{a\alpha b\beta}C^{c'\gamma'}_{a\alpha b\beta} &= \delta_{cc'}\delta_{\gamma\gamma'} \\
\sum_{c\gamma}C^{c\gamma}_{a\alpha b\beta}C^{c\gamma}_{a\alpha' b\beta'} &= \delta_{\alpha\alpha'}\delta_{\beta\beta'}
\end{aligned}
$$

We obtain that

$$
\begin{aligned}
&\left\langle \alpha_{\lambda}^{*LM}(\cos\theta_1)\alpha_{\lambda'}^{*L'M'}(\cos\theta_2)\right\rangle_{SI} \\
&= \sum_{\ell_1\ell_3}\left(\prod_{\ell_1}\delta_{L0}\right)\left(\prod_{\ell_3}\delta_{L'0}\right)a_\lambda(l_1,l_1,L,\cos\theta_1)a_{\lambda'}(l_3,l_3,L',\cos\theta_2)C_{l_1}C_{l_3} \\
&= \left(\sum_{\ell_1}\sqrt{2\ell_1+1}a_\lambda(l_1,l_1,0,\cos\theta_1)C_{l_1}\right)\left(\sum_{\ell_3}\sqrt{2\ell_3+1}a_\lambda(l_3,l_3,0,\cos\theta_2)C_{l_3}\right) \\
&= \langle C(\theta_1)\rangle\langle C(\theta_2)\rangle .
\end{aligned}
\tag{4.37}
$$

Ignoring this term, as there cannot be a monopolar $(L = 0)$ violation of isotropy. A monopolar isotropy violating field is equivalent to rescaling the temperature anisotropies and will be indistinguishable from a change in the power spectral amplitude.

Now using 2nd term, we will show 2nd and 3rd terms are similar and contribute to nSI terms in variance for $L > 0$.

$$
\begin{aligned}
&\left\langle \alpha_{\lambda}^{LM}(\cos\theta_1)\alpha_{\lambda'}^{*L'M'}(\cos\theta_2)\right\rangle_{nSI} \\
&= \sum_{m_1 m_2 m_3 m_4} \sum_{\ell_1\ell_2\ell_3\ell_4} (-1)^{m_2} C^{LM}_{l_1 m_1 l_2 -m_2} a_{\lambda}(l_1, l_2, L, \cos\theta_1)(-1)^{m_3+m_4} \\
&\times (-1)^{m_4} C^{L'M'}_{l_3 m_3 l_4 -m_4} a_{\lambda'}(l_3, l_4, L', \cos\theta_2) C_{l_1} C_{l_2} \delta_{l_1 l_3}\delta_{m_1 m_3}\delta_{l_2 l_4}\delta_{m_2 m_4} \\
&= \sum_{m_1 m_2}\sum_{\ell_1\ell_2} (-1)^{m_2+m_2} C^{LM}_{l_1 m_1 l_2 -m_2} C^{L'M'}_{l_1 m_1 l_2 -m_2} \\
&\times a_{\lambda}(l_1, l_2, L, \cos\theta_1) a_{\lambda'}(l_1, l_2, L', \cos\theta_2) C_{l_1} C_{l_2} \\
&= \sum_{\ell_1\ell_2}\left(\sum_{m_1 m_2} C^{LM}_{l_1 m_1 l_2 -m_2} C^{L'M'}_{l_1 m_1 l_2 -m_2}\right) \\
&\times a_{\lambda}(l_1, l_2, L, \cos\theta_1) a_{\lambda'}(l_1, l_2, L', \cos\theta_2) C_{l_1} C_{l_2} \\
&= \sum_{\ell_1\ell_2} (\delta_{LL'}\delta_{MM\prime})\, a_{\lambda}(l_1, l_2, L, \cos\theta_1) a_{\lambda'}(l_1, l_2, L', \cos\theta_2) C_{l_1} C_{l_2} \\
&= \sum_{\ell_1\ell_2} a_{\lambda}(l_1, l_2, L, \cos\theta_1) a_{\lambda'}(l_1, l_2, L, \cos\theta_2) C_{l_1} C_{l_2}
\end{aligned}
\tag{4.38}
$$

We can show similary that another term will result into same expression hence,

$$
\left\langle \alpha_{\lambda}^{LM}(\cos\theta_1)\alpha_{\lambda'}^{*L'M'}(\cos\theta_2)\right\rangle_{nSI} = \sum_{\ell_1\ell_2} 2a_{\lambda}(l_1, l_2, L, \cos\theta_1) a_{\lambda'}(l_1, l_2, L, \cos\theta_2) C_{l_1} C_{l_2}
\tag{4.39}
$$

Now using this relations, the reconstruction noise,

$$N_1 = \sum_{\theta_1\theta_2} \frac{\sum_{\ell_1\ell_2} 2a_\lambda(l_1,l_2,L,\cos\theta_1)a_{\lambda'}(l_1,l_2,L,\cos\theta_2)C_{l_1}C_{l_2}}{G^1_\lambda(\cos\theta_1)G^1_{\lambda'}(\cos\theta_2)}. \tag{4.40}$$

To arrive at the minimum variance estimator, we seek an optimally weighted linear combination

$$\hat{\beta}_{1M} = \sum_\theta w^L_\lambda(\cos\theta)\frac{\alpha^{1M}_\lambda(\cos\theta)}{G^1_\lambda(\cos\theta)} + \beta_{1M}\,, \tag{4.41}$$

where $w^L_\lambda(\cos\theta)$ are the weights satisfies the constraint $\sum_\theta w^L_\lambda(\cos\theta) = 1$. These weight factors should be chosen to minimize the reconstruction noise.

$$(\hat{\sigma}_\beta)^2 = \sum_{\theta_1\theta_2} w^L_\lambda(\cos\theta_1)w^L_\lambda(\cos\theta_2)\frac{\left\langle \alpha^{*1M}_\lambda(\cos\theta_1)\alpha^{1M'}_{\lambda'}(\cos\theta_2)\right\rangle}{G^1_\lambda(\cos\theta_1)G^1_{\lambda'}(\cos\theta_2)} + |\beta_1|^2\,. \tag{4.42}$$

Using the *Lagrange multiplier* method, we obtain, as a solution of matrix equation for the $1\times N_{obs}$ weights array as

$$\frac{\partial}{\partial w} w^T C w = 0$$

In the above, the matrix $C = \langle dd^T\rangle$ represents the covariance matrix with dimensions $N_{\rm obs}\times N_{\rm obs}$ for the temperature data maps. Here, $\langle ..\rangle$ denotes the average taken over all pixels within the region of interest.

Further, the weights array satisfies the constraint $w^T a = 1$, where a is an array of unity elements. By using the Lagrange mutliplier conditions, this contraint equation can be given as

$$\frac{\partial}{\partial w}\left[w^T C w + \lambda(1 - w^T a)\right] = 0$$

Solving the system of equations, we can determine the weights given as

$$w^T = a^T C^{-1} (aC^{-1}a)^{-1}.$$

Using this formalism, we can calculate the weights and subsequently compute the signal strength for the non-statistical isotropy (nSI) estimator. It is important to note that this estimator provides estimates for mBipoSH angular functions. We can also directly compute the relevant signal strength from correlation function computations. Similarly, when employing this for a Doppler-like effect at $L = 1$ dipole anisotropy, we can express it as

$$C\left(\hat{n}_1, \hat{n}_2\right) = C_{SI}(\cos\theta) + C_{nSI}(\hat{n}_1, \hat{n}_2). \tag{4.43}$$

Considering the SI part as noise, the signal strength of the nSI encoded in the other part of the correlation function can be expanded as

$$C\left(\hat{n}_1, \hat{n}_2\right) = \beta^{1N} F_{1N}(\hat{n}_1, \hat{n}_2) + C_{SI}(\cos\theta). \tag{4.44}$$

In this case, the velocity signal strength can be expressed as

$$\hat{\beta}^{1N} = \sum_{n_1, n_2} w_{n_1, n_2} \frac{C\left(\hat{n}_1, \hat{n}_2\right)}{F_{1N}\left(\hat{n}_1, \hat{n}_2\right)}. \tag{4.45}$$

The variance term for such analysis can be written as

$$(\hat{\sigma}_\beta)^2 = \sum_{n_1, n_2, n_3, n_4} w_{n_1, n_2} w_{n_3, n_4} \frac{C\left(\hat{n}_1, \hat{n}_2\right)}{F_{1N}\left(\hat{n}_1, \hat{n}_2\right)} \frac{C\left(\hat{n}_3, \hat{n}_4\right)}{F_{1N}\left(\hat{n}_3, \hat{n}_4\right)} + |\beta_1|^2. \tag{4.46}$$

The weights defined can be solved using a method similar to that defined in the earlier approach. Consequently, the signal strength can be directly calculated from the temperature fluctuations values extracted from the measured CMB maps, offering a novel method for computing the nSI signal strengths. Moreover, this technique is applicable to partial sky maps as well.

4.5 Analysis of Planck Data

In this part, we aim to make plots showing how the mBipoSH isotropic angular correlation functions behave based on the data collected by the Planck satellite.

To ensure our results are accurate, we use two different sets of maps that have been cleaned of foreground signals. SEVEM uses the template fitting method to extract the clean CMB map free from foregrounds, whereas SMICA gives the foreground-cleaned maps by linearly combining the observed CMB maps across different frequencies with multipole-dependent weights.

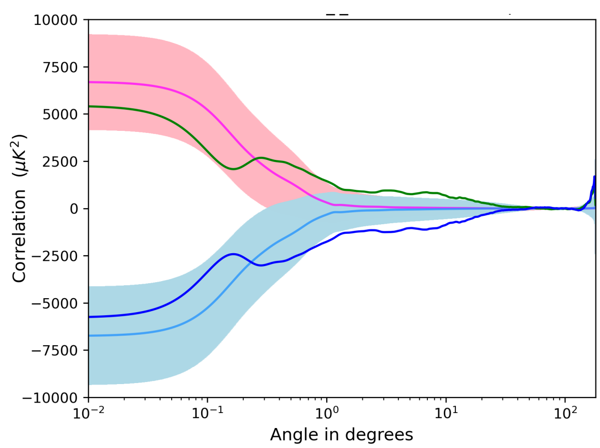

Figure 4.6: Angular mBipoSH correlation functions from SEVEM Foreground-cleaned Planck data for L=1. Green and blue lines represent the extracted mBipoSH functions from the map, while light blue and red depict theoretical Doppler boost-only plots with error bars.

In the given figures 4.6 and 4.7, we plot the mBipoSH angular correlation function corresponding to $L = 1$ dipolar anisotropy having l and $l + 1$ like correlations in the harmonic space, which is mainly dominated by Doppler boost at smaller angles and at large angular separations, the Cosmic Hemispherical Asymmetry nSI effect. We observe that our results from SEVEM match well with the expactations

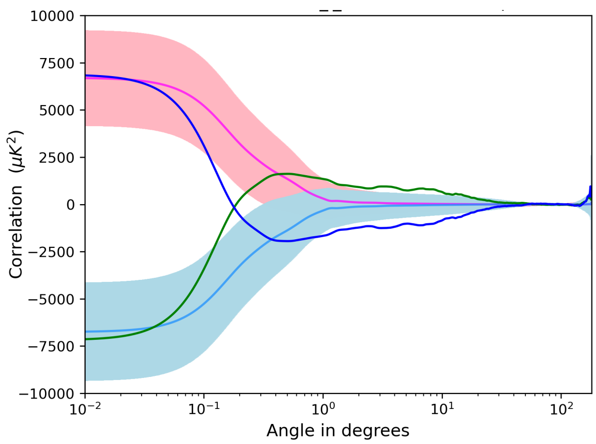

Figure 4.7: Angular mBipoSH correlation functions from SMICA Foreground-cleaned Planck data for L=1. Green and blue lines represent the extracted mBipoSH functions from the map, while light blue and red depict theoretical Doppler boost-only plots with error bars.

from theoretical analyses. However, to understand for the deviations between SEVEM and SMICA methods, we need to investigate in depth multiple issues including an assessment of the foreground residuals present in both the cleaned maps. We defer the pursuit of this investigation in future work since this would involve more detailed understanding of the analysis underlying the two approaches to foreground cleaning .

4.6 Discussions

The mBipoSH basis provides a natural extension of the standard CMB correlation function by extending an expanded set of isotropic correlation functions for the nSI CMB maps. We show the effectiveness of this basis in capturing well-known sources of nSI violation effects, such as Doppler boost, CHA and Non circular beam. This new basis introduces a new real-space-based estimator for studying nSI maps. We illustrate this by successfully capturing the Doppler boost effect and CHA effect dipolar anisotropy at $L = 2$ using a set of two additional angular isotropic correlation functions. Additionally, we model systematics from non-circular beam of the instrument under the $L = 2$ quadrupole anisotropy and successfully capture it with three correlation functions. Subsequently, we construct the real-space-based estimations for the signal strength of the nSI effects. We find that mathematically, the nSI effects can be captured in the real-space estimator and can be studied using partial sky maps. Finally, in this chapter, we present a preliminary analysis of the Planck sky SMICA and SEVEM maps, which are the foreground-cleaned maps from Planck produced by two independent approaches and observe that the result at the $L = 1$ dipole signal for one matches well with the dominant Doppler boost signal. However, our result shows that the further investigation of the maps at large angles is necessary to better understand residual foreground contributions. This serves as a direction for future work. In summary, the mBipoSH method proves to be an efficient new approach for capturing nSI effects in the CMB data in terms of a set of isotropic correlation functions.

CHAPTER 5

CONCLUSION

5.1 Summary

In this thesis, we have studied a novel estimator to effectively analyze the non-statistical isotropic features in the CMB data. Our estimator extends the well-known and tested BipoSH estimator from harmonic space to real-space cases, allowing for the study of nSI CMB sky maps and making it suitable for examining partial CMB sky maps. Our framework is based on the reduction of bipolar spherical harmonics basis as studied by Manakov et al. in the context of angular distributions in atomic processes. This method provides us with a 'minimal' basis to study the nSI features and offers an expansion in a set of isotropic correlation functions named here as mBipoSH angular functions, thus presenting a new method for analyzing CMB maps beyond Statistical isotropy (SI) assumptions. In this thesis, we have extended these cases to a general CMB sky map, tested our approach on well-known instances of nSI violation, provided the mathematical formulation, and demonstrated the efficacy of our results on a set of simulated maps, which agree well with the features of those nSI signals. Lastly, we have introduced a new real-space-based estimation criterion for studying nSI signals from partial CMB sky maps. Our construction represents a generally applicable structure for data distributed on the 2D sphere, with a varied range of applicability for celestial and geographical maps in studying patterns.

5.1.1 BipoSH basis and its irreducible reduction

The BipoSH basis, consisting of the tensor product of the two spherical harmonic basis functions, forms the most general basis for studying the two-point correlation of data distributed on the 2D sphere. The BipoSH basis has been successfully employed to capture non-statistical isotropy (nSI) from the CMB maps. We investigate a possible irreducible reduction of this basis, based on the observation that any tensor of rank L can be constructed from L components. Utilizing this structure, we construct functions that depend on the angular separation, θ and expand the most general correlation function based on this basis. We define new functions in this basis as mBipoSH functions, demonstrating that any nSI feature in the CMB map can be effectively captured by $L+1$ of these mBipoSH functions in the case of even parity and L mBipoSH functions in the case of odd parity. The parity structure in the two-point correlation naturally emerges in this new basis.

5.1.2 Application to the CMB sky maps

Within the framework developed in this thesis, we studied well-known cases of non-statistical isotropy (nSI) violation. Specifically, we examined the Doppler boost, Cosmic Hemispherical Asymmetry (CHA), and Non-circular Beam Systematics cases using the developed mBipoSH correlation functions. The results from simulated CMB sky maps with the Doppler boost feature, indicate that these nSI signals peak at very small angles, clearly highlighting why the Planck satellite with improved resolution could detect the signal clearly. Additionally, the results from CHA were studied using two mBipoSH functions, revealing that CHA is subdominant at lower angles compared to the Doppler boost but becomes slightly more relevant at higher angles. We observe that the signal is prominent at 2-3 σ versus the null realization of the signal, drawing a decisive inference regarding the presence of the cosmic hemispherical effect versus random realizations of the cosmic microwave background (CMB) sky. Furthermore, the results from non-circular beam systematics demonstrate that the exact analytic form of the nSI signal can be captured by three istropic correlation functions at L=2 quadrupole, and the effect of the systematics can be effectively probed by the mBipoSH method.

We developed a minimum variance-based estimator for our developed mBipoSH functions. This estimator is crucial as it measures the signal strength of nSI cases from the real sky maps, which consist of temperature fluctuations/polarization values from the pixels, making it suitable for ground-based missions capturing partial sky maps. The results from the L=1 dipole, having l and $l+1$ correlations, from the Planck foreground cleaned maps SMICA and SEVEM, agree well with the predicted signals from the simulated maps. We plan to study them more thoroughly in the near future to investigate the effects of various contributions such as residuals, for a detailed study of the L=1 nSI effect.

5.2 Future Work

The method proposed in this thesis has opened up many possibilities for future investigations. In the future, we plan to thoroughly study the various sources of nSI features in the CMB maps using mBipoSH correlation functions, such as nontrivial topologies and weak lensing. We aim to effectively analyze the Planck data maps for nSI features such as Systematics and CHA in detail and then estimate nSI features such as boost velocity and lensing potential from the CMB sky maps, both from the Planck data maps and from the recent ACT-based partial sky maps, using the pixel sky-based minimum variance method. Additionally, we intend to develop a Hamiltonian Monte Carlo-based posterior estimator for these effects in the real-space data observations. Furthermore, we plan to carry out the whole analysis using CMB polarization-based methods.

Appendices

APPENDIX A

SPHERICAL COORDINATE SYSTEM

Spherical coordinates are extensively used in angular momentum theory, proving particularly useful for handling problems having spherically symmetric datasets. Within this framework, the covariant spherical coordinates x_μ (with $\mu = \pm 1, 0$) are defined by the following relations

$$\begin{aligned} x_{+1} &= -\frac{1}{\sqrt{2}}(x+iy) = -\frac{1}{\sqrt{2}} r \sin\vartheta e^{i\varphi}, \\ x_0 &= z = r\cos\vartheta, \\ x_{-1} &= \frac{1}{\sqrt{2}}(x-iy) = \frac{1}{\sqrt{2}} r \sin\vartheta e^{-i\varphi}. \end{aligned} \tag{A.1}$$

The corresponding contravariant spherical coordinates x^μ (where $\mu = \pm 1, 0$) can be written as

$$\begin{aligned} x^{+1} &= -\frac{1}{\sqrt{2}}(x-iy) = -\frac{1}{\sqrt{2}} r \sin\vartheta e^{-i\varphi}, \\ x^0 &= z = r\cos\vartheta, \\ x^{-1} &= \frac{1}{\sqrt{2}}(x+iy) = \frac{1}{\sqrt{2}} r \sin\vartheta e^{i\varphi}. \end{aligned} \tag{A.2}$$

The transformation between covariant and contravariant spherical coordinates can be achieved by using

$$\begin{aligned} x^\mu &= (-1)^\mu x_{-\mu}, \quad x_\mu = (-1)^\mu x^{-\mu}, \\ x^\mu &= x^*_\mu, \quad x_\mu = x^{\mu *}. \end{aligned} \tag{A.3}$$

The covariant and contravariant spherical basis vectors $\mathbf{e}_\mu (\mu = \pm 1, 0)$ are defined by

$$\begin{aligned}
\mathbf{e}_{+1} &= -\frac{1}{\sqrt{2}}\left(\mathbf{e}_x + i\mathbf{e}_y\right), \\
\mathbf{e}_0 &= \mathbf{e}_z, \\
\mathbf{e}_{-1} &= \frac{1}{\sqrt{2}}\left(\mathbf{e}_x - i\mathbf{e}_y\right), \\
\mathbf{e}^{+1} &= -\frac{1}{\sqrt{2}}\left(\mathbf{e}_x - i\mathbf{e}_y\right), \\
\mathbf{e}^0 &= \mathbf{e}_z, \\
\mathbf{e}^{-1} &= \frac{1}{\sqrt{2}}\left(\mathbf{e}_x + i\mathbf{e}_y\right).
\end{aligned} \tag{A.4}$$

These spherical basis vectors form a complete and orthonormal basis defined as

$$\mathbf{e}_\mu \mathbf{e}^\nu = \mathbf{e}_\mu \mathbf{e}_\nu^* = \delta_{\mu\nu}. \tag{A.5}$$

Spherical basis vectors follow the given relations involving the vector product

$$\begin{aligned}
&\mathbf{e}_\mu \times \mathbf{e}_\nu = i\sqrt{2}C_{1\mu 1\nu}^{1\lambda}\mathbf{e}_\lambda, \quad \mathbf{e}^\mu \times \mathbf{e}^\nu = -i\sqrt{2}C_{1\mu 1\nu}^{1\lambda}\mathbf{e}^\lambda, \\
&\mathbf{e}_\mu \times \mathbf{e}_\nu = -i\varepsilon_{\mu\nu\lambda}\mathbf{e}^\lambda, \quad \mathbf{e}^\mu \times \mathbf{e}^\nu = i\varepsilon_{\mu\nu\lambda}\mathbf{e}_\lambda.
\end{aligned} \tag{A.6}$$

The mathematical expression for the function $\varepsilon_{\mu\nu\lambda}$ can be written as

$$\varepsilon_{\mu\nu\lambda} = \begin{cases} +1 & \text{if } (\mu, \nu, \lambda) \text{ is an even permutation of } (+1, 0, -1), \\ -1 & \text{if } (\mu, \nu, \lambda) \text{ is an odd permutation of } (+1, 0, -1), \\ 0 & \text{if at least two indices among } \mu, \nu, \lambda \text{ are equal.} \end{cases} \tag{A.7}$$

A spherical harmonic given as $Y_{lm}(\vartheta, \varphi)$ is a complex-valued function of two real variables, ϑ and φ, where variables take values $0 \leq \vartheta \leq \pi$ and $0 \leq \varphi < 2\pi$. It is continuous, bounded, and single-valued. This function is defined by two parameters, l and m, where l ranges from 0 to ∞, and m ranges from $-l$ to l. For a fixed value of l, there exist $2l + 1$ functions corresponding to different values of m.

Derivatives of $Y_{lm}(\vartheta, \varphi)$ are also single-valued, continuous, and finite functions.

Spherical harmonics provide a complete and orthonormal basis for analyzing spherical functions, playing a crucial role in the study of atomic physics and quantum mechanics. These functions represent the possible states of orbital angular momentum on a sphere. This helps our understanding of particle distribution in a spherical space. Here, l describes the magnitude of the orbital angular momentum, while m specifies its orientation. When we square the orbital angular momentum operator, denoted as $\widehat{\mathbf{L}}^2$, we obtain $l(l+1)$ as the eigenvalue. Additionally, the projection of the orbital angular momentum operator, $\widehat{L}_z$, gives m as its eigenvalue.

The spherical harmonics $Y_{lm}(\vartheta, \varphi)$ follow the commutation relations corresponding to rank-increasing and rank-decreasing operators, as given by

$$\left[\widehat{L}_\mu, Y_{lm}(\vartheta, \varphi)\right] = \sqrt{l(l+1)}C^{lm+\mu}_{lm1\mu} Y_{lm+\mu}(\vartheta, \varphi). \tag{A.8}$$

The simpler form can be represented as

$$\begin{aligned} \widehat{L}_{\pm 1} Y_{lm}(\vartheta, \varphi) &= \mp \sqrt{\frac{l(l+1) - m(m \pm 1)}{2}} Y_{lm\pm 1}(\vartheta, \varphi), \\ \widehat{L}_0 Y_{lm}(\vartheta, \varphi) &= m Y_{lm}(\vartheta, \varphi). \end{aligned} \tag{A.9}$$

The mathematical form for the spherical harmonic basis can be given as

$$Y_{lm}(\vartheta, \varphi) = e^{im\varphi} \sqrt{\frac{2l+1}{4\pi} \frac{(l-m)!}{(l+m)!}} P_l^m(\cos\vartheta). \tag{A.10}$$

Explicit analytical form of a few spherical harmonic functions can be presented

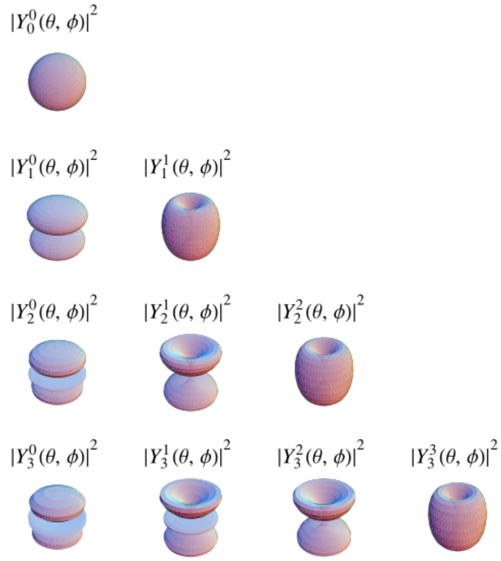

Figure A.1: The visual representation of the first few spherical harmonic basis components. Credit- wolfram.com/sphericalharmonics

as

$$
\begin{aligned}
Y_{00}(\vartheta, \varphi) &= \frac{1}{2\sqrt{\pi}}, \\
Y_{1+1}(\vartheta, \varphi) &= -\frac{1}{2}\sqrt{\frac{3}{2\pi}} \sin\vartheta e^{i\varphi}, \\
Y_{10}(\vartheta, \varphi) &= \frac{1}{2}\sqrt{\frac{3}{\pi}} \cos\vartheta, \\
Y_{1-1}(\vartheta, \varphi) &= \frac{1}{2}\sqrt{\frac{3}{2\pi}} \sin\vartheta e^{-i\varphi}, \\
Y_{2+2}(\vartheta, \varphi) &= \frac{1}{4}\sqrt{\frac{3\cdot 5}{2\pi}} \sin^2\vartheta e^{i2\varphi}, \\
Y_{2+1}(\vartheta, \varphi) &= -\frac{1}{2}\sqrt{\frac{3\cdot 5}{2\pi}} \cos\vartheta \sin\vartheta e^{i\varphi}, \\
Y_{20}(\vartheta, \varphi) &= \frac{1}{4}\sqrt{\frac{5}{\pi}} (3\cos^2\vartheta - 1).
\end{aligned}
\tag{A.11}
$$

APPENDIX B

IMPORTANT RELATIONS

Orthonomality of the Spherical Harmonics is given as

$$\int d\Omega_{\hat{n}} Y_{\ell m}(\hat{n}) = \sqrt{4\pi}\delta_{\ell 0}\delta_{m0} \tag{B.1}$$

$$\int d\Omega_{\hat{n}} Y_{l_1 m_1}(\hat{n}) Y^*_{l_2 m_2}(\hat{n}) = \delta_{l_1 l_2}\delta_{m_1 m_2} \tag{B.2}$$

$$\int d\Omega_{\hat{n}} Y_{l_1 m_1}(\hat{n}) Y_{l_2 m_2}(\hat{n}) Y^*_{\ell_3 m_3}(\hat{n}) = \sqrt{\frac{(2l_1+1)(2l_2+1)}{4\pi(2\ell_3+1)}} C^{\ell_3 0}_{l_1 0 l_2 0} C^{\ell_3 m_3}_{l_1 m_1 l_2 m_2} \tag{B.3}$$

The symmetry property of spherical harmonics is given by

$$Y^*_{lm}(\hat{n}) = (-1)^m Y_{l-m}(\hat{n}). \tag{B.4}$$

Spherical harmonic expansion of Legendre polynomials:

$$P_l\left(\hat{n}\cdot\hat{n}'\right) = \frac{4\pi}{2l+1}\sum_{m=-l}^{l} Y^*_{lm}(\hat{n}) Y_{lm}\left(\hat{n}'\right). \tag{B.5}$$

Symmetry properties of Clebsch-Gordan coefficients:

$$\begin{aligned} C^{c\gamma}_{a\alpha b\beta} &= (-1)^{a+b-c} C^{c\gamma}_{b\beta a\alpha}, \\ C^{c\gamma}_{a\alpha b\beta} &= (-1)^{a+b-c} C^{c-\gamma}_{a-\alpha b-\beta}. \end{aligned} \tag{B.6}$$

Summation rules of Clebsch-Gordan coefficients:

$$\begin{aligned}
\sum_{\alpha\beta} C^{c\gamma}_{a\alpha b\beta} C^{c'\gamma'}_{a\alpha b\beta} &= \delta_{cc'}\delta_{\gamma\gamma'}\{abc\}\{abc'\}, \\
\sum_{a\gamma} C^{c\gamma}_{a\alpha b\beta} C^{c\gamma}_{a\alpha b'\beta'} &= \frac{2c+1}{2b+1}\delta_{bb'}\delta_{\beta\beta'}\{abc\}\{ab'c\}, \\
\sum_{c\gamma} C^{c\gamma}_{a\alpha b\beta} C^{c\gamma}_{a\alpha' b\beta'} &= \delta_{\alpha\alpha'}\delta_{\beta\beta'}\{abc\}.
\end{aligned} \tag{B.7}$$

Here, the $3j$-symbol $\{abc\}$ is defined by

$$\{abc\} = \begin{cases} 1 & \text{if } a+b+c \text{ is integer and } |a-b| \leq c \leq (a+b), \\ 0 & \text{otherwise.} \end{cases} \tag{B.8}$$

The orthonormality relation of $\chi^{\ell}(\omega)$ is given by

$$\int_0^{\pi} \chi^{\ell_1}(\omega)\chi^{\ell_2}(\omega)\sin^2\frac{\omega}{2}d\omega = \frac{\pi}{2}\delta_{\ell_1\ell_2}. \tag{B.9}$$

The orthonormality of $D^{\ell}_{MM}(\mathcal{R})$ is expressed as

$$\int d\mathcal{R} D^{*\ell}_{MM'}(\mathcal{R}) D^{l}_{mm'}(\mathcal{R}) = \frac{8\pi^2}{2l+1}\delta_{l\ell}\delta_{mM'}\delta_{m'M} \tag{B.10}$$

$$\sum_{mm'} D^{\ell}_{mm'}(R_1)\, D^{\ell}_{m'm}(R_2) = \chi_{\ell}(R_1 R_2)\,. \tag{B.11}$$

APPENDIX C

mBipoSH FUNCTIONS

In this appendix, we present the reduction formulae for Bipolar spherical harmonics with ranks 1, 2, and 3. The notation $x = \cos\theta = \hat{n} \cdot \hat{n}'$ and $l_{\max} = \max(l, l')$ will be used consistently throughout this section.

C.0.1 Rank 1 Reduction Formula

We begin with the reduction formula for Bipolar spherical harmonics with rank 1.

The spherical harmonic function $Y^{ll'}_{1M}(n, n')$ for the odd parity case having l, l correlations is defined as:

$$Y^{ll'}_{1}(n, n') = \frac{i(-1)^{l+1}}{4\pi} \left[\frac{3(2l+1)}{l(l+1)}\right]^{\frac{1}{2}} P^{(1)}_{l}(x) \left[\hat{n} \times \hat{n}'\right]. \tag{C.1}$$

Similarly, the even parity case for $l, l+1$ correlations, $Y^{ll'}_{1m}(n, n')$ is given as:

$$Y^{ll'}_{1m}(n, n') = -\frac{1}{4\pi} \frac{\sqrt{3}}{l_{\max}} \left((-1)^{l'} P^{(1)}_{l}(x)\hat{n} + (-1)^{l} P^{(1)}_{l}(x)\hat{n}'\right). \tag{C.2}$$

C.0.2 Rank 2 Reduction Formula

The reduction formula for Bipolar spherical harmonics with rank 2 is more involved. We start with even parity with l, l correlations,

$$\begin{aligned} Y^{ll}_{2m}(n, n') = (-1)^{l+1} \frac{30(2l+1)}{4\pi\sqrt{(2l-1)(l+1)(2l+3)}} & P^{(1)}_{l}(x) \left(\hat{n} \otimes \hat{n}'\right)_{2m} \\ & + P^{(2)}_{l}(x) \left[\hat{n} \times \hat{n}'\right]_{2m}. \end{aligned} \tag{C.3}$$

The equation for Bipolar harmonics corresponding to odd parity with $l' = l \pm 1$ correlations is given as

$$
\begin{aligned}
Y^{ll'}_{2m}(n,n') = i(-1)^l \frac{10}{4\pi\sqrt{l_{\max}(l_{\max}+1)}} P^{(2)}_{lm}(x)\left(\hat{n}\otimes[\hat{n}\times\hat{n}']\right)_{2m} \\
+ P^{(2)}_{lm}(x)\left(\hat{n}'\otimes[\hat{n}\times\hat{n}']\right)_{2m}.
\end{aligned}
\tag{C.4}
$$

Further, an additional even parity case corresponding to $l' = l \pm 2$ correlations given as

$$
\begin{aligned}
Y^{ll'}_{2m}(n,n') = (-1)^l \frac{\sqrt{5}}{4\pi\sqrt{l_{\max}(2l_{\max}-1)(l_{\max}-1)}} P^{(2)}_{l}(x)\left(\hat{n}\otimes\hat{n}\right)_{2m} \\
- 2P^{(2)}_{l}(x)\left(\hat{n}'\otimes\hat{n}\right)_{2m} \\
+ P^{(2)}_{l}(x)\left(\hat{n}'\otimes\hat{n}'\right)_{2m}.
\end{aligned}
\tag{C.5}
$$

C.0.3 Rank 3 Reduction Formula

Moving on to rank 3, the spherical harmonic function in terms of minimal bipolar spherical harmonics for even parity $l = l' \pm 1$ and $l = l' \pm 3$ correlations is defined as

$$
\begin{aligned}
Y^{ll'}_{3m}(n,n') = C(l,l')\left(P^{(3)}_{l}(x)\hat{n}\hat{n}\right)_{3m} + P^{(3)}_{l}(x)\hat{n}'_{3m} \\
- \left(\frac{3P^{(3)}_{l+1}(x)(l'-l+3)(l+l'+4)}{2}\right) P^{(2)}_{l}(x)\left(\hat{n}\otimes\hat{n}\right)_{3m}.
\end{aligned}
\tag{C.6}
$$

The cases corresponding to odd parity $l = l'$ and $l = l' \pm 2$ correlations are given ass

$$Y^{ll'}_{3m}(n,n') = -iC(l,l')\left(P^{(3)}_l(x)[\hat{n}\times\hat{n}]_{3m} + P^{(3)}_l(x)[\hat{n}\otimes\hat{n}']_{3m}\right) + \frac{l'+l+2(l'+l+3)}{2}. \tag{C.7}$$

The coefficient $C(l,l')$ is given by

$$C(l,l') = \frac{6(-1)^{l+1}}{\pi}\left[\frac{210(2l+1)(2l'+1)(l'-3)!}{(l'-l+3)!(l+1)!(l'+4)!}\right]^{1/2}. \tag{C.8}$$

BIBLIOGRAPHY

[1] S. Mukherjee and T. Souradeep, Phys. Rev. D **89**, 063013 (2014).

[2] D. Fixsen, The Astrophysical Journal **707**, 916 (2009).

[3] A. Hajian and T. Souradeep, The Astrophysical Journal **597**, L5 (2003).

[4] A. Hajian, T. Souradeep, and N. Cornish, The Astrophysical Journal **618**, L63–L66 (2004).

[5] N. L. Manakov, S. I. Marmo, and A. V. Meremianin, Journal of Physics B: Atomic, Molecular and Optical Physics **29**, 2711 (1996).

[6] D. A. Varshalovich, A. N. Moskalev, and V. K. Khersonskii, *Quantum Theory of Angular Momentum* (World Scientific, Singapore, 1988).

[7] S. Mitra, A. S. Sengupta, and T. Souradeep, Phys. Rev. D **70**, 103002 (2004).

[8] N. Joshi, S. Jhingan, T. Souradeep, and A. Hajian, Phys. Rev. D **81**, 083012 (2010).

[9] S. Mukherjee, A. De, and T. Souradeep, Phys. Rev. D **89**, 083005 (2014).

[10] S. Kumar *et al.*, Phys. Rev. D **91**, 043501 (2015).

[11] Planck Collaboration *et al.*, **571**, A27 (2014).

[12] P. Ade *et al.*, Astronomy & Astrophysics **594**, A16 (2016).

[13] S. Saha *et al.*, JCAP **10**, 072 (2021).

[14] A. Lewis and A. Challinor, CAMB: Code for Anisotropies in the Microwave Background, Astrophysics Source Code Library, record ascl:1102.026, 2011.

[15] G. Hinshaw *et al.*, The Astrophysical Journal Supplement Series **208**, 19 (2013).

[16] S. Shaikh *et al.*, Journal of Cosmology and Astroparticle Physics **2019**, 007 (2019).

[17] S. Mitra, A. S. Sengupta, and T. Souradeep, Physical Review D **70**, (2004).

[18] N. Joshi *et al.*, Revealing Non-circular beam effect in WMAP-7 CMB maps with BipoSH measures of Statistical Isotropy, 2013.

[19] W. Hu and T. Okamoto, The Astrophysical Journal **574**, 566 (2002).

[20] D. Hanson, G. Rocha, and K. Górski, Monthly Notices of the Royal Astronomical Society **400**, 2169 (2009).

[21] A. Rotti, M. Aich, and T. Souradeep, WMAP anomaly : Weak lensing in disguise, 2011.

[22] M. Kamionkowski and T. Souradeep, Phys. Rev. D **83**, 027301 (2011).

[23] G. Hinshaw *et al.*, Astrophys. J. Suppl. **180**, 225 (2009).

[24] C. J. Copi, D. Huterer, D. J. Schwarz, and G. D. Starkman, Adv. Astron. **2010**, 847541 (2010).

[25] N. Aghanim *et al.*, Astron. Astrophys. **641**, A1 (2020).

[26] K. M. Gorski *et al.*, The Astrophysical Journal **622**, 759 (2005).

[27] C. R. Harris *et al.*, Nature **585**, 357 (2020).

[28] P. Virtanen *et al.*, Nature Methods **17**, 261 (2020).

[29] J. D. Hunter, Computing in Science & Engineering **9**, 90 (2007).

[30] S. Das, arXiv preprint arXiv:1902.02328 (2019).

[31] L. G. Book, M. Kamionkowski, and T. Souradeep, Phys. Rev. D **85**, 023010 (2012).

[32] Dipanshu, T. Souradeep, and S. Hirve, The Astrophysical Journal **954**, 181 (2023).

[33] S. Mukherjee *et al.*, Journal of Cosmology and Astroparticle Physics **2016**, 042 (2016).

[34] A. Hajian and T. Souradeep, The Cosmic Microwave Background Bipolar Power Spectrum: Basic Formalism and Applications, 2004.

[35] T. Souradeep and A. Hajian, Pramana **62**, 793–796 (2004).

[36] M. Aich and T. Souradeep, Phys. Rev. D **81**, 083008 (2010).

[37] S. Mitra *et al.*, Monthly Notices of the Royal Astronomical Society **394**, 1419 (2009).

[38] S. Das and T. Souradeep, Journal of Cosmology and Astroparticle Physics **2015**, 012 (2015).

[39] P. K. Aluri, N. Pant, A. Rotti, and T. Souradeep, Phys. Rev. D **92**, 083015 (2015).

[40] M. Aich, A. Rotti, and T. Souradeep, Weak lensing in non-statistically isotropic universes, 2015.

[41] S. Mukherjee and T. Souradeep, Phys. Rev. Lett. **116**, 221301 (2016).

[42] N. Pant *et al.*, Journal of Cosmology and Astroparticle Physics **2016**, 035 (2016).

[43] S. Basak, A. Hajian, and T. Souradeep, Phys. Rev. D **74**, 021301 (2006).